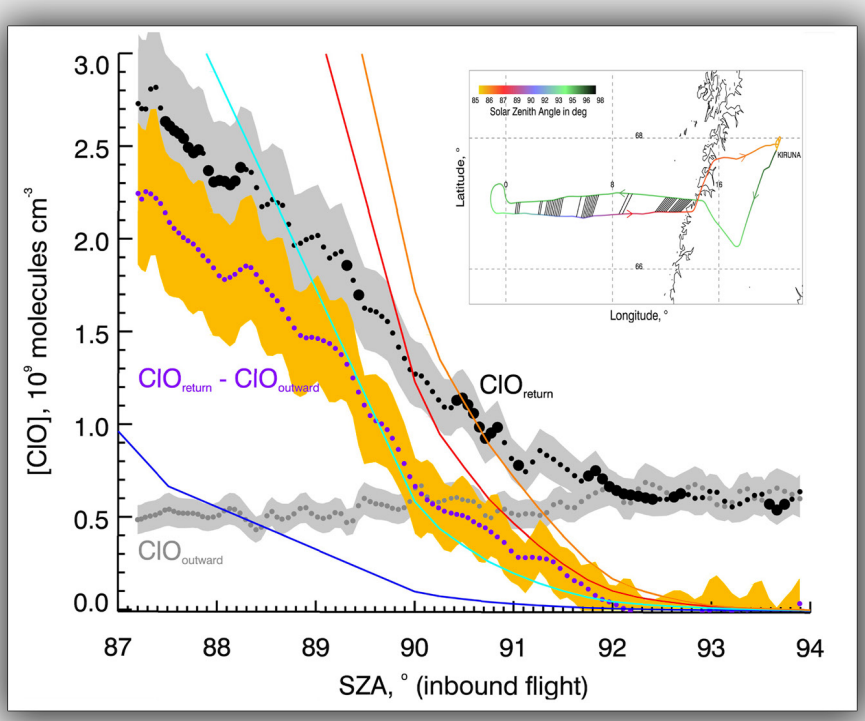

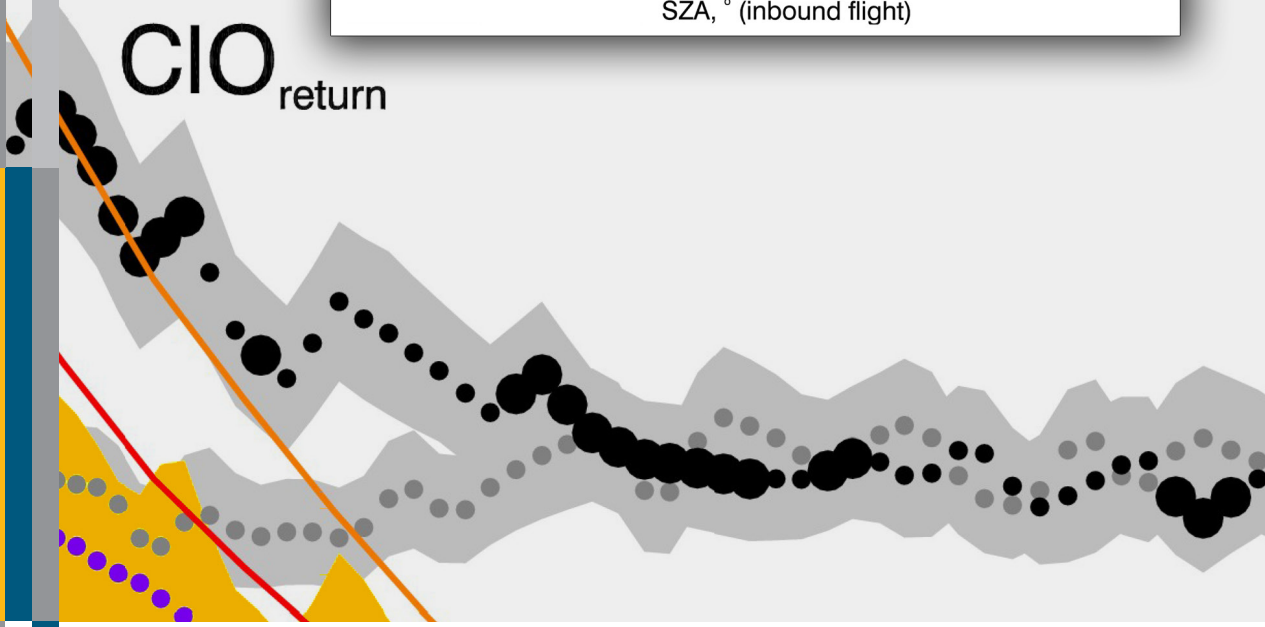

Stratospheric ClOOCl chemistry at high solar zenith angles

Olga Suminska-Ebersoldt

Member of the Helmholtz Association

JÜLICH
FORSCHUNGSZENTRUM

Schriften des Forschungszentrums Jülich
Reihe Energie & Umwelt / Energy & Environment Band / Volume 151

Forschungszentrum Jülich GmbH
Institut für Energie- und Klimaforschung (IEK)
Stratosphäre (IEK-7)

Stratospheric ClOOCl chemistry at high solar zenith angles

Olga Suminska-Ebersoldt

Schriften des Forschungszentrums Jülich
Reihe Energie & Umwelt / Energy & Environment Band / Volume 151

ISSN 1866-1793 ISBN 978-3-89336-817-4

Bibliographic information published by the Deutsche Nationalbibliothek.
The Deutsche Nationalbibliothek lists this publication in the Deutsche Nationalbibliografie; detailed bibliographic data are available in the Internet at http://dnb.d-nb.de.

Publisher and Distributor:	Forschungszentrum Jülich GmbH Zentralbibliothek 52425 Jülich Phone +49 (0) 24 61 61-53 68 · Fax +49 (0) 24 61 61-61 03 e-mail: zb-publikation@fz-juelich.de Internet: http://www.fz-juelich.de/zb
Cover Design:	Grafische Medien, Forschungszentrum Jülich GmbH
Printer:	Grafische Medien, Forschungszentrum Jülich GmbH
Copyright:	Forschungszentrum Jülich 2012

Schriften des Forschungszentrums Jülich
Reihe Energie & Umwelt / Energy & Environment Band / Volume 151

D 468 (Diss., Wuppertal, Univ., 2012)

ISSN 1866-1793
ISBN 978-3-89336-817-4

The complete volume is freely available on the Internet on the Jülicher Open Access Server (JUWEL) at http://www.fz-juelich.de/zb/juwel

Abstract

The photolysis rate constant of dichlorine peroxide (ClOOCl, ClO dimer), J_{ClOOCl}, is a critical parameter in catalytic cycles destroying ozone (O_3) in the polar stratosphere. In the atmospherically relevant wavelength region (310 – 500 nm), significant discrepancies between laboratory measurements of ClOOCl absorption cross sections and spectra cause a large uncertainty in J_{ClOOCl}. Previous investigations of the consistency of published J_{ClOOCl} with atmospheric observations of chlorine monoxide (ClO) and ClOOCl have focused on the photochemical equilibrium between ClOOCl formation and photolysis, and thus could only constrain the ratio of J_{ClOOCl} and the ClOOCl formation rate constant k_{rec}.

Here, the atmospherically effective J_{ClOOCl} was constrained independent of k_{rec}, using ClO measured in the same air masses before and directly after sunrise during an aircraft flight that was carried out as a part of the RECONCILE field campaign in winter 2010 over Kiruna, Sweden. Over sunrise, when the ClO/ClOOCl system comes out of thermal equilibrium, the influence of the ClO recombination reaction is negligible and the ClO concentration increase results from the photolysis of ClOOCl. J_{ClOOCl} values based on four absorption cross sections and spectra were estimated for the atmospheric conditions on the flight track and resulting ClO concentration increases were compared with the observed ClO rise.

The analysis shows, that the increase in measured ClO concentrations was significantly faster than expected from J_{ClOOCl} based on the absorption spectrum proposed by Pope et al. (2007), but did not warrant cross sections larger than recently published values by Papanastasiou et al. (2009). In particular, the existence of a significant ClOOCl absorption band longwards of 420 nm is not supported by the observations. The observed night-time ClO is not consistent with a ClO/ClOOCl thermal equilibrium constant significantly higher

than the one proposed by Plenge et al. (2005).

Another important uncertainty factor for J_{ClOOCl}, and for photolysis rates in general, is the actinic flux, i.e. the radiation available to drive photochemical reactions. Comprehensive sensitivity studies were carried out to investigate the influence of ozone, albedo, aerosol and clouds on the UV/Vis actinic flux in the lower stratosphere using two different radiation transfer models.

The sensitivity studies revealed that at high solar zenith angles albedo and tropospheric clouds do not influence actinic flux and thus J_{ClOOCl} significantly. The impact of ozone and aerosol is larger, but still less important than the differences between J_{ClOOCl} based on various absorption cross sections and spectra.

The method used in this study enabled estimation of J_{ClOOCl} separately from k_{rec}. The results of the analysis are consistent with previous studies and confirm our understanding of processes governing ozone loss in polar regions.

Zusammenfassung

Die Photolyserate von Dichlordioxid (ClOOCl, ClO-Dimer), J_{ClOOCl}, ist ein kritischer Parameter in katalytischen Zyklen, die das Ozon (O_3) in der polaren Stratosphäre zerstören. In dem atmosphärisch relevanten Wellenlängenbereich (310 bis 500 nm) führen die erheblichen Diskrepanzen zwischen unterschiedlichen Labormessungen der ClOOCl Absorptionsquerschnitte und -spektren zu einer großen Unsicherheit in J_{ClOOCl}. Vorherige Untersuchungen der Konsistenz der veröffentlichten J_{ClOOCl}-Werte mit atmosphärischen Beobachtungen von Chlormonoxid (ClO) und ClOOCl haben sich auf das photochemische Gleichgewicht zwischen ClOOCl Bildung und Photolyse konzentriert. Diese konnten jedoch nur das Verhältnis von J_{ClOOCl} zur ClOOCl Bildungsrate k_{rec} einschränken.

Hier wurde die atmosphärisch wirksame Photolyserate J_{ClOOCl} unabhängig von k_{rec} bestimmt, indem ClO in den gleichen Luftmassen jeweils vor und direkt nach Sonnenaufgang während eines Flugs, im Rahmen der RECONCILE Messkampagne im Winter 2010 in Kiruna, Schweden, gemessenen wurde. Während des Sonnenaufgangs, wenn das ClO/ClOOCl System aus dem thermischen Gleichgewicht herauskommt, ist der Einfluss der ClO Rekombinationsreaktion vernachlässigbar und der ClO-Konzentrationsanstieg resultiert ausschließlich aus der Photolyse von ClOOCl. J_{ClOOCl}-Werte, basierend auf vier Absorptionsquerschnitten und -spektren, wurden für die atmosphärischen Bedingungen auf dem Flugweg geschätzt und die daraus resultierenden ClO-Konzentrationsanstiege wurden mit dem beobachteten ClO-Anstieg verglichen.

Die Analyse zeigt, dass die Zunahme der gemessenen ClO-Konzentrationen deutlich schneller verläuft, als zum Beispiel das Absorptionsspektrum von den Pope et al. (2007) erwarten lassen würde. Auf der anderen Seite würde das ClO früher und schneller als beobachtet ansteigen, wenn die Querschnitte deutlich über den Werten von Papanasta-

siou et al. (2009) lägen. Insbesondere die Existenz einer bedeutenden ClOOCl Absorptionsbande oberhalb von 420 nm erscheint mit den Beobachtungen nicht vereinbar. Das nachts beobachtete ClO ist nicht konsistent mit einer thermischen Gleichgewichtkonstante ClO/ClOOCl oberhalb der von Plenge et al. (2005) publizierten.

Ein weiterer wichtiger Unsicherheitsfaktor für J_{ClOOCl} und die Photolyseraten im Allgemeinen ist der aktinischen Fluss, das heißt, die für photochemische Reaktionen zur Verfügung stehende Strahlung. Um den Einfluss von Ozon, Albedo, Aerosol und Wolken auf den UV/Vis aktinischen Fluss in der unteren Stratosphäre zu untersuchen, wurden Sensitivitätsstudien durchgeführt. Diese zeigen, dass bei hohen Zenitwinkeln Albedo und troposphärische Wolken keinen Einfluss auf den aktinischen Fluss und damit auch auf J_{ClOOCl} haben. Die Auswirkungen von Ozon und Aerosol sind größer, aber immer noch weniger wichtig als die Unterschiede zwischen J_{ClOOCl} basierend auf verschiedenen Absorptionsquerschnitten und -spektren.

Die in dieser Studie verwentete Methode ermöglichte eine Schätzung von J_{ClOOCl} unabhängig von k_{rec}. Die Ergebnisse der Analyse stehen im Einklang mit früheren Studien und bestätigen unser Verständnis der Prozesse, die den Ozon-Verlust in den Polargebieten regulieren.

Contents

1 Ozone in the stratosphere

Ozone (O_3) is one of the most important species in the Fatmosphere. It governs the amount of solar UV radiation reaching the Earth's surface and influences strongly the temperature profile of the atmosphere. The region of increased O_3 concentrations located in the stratosphere between 20 and 30 km altitude is called the ozone layer. The altitude, thickness and ozone concentrations in this layer depend on available solar radiation, chemical composition of the air masses and on transport. It all results in longitudinal, latitudinal and seasonal variability in the distribution of ozone. Figure 1.1 shows a comparison of vertical profiles of ozone at two different equivalent latitudes[1] calculated on the basis of a climatology deduced from Halogen Occultation Experiment (HALOE) satellite measurements (Grooß and Russell, 2005).

During the last century, the concentrations of anthropogenically released gases strongly increased. Gases emitted at the surface such as carbon dioxide (CO_2), methane (CH_4), nitrous oxide (N_2O) and fluorinated gases like e.g. chlorofluorocarbons (CFCs) absorb the IR radiation of the Earth and re-emit it in all directions increasing the temperature in the troposphere and influencing the atmospheric transport and mixing. Increased concentrations of CO_2 and CFCs also result in cooling of the stratosphere (Thompson and Solomon, 2002).

The climate changes affect ozone leading to distortion in its distribution and hence also in atmospheric temperatures, which influence the lower levels of the atmosphere down to the surface (Gillett and Thompson, 2003). Due to the coupling between ozone and climate change, the modelling of the future climate requires full understanding of the ozone production and depletion under the changing conditions. First however, the chemical processes

[1] equivalent latitude is calculated from potential vorticity or from passive tracer simulations. Each isoline of equivalent latitude corresponds to an isoline of an atmospheric tracer and encloses the same area as the latitude line of equivalent value

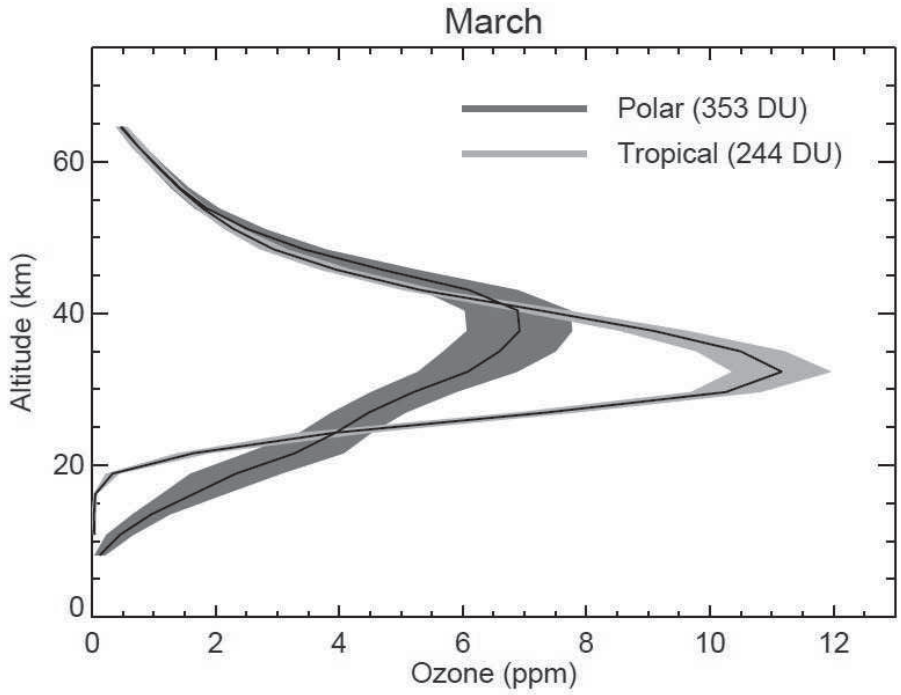

Figure 1.1: The vertical profile of the ozone mixing ratio for polar (equivalent latitude 72.5°N) and tropical (equivalent latitude 2.5°N) conditions in March. In the right corner, the total ozone for this latitudes in Dobson units[2] is given. The ozone data are deduced from satellite measurements (Grooß and Russell, 2005). The figure is adopted from Müller (2010).

governing ozone have to be well known. One of the processes that have to be investigated is the catalytic ClO dimer (dichlorine peroxide, ClOOCl) cycle, in which the polar ozone is intensely depleted during the winter/spring time. This cycle and its parametrisation are the main issue of this thesis and are described in detail in Section 2.

[2]Dobson unit (DU) is a unit of measurement of atmospheric ozone columnar density. 1 DU is defined to be 0.01 mm thickness at standard atmospheric temperature (273.15 K) and pressure (100 kPa).

1.1 Natural stratosphere

1.1.1 Stratospheric ozone chemistry

The atmospheric ozone research started with the studies of Hartley (1881), who investigated the spectroscopic properties of ozone and their influence on the solar radiation penetrating the Earth's atmosphere. The beginning of the regular measurements of O_3 is dated to 1926, when the first column measurements were published by Dobson and Harrison. At that time, the ozone formation mechanism was still unclear. First in 1930, Chapman proposed the photochemical theory of the formation of ozone:

$$O_2 + h\nu \xrightarrow{\lambda<242\text{nm}} O + O \qquad \text{R1}$$

$$O + O_2 + M \rightarrow O_3 + M \qquad \text{R2}$$

$$O_3 + h\nu \xrightarrow{\lambda<320\text{nm}} O + O_2 \qquad \text{R3}$$

$$O + O_3 \rightarrow O_2 + O_2 \qquad \text{R4}$$

The four reactions are today known as the Chapman reactions. In Reaction R1, an oxygen molecule, O_2, absorbs a photon or quantum of electromagnetic radiation. The energy contained in the photon is sufficient to split the oxygen molecule into two highly reactive oxygen atoms, O, called singlet oxygen. In the second reaction singlet oxygen spontaneously combines with another oxygen molecule to create a molecule of ozone. M denotes a collision partner (N_2 or O_2) that is not affected by the reaction. Since Reaction R1 generates 2 singlet oxygen atoms, Reaction R2 generates 2 molecules of ozone for every photon of UV radiation absorbed in Reaction R1. These ozone molecules can be split by UV radiation within a wavelength between 200 and 320 nm into its constituent parts, a molecule of oxygen and a singlet oxygen atom. Reaction R3 consumes a molecule of ozone while absorbing a photon of UV, but because the reaction generates a singlet oxygen, there is no net loss of ozone, since

the singlet oxygen simply proceeds to generate more ozone via Reaction R2. In Reaction R4 the second ozone molecule combines with a singlet oxygen creating two oxygen molecules.

Up to 1960', the Chapman cycle was accepted as sufficient to describe the observed vertical distribution of ozone. However, the measurements of the rate constant of the Chapman reactions (Benson and Axworthy, 1957; Jones and Davidson, 1962) demonstrated that additional reactions are needed to explain the ozone destruction (Hunt, 1966; Schiff, 1969). At the beginning, only the reactions involving OH and HO_2 radicals were assumed to lead to a significant catalytic ozone loss (Hampson, 1964). In 1970 Crutzen proposed that NO catalysed reactions control the ozone concentrations in the middle stratosphere and a few years later, in 1974, Stolarski and Cicerone suggested the possibility of chlorine catalysed ozone loss.

The catalytic ozone loss cycles can be summarised in the form:

$$XO + O \rightarrow X + O_2 \qquad \text{R5}$$

$$X + O_3 \rightarrow XO + O_2 \qquad \text{R6}$$

$$O + O_3 \rightarrow O_2 + O_2$$

where the net reaction is identical to Chapman Reaction R4. Depending on the cycle X = H, OH, NO or Cl. The importance of every cycle increases strongly between 25 and 40 km due to large increase of atomic oxygen with altitude. In this range, the NO_x cycle dominates O_3 loss, below 25 km and above 45 km HO_x is the strongest loss cycle. The loss through the ClO_x cycle depends on the stratospheric chlorine loading and peaks at about 40 km.

Hydrogen oxide radicals ($HO_x \approx HO_2 + HO + H$) in the stratosphere originate from oxidation of water vapour, H_2, and CH_4 transported from the troposphere.

Most of the nitric oxide (NO) in atmosphere comes from nitrous oxide (N_2O), which is a byproduct of bacterial denitrification and nitrification processes occurring mainly in soils below natural vegetation and in the oceans. The most important anthropogenic source

are agricultural activities. N_2O is inert in the troposphere. In the stratosphere it is removed by photolysis and reaction with excited oxygen atoms, providing the major input of $NO_x(\approx NO + NO_2)$ to the stratosphere. NO_x is also a result of lightening and oxidation of atmospheric N_2 at the high temperatures of aircraft engines. The influence of NO radical on ozone was considered first at the beginning of 1970s when the United States and other countries considered the launch of a supersonic aircraft fleet flying in the stratosphere (Crutzen, 1970; Johnston, 1971).

The largest natural sources of chlorine in the atmosphere are evaporated ocean spray as sea salt (sodium chloride NaCl) particles and volcanoes. Most of the species containing chlorine, which are emitted at the Earth's surface cannot reach the stratosphere due to their high reactivity and high water solubility. Only chloromethane (CH_3Cl) is stable enough to be regarded as a natural source of stratospheric chlorine. It is produced by biomass burning, marine algae and phytoplankton, polypore fungi involved in wood rotting and salt tolerant plants (Studer, 2001). The dominant process for the removal of chloromethane from the atmosphere is the reaction with tropospheric hydroxyl (OH) radicals. From the known rate of this reaction, an average global lifetime for chloromethane of about one year was estimated (WMO, 2010). Only a relatively small part of the tropospheric chloromethane is transported to the stratosphere, where it is subsequently destroyed photolytically (Studer, 2001).

Even though, chloromethane contributed about 17% of the total chlorine in the stratosphere in 2008 (WMO, 2010), the influence of chlorine from natural chloromethane on the stratospheric ozone is insignificant due to its small ozone depletion potential (e.g. 2% of the potential of anthropogenic $CFCl_3$; WMO, 2010). By far the most of the chlorine threatening ozone originates from anthropogenic chlorofluorocarbons (CFCs), which were used until the 1990' in essentially all refrigeration and air conditioning systems. A less significant source of chlorine and a very important source of bromine in the stratosphere are halons[3], frequently used as fire extinguishing agents. The chemical processes involving CFCs are described in Section 1.2.1.

[3]compounds consisting of bromine, fluorine, and carbon.

In the next section, the dynamics of the stratosphere with a focus on the processes influencing ozone distribution is described. A comprehensive picture of the formation of the ozone hole and differences between the ozone loss over the Antarctic and the Arctic are given in Section 1.2.

1.1.2 Dynamics of the stratosphere

The largest production of ozone in the stratosphere takes place near the Equator, where the energetic short-wave sun radiation necessary for oxygen photolysis (R1) is most intense. From here ozone is transported poleward and downward by the so called Brewer-Dobson (B-D) circulation as shown in Figure 1.2. In the high latitude regions ozone can accumulate on the time scale of seasons. Transport due to the B-D circulation is the strongest during the winter and spring resulting in the extra-tropical lower stratosphere during that period (shown in Figure 1.2 with a black dashed line).

The maximum ozone mixing ratio occurs in the tropics in the altitude range between $\sim 30 - 40$km (cf. Fig. 1.1). The total ozone over the tropics (Fig. 1.1 and Fig. 1.3) shows however very low values due to low ozone mixing ratios in the atmospheric layers below and above the maximal mixing ratio region. In the tropics ozone has a short life time resulting from the photochemical equilibrium between the production and destruction processes. For this reason, the tropical upper-stratosphere cannot be a source of the extratropical stratospheric ozone. In the lower stratosphere ($20 - 25$ km), the photochemical life time is several months and longer, what enables the transport of ozone to other regions of the Earth's atmosphere. Variations in the ozone concentrations in this region control changes in total column ozone abundance (Müller, 2010).

The difference in the total column of ozone over the poles shown in Figure 1.3 is connected with the asymmetry in the Brewer-Dobson circulation. The topography of the Earth differs strongly when comparing the hemispheres. This influences the planetary waves activity (orange wiggly arrows in the Fig. 1.2), which regulates the circulation speed. The circulation is stronger during the northern hemispheric winter than during southern hemispheric winter resulting in larger extra-tropical total ozone columns in the northern hemisphere than in the southern hemisphere.

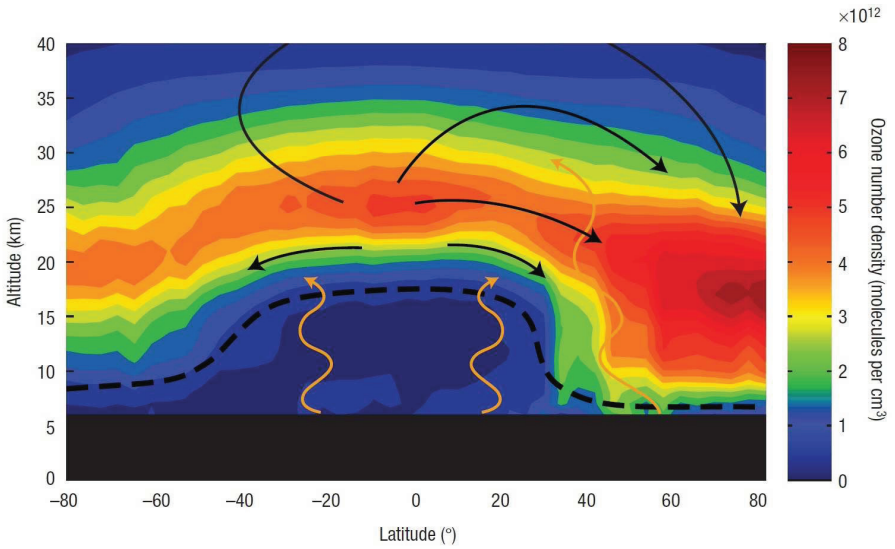

Figure 1.2: Brewer-Dobson circulation and stratospheric ozone. The black arrows show schematically the Brewer-Dobson circulation. The ozone distribution as measured by the OSIRIS satellite instrument in March 2004 is represented by colour scale. The circulation is forced by waves propagating up from the troposphere (orange wiggly arrows), especially in the winter hemisphere, and it strongly shapes the distribution of ozone by transporting it from its source region in the tropical stratosphere to the high-latitude lower stratosphere. The dashed line represents the tropopause, or the boundary between the troposphere and stratosphere. The Figure is adopted from Shaw and Shepherd (2008).

The planetary waves activity contributes also to the breakdown of the northern and southern polar vortex. The vortex is a planetary-scale cyclonic circulation, centred in the polar winter regions. During the winter, the very cold air over Antarctic and Arctic is surrounded by warmer air at lower latitudes. This creates a low pressure region with strong winds blowing around the region at the boundary between warm and cold air. The rotating air, a strong polar vortex, isolates the stratosphere above the poles from the rest of the stratosphere. The vortex is most powerful in the hemisphere's winter, when the temperature gradient is steepest, and disappears in summer. Temperatures in the vortex can reach below 195 K in the lower stratosphere. These low temperatures allow the formation of polar stratospheric clouds, which are an important feature for ozone depletion (see Section 1.2.2).

Due to the differences in planetary waves activity in the hemispheres, the Arctic polar

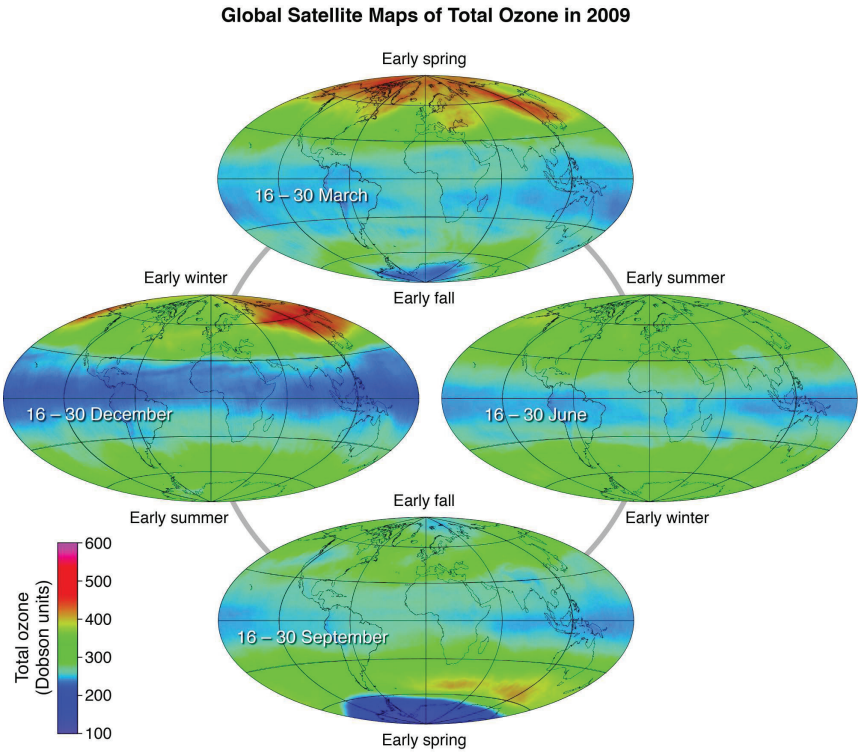

Figure 1.3: Total ozone in 2009. The seasonal, zonal and meridional variations are demonstrated with two-week averages of total ozone in 2009 asmeasured with the Ozone Monitoring Instrument (OMI) placed on NASA's Aura satellite. Figure taken from WMO 2010.

vortex is smaller and less persistent than the Antarctic polar vortex. In Section 1.2.4 the ozone losses over the Antarctic and the Arctic are presented separately.

The polar vortex breaks down in spring, when the solar radiation is again available, the temperatures of the vortex air rise and its segments drift equatorward. The final warming usually occurs in early spring in the northern hemisphere, but it can be very late in the season in the southern hemisphere.

1.2 Anthropogenic perturbations to stratospheric ozone

The idea, that the ozone layer can be threatened by anthropogenically produced gases was formulated first in late fifties of the last century. At that point, the impact of nuclear weapons on the ozone layer was discussed (a review of the history of ozone research is given by Müller, 2009). In the seventies the influence of supersonic transport was investigated (Crutzen, 1971; Johnston, 1971). The research programmes greatly improved the knowledge of ozone chemistry and indicated halogens as very important factor in the ozone loss.

In 1974 Stolarski and Cicerone presented the catalytic chlorine cycle (R5-R6, X = Cl). In the same year Molina and Rowland proposed anthropogenic $CFCl_3$ (CFC-11) and CF_2Cl_2 (CFC-12) as possible sources of chlorine in the stratosphere and concluded *'It seems quite clear that the atmosphere has only a finite capacity for absorbing Cl atoms produced in the stratosphere, and that important consequences may result. (...) More accurate estimates of this absorptive capacity need to be made in the immediate future in order to ascertain the levels of possible onset of environmental problems'*. Early model studies on the stratospheric chemistry (Crutzen, 1974; Rowland and Molina, 1975) confirmed the importance of chlorine and predicted that enhanced levels of chlorine in the stratosphere would lead to a depletion of upper stratospheric ozone via the catalytic chlorine cycle. In their article, Stolarski and Cicerone indicated also that *'nothing is known of possible heterogeneous reactions of Cl atoms with particulate matter in the stratosphere'* pointing out another field of stratospheric chemistry, that had to be studied: the heterogeneous chemistry. One year later, Cadle et al. presented studies, in which they considered influence of heterogeneous reactions in the stratosphere on ozone loss. The importance of this theory was not acknowledged until 1986, when Solomon et al. suggested, that the heterogeneous reaction $HCl + ClONO_2$ leads to liberation of Cl_2 from the stable reservoir gases and hence enhancement of the chlorine ability to destroy ozone. The knowledge gathered in the studies presented in this paragraph enabled the understanding of the massive ozone depletion in the late winter/early spring in polar regions described for the first time in 1985 by Farman et al..

Farman et al. reported that in the Antarctic spring strongly reduced total column ozone

above the British Antarctic Survey research station at Halley. They suggested also the possible relationship between ozone loss and the rise in the tropospheric CFCs mixing ratios. The plot from the original Farman et al. publication illustrating the O_3 and CFCs data sets is shown in Figure 1.4.

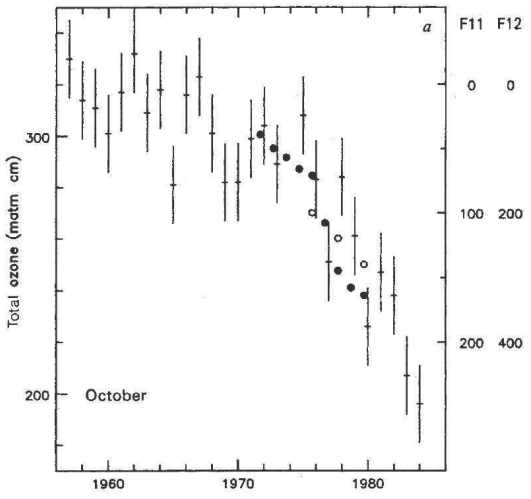

Figure 1.4: Ozone loss measured by Farman et al. (1985) at Halley Bay and Southern Hemisphere mixing ratios of CFC-11 (F11) CFC-12 (F12). The full circles correspond to CFC-11, the unfilled circles show the CFC-12 mixing ratios. Both data sets are given in parts per trillion per volume (ppt). Note that the CFC-11 and CFC-12 decrease up the figure.

The discovery by Farman et al., which was based on a series of measurements by classical Dobson instruments was soon confirmed by satellite measurements showing that the ozone depletion extended over roughly the entire Antarctic continent (Stolarski et al., 1986). These findings reinforced the studies on the stratospheric ozone and led to the first international agreement to be signed, the Montreal Protocol (1987), regulating the use of CFCs and halons.

In the next three Sections, the stratospheric chemistry of chlorine coming from anthropogenic source gases and the ozone depletion processes in the polar region are described. Sections 1.2.4 and 1.2.5 give an overview of the differences in the ozone loss on the southern and northern hemisphere.

1.2.1 Chlorine in the stratosphere

83% of stratospheric chlorine comes from human-made source gases (WMO, 2010):

- chlorofluorocarbons (CFCs): CF_2Cl_2 (CFC-12), $CFCl_2$ (CFC-11), $CFCl_2CF_2Cl$ (CFC-113)
- hydrochlorofluorocarbons (HCFCs): e.g. HCF_2Cl (HCFC-22)
- carbon tetrachloride CCl_4
- methyl chloroform CH_3CCl_3
- halons: e.g. $CBrClF_2$ (Halon-1211) and
- other gases.

These gases are stable in the troposphere and are photolysed by UV solar radiation available in the stratosphere:

$$CFCl_3 + h\nu \rightarrow CFCl_2 + Cl \qquad \text{R7}$$

$$CF_2Cl_2 + h\nu \rightarrow CF_2Cl + Cl \qquad \text{R8}$$

The highly reactive chlorine atoms released in this way react with methane, ozone or other species and form so-called reservoir gases, the most important being HCl and $ClONO_2$:

$$Cl + CH_4 \rightarrow HCl \qquad \text{R9}$$

$$Cl + O_3 \rightarrow ClO + O_2 \qquad \text{R10}$$

$$ClO + NO_2 \rightarrow ClONO_2 \qquad \text{R11}$$

Chlorine trapped in those species can not react with ozone. The ozone depletion can start after 'activation' of the Cl atoms, i.e. when Cl is liberated from the reservoir species. The activation is normally done by photolysis, hence in the winter hemisphere, under lack of solar radiation, the reservoir gases can be slowly removed from the stratosphere. In 'normal' stratospheric gas phase chemistry, only slight ozone depletion is therefore expected. However, the reservoir species are transported down into the lower stratosphere in the winter

as a result of the Brewer-Dobson circulation pattern (cf. Section 1.1.2). Here they can be activated by heterogeneous reaction on the surfaces of polar stratospheric clouds (PSCs) and cold aerosol particles (cf. Section 1.2.2). Also bromine reservoir species such as $BrONO_2$ can be activated by heterogeneous reactions.

Atmospheric concentrations of CFCs and halons continued to increase until the past ten years when the rise first slowed down and was then reversed (WMO, 2010). Today, although production of practically all such substances has ceased because of the provisions of the Montreal Protocol and its amendments and adjustments, halogen source gases are still present in existing fire extinguishing equipment, chemical stockpiles, foams etc., so that emissions continue.

In the next section, the heterogeneous chemistry as a necessary factor for the massive ozone loss in the polar regions in winter-spring period is introduced. In Section 1.2.3, the last step of the polar ozone depletion, the ClO dimer and ClO-BrO cycles, is described. Sections 1.2.4 and 1.2.5 summarize the processes and give an overlook of the ozone loss over the southern and northern poles.

1.2.2 Heterogeneous chemistry

The activation of chlorine tied in the reservoir gases HCl and $ClONO_2$ occurs by photolysis or by heterogeneous reactions. In the polar regions in winter, solar radiation is not available, so the liberation of the Cl_2 is possible only in reactions on surfaces of liquid or solid polar stratospheric clouds (PSCs) or binary H_2SO_4/H_2O aerosols.

The main compound of PSCs is nitric acid (HNO_3), for which the most important chemical source in the stratosphere is the three-body gas-phase reaction between OH and NO_2. In midwinter, the downward flux of mesospheric air results in enhanced abundances of NO_x in the polar stratosphere. These conditions lead to the formation of nitric acid through a height-dependent combination of water-ion cluster chemistry and heterogeneous conversion on sulphate aerosols involving the night-time odd nitrogen reservoir N_2O_5 (Urban et al., 2009).

The sulphuric acid (H_2SO_4) comes from carbonyl sulphide (COS) and sulphur dioxide (SO_2) carried into the stratosphere via tropical lifting by the Brewer-Dobson circulation,

or by direct injection into the stratosphere from volcanic eruptions. The largest sources of COS are the oceans (Kettle et al., 2002), whereas SO_2 is a product of burning of sulphur or of burning of materials that contain sulphur.

Water in the stratosphere comes mostly from evaporation of moisture at the Earth's surface that enters the stratosphere in the tropics and is further distributed by the Brewer-Dobson circulation. The stratospheric water vapour results also from methane oxidation in the upper stratosphere coupled with subsequent downward transport (Rosenlof, 2003).

When the temperature in the stratospheric polar vortex drops below 195 K, HNO_3, H_2SO_4 and water condense to form cold binary aerosol and Type I Polar Stratospheric Clouds. The structure and composition of the Type I PSC have been the topic of extensive research over the last few years. It is believed that Type I PSCs are composed of a supercooled liquid ternary solution of nitric acid, sulfuric acid, and water ice, as well as frozen nitric acid trihydrates (NAT). At temperatures below 188 K, H_2O molecules condense to form ice crystals building Type II Polar Stratospheric Clouds. Type II particles are large enough (10 microns in diameter) to fall out of the stratosphere at about 1.5 kilometers per day, causing dehydration (removal of HO_x) of the stratosphere. Type I cloud particles are about 1 micron in diameter and remain longer in the stratosphere. Their sedimentation time is approximately 10 meters per day. However, solid PSC built out of NAT particles can grow to larger sizes (20 – 40 microns in diameter, so called 'NAT rocks') than liquid PSC particles and finally sediment to the lower altitudes leading to a denitrification of the stratosphere. The sedimentation of large HNO_3 containing particles leads to an irreversible removal of nitrogen and thus limits the chlorine deactivation (R11) in springtime allowing the ozone-destroying catalytic cycle to last longer (Khosrawi et al., 2011).

Because the Antarctic stratosphere is much colder than the Arctic stratosphere, polar stratospheric clouds are more abundant in the Antarctic. They form early in the winter, and persist into the spring, enabling the ozone hole to build. Cold binary aerosol can exist at temperatures near 195 K and is an important contributor to chlorine chemistry and polar ozone loss specially in the Arctic, where the PSCs are not so frequent (Drdla and Müller, 2010).

PSCs and aerosols provide surfaces for heterogeneous chemical reactions, which lead to increased ozone depletion. After the reactant species make contact with the particles by kinetic motion, the reactants are absorbed onto the surface of the particle by either physical or chemical bonding, where they diffuse into the body of the particle or remain on the surface. When the reactants meet on (or in) the particle, different products can form. These products will then diffuse into the particle, remain on the surface, or be desorbed (emitted) from the particle. Since the studies of Solomon et al. (1986) heterogeneous reactions are one of the main research topics in stratospheric chemistry, as they are very important factor behind the Antarctic ozone hole phenomenon. The importance of these reactions results from the liberation of chlorine from relatively benign chlorine forms into highly reactive forms (Cl_2):

$$ClONO_2 + HCl \rightarrow Cl_2 + HNO_3 \qquad \text{R12}$$

$$ClONO_2 + H_2O \rightarrow HOCl + HNO_3 \qquad \text{R13}$$

$$N_2O_5 + HCl \rightarrow ClONO_2 + HNO_3 \qquad \text{R14}$$

$$N_2O_5 + H_2O \rightarrow 2 \times HNO_3 \qquad \text{R15}$$

$$HOCl + HCl \rightarrow Cl_2 + H_2O \qquad \text{R16}$$

HNO_3 remains on PSC/aerosol and is slowly removed from the stratosphere by sedimentation, whereas Cl_2 is released and its concentration rises through the polar winter. When solar radiation is again available in late winter and spring, Cl_2 is photolysed:

$$Cl_2 + h\nu \rightarrow 2 \times Cl. \qquad \text{R17}$$

Like singlet oxygen, the chlorine radical is highly reactive. It combines spontaneously with a molecule of ozone and has enough energy to split it. One oxygen atom from the ozone molecule combines with the chlorine radical to form chlorine monoxide, ClO, leaving the

other two atoms as molecular oxygen, O_2. The denitrification due to sedimentation of HNO_3 hinders deactivation of chlorine (R11) and hence increases the ozone depleting potential of $ClO_x (\approx ClO + 2ClOOCl)$. The ClO_x chemistry leading to polar ozone loss is described in the following section.

1.2.3 Stratospheric ClO/ClOOCl chemistry

Once chlorine is activated on PSCs (Solomon et al., 1986) or background aerosol (Drdla and Müller, 2010) in the polar stratosphere and sunlight is available, photochemical ozone loss occurs essentially via two catalytic cycles: the ClO dimer cycle (Molina and Molina, 1987), where ClOOCl is the dimer:

$$ClO + ClO + M \underset{k_{diss}}{\overset{k_{rec}}{\rightleftharpoons}} ClOOCl + M \qquad \text{R18}$$

$$ClOOCl + h\nu \xrightarrow{J_{ClOOCl}} Cl + ClOO \qquad \text{R19}$$

$$ClOO + M \rightarrow Cl + O_2 + M \qquad \text{R20}$$

$$2 \times (Cl + O_3 \rightarrow ClO + O_2) \qquad \text{R21}$$

$$2O_3 + h\nu \rightarrow 3O_2$$

and the ClO-BrO cycle (McElroy et al., 1986):

$$BrO + ClO \rightarrow Br + Cl + O_2 \qquad \text{R22}$$

$$Br + O_3 \rightarrow BrO + O_2 \qquad \text{R23}$$

$$Cl + O_3 \rightarrow ClO + O_2 \qquad \text{R21}$$

$$2O_3 + h\nu \rightarrow 3O_2$$

The cycles are connected by ClO, which concentration influences the rate of the ClO-BrO cycle and of the ClO dimer cycle. Figure 1.5 illustrates the two cycles schematically.

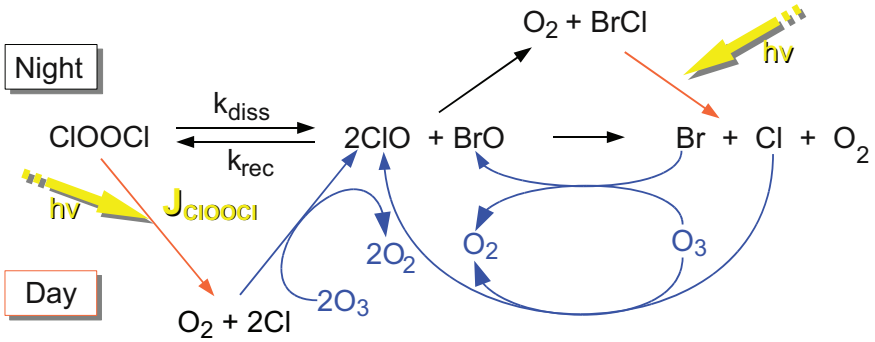

Figure 1.5: Polar ozone destruction cycles. On the left hand side the ClO dimer cycle is sketched, on the right hand side the ClO-BrO cycle. Black arrows indicate reactions taking place without sun radiation, photolysis and ozone depletion reactions are marked with respectively orange and blue colour. k_{rec}, k_{diss} and J_{ClOOCl} correspond to recombination constant of ClO, dissociation constant and photolysis rate of ClOOCl.

In the stratosphere, chlorine is approximately 150 times more abundant than bromine. Nonetheless, the ClO-BrO cycle is important as bromine atoms are about 60 times more efficient than chlorine atoms in destroying ozone (WMO, 2010). Outside of the polar regions, both cycles are of only minor importance due to low concentration of ClO. The ClO dimer cycle is negligible also because it is only effective at the low temperatures in polar winter and spring (ClOOCl is thermally unstable at typical stratospheric temperatures). Furthermore, outside of the polar regions, denitrification does not occur and ClO can be trapped in $ClONO_2$ reservoir.

To maintain a large ClO abundance through the photolysis of ClOOCl, sunlight is necessary. However, in contrast to the short-wave UV radiation (wavelengths less than 242 nm) required to produce atomic oxygen and hence to produce ozone, the photolysis of ClOOCl

proceeds at rather long UV wavelengths. The radiation between 200 and 450 nm needed for photolysis of ClOOCl prevails under conditions of low sun at the poles, hence ClOOCl is photolysed already in spring before the ozone production can be started. Therefore the two presented cycles account for the majority of the ozone loss observed in late winter-spring in the polar stratosphere (WMO, 2010). Despite a great number of studies on the cycles, the kinetic parameters of the reactions constituting ClO dimer cycle still remain a matter of scientific debate, so that it cannot be claimed that a full quantitative understanding of polar ozone loss has been reached. In Section 2 the parameters and their influence on the cycle are introduced.

The processes introduced in this chapter lead to massive ozone depletion over the Antarctic and Arctic. However, due to differences in the topography of the southern and northern hemisphere, the ozone loss is significantly greater over the Antarctic. The following sections describe and compare the ozone losses over the two polar regions.

1.2.4 Antarctic: Ozone hole

The ozone hole as a term describing the phenomenon of low total ozone values in the Antarctic spring was first used by Stolarski et al. (1986): *'The deep minimum, or hole...'*. The ozone hole is typically defined as the geographical region contained within the 220-Dobson unit contour in total ozone maps. The maximum of such area reaches 25 millions square kilometres, which is nearly twice the area of Antarctic. Minimum values of total ozone averaged in late September/mid October period over Antarctic are near 100 DU, where normal values for southern polar spring are equal approximately 350 DU (WMO, 2010). The maximal ozone loss over Antarctic occurs at 70 hPa (~18 km) and reaches frequently more than 90% and ozone mixing ratios of less than 0.1 ppm. Figure 1.6 shows an overview of the total ozone over Antarctic in October during the last 40 years.

1.2.5 Arctic: Ozone loss

The Arctic winter stratosphere is in three aspects similar to the Antarctic counterpart. In both cases a cold polar vortex is separated from midlatitude air masses, the strong adiabatic descent in winter transports air from upper stratosphere and partly from the mesosphere to

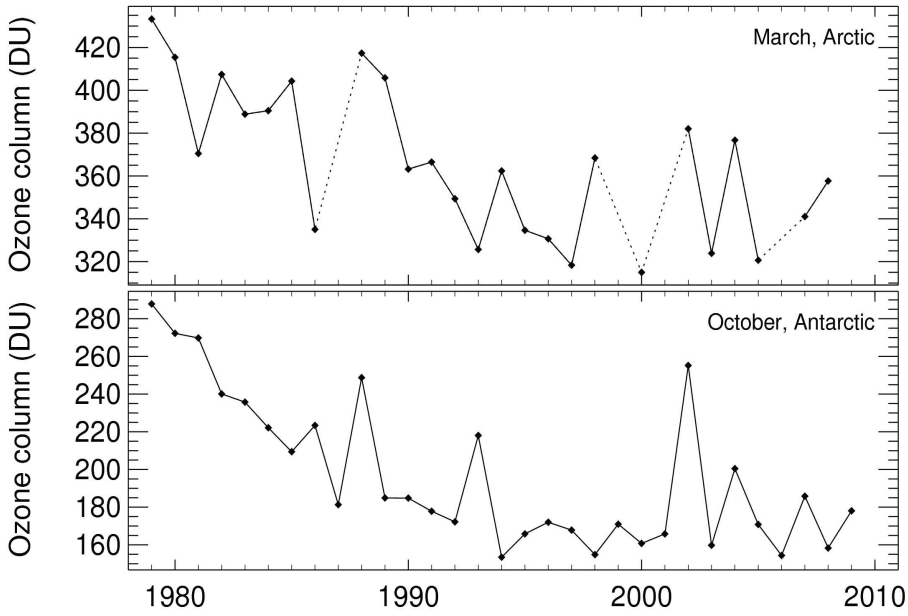

Figure 1.6: Time series of minimum of daily average column ozone poleward 63° equivalent latitude for March in the Arctic (upper panel) and October in the Antarctic (lower panel). Winters in which the vortex broke up before March (1987, 1999, 2001, and 2009) are plotted with dashed lines. Data were taken from version 2.7 of the NIWA (National Institute of Water and Atmospheric Research) combined ozone database. Figure adapted from Müller et al. (2008).

the lower stratosphere and the isolated air is rich with the reactive halogen gases. However, due to the more extensive topography of the northern polar regions, the Arctic polar vortex is warmer and much more variable than the Antarctic vortex (cf. Section 1.1.2). It results in a stronger interannual variability in both chemical loss of ozone and in dynamical supply of ozone-rich air to high latitudes. Therefore, the total ozone in the polar spring in Arctic are approximately 200 DU larger than in Antarctic, as shown in Fig. 1.6. Nonetheless, in particularly cold winters and in winters with an enhanced burden of volcanic aerosol, substantial chemical loss of ozone has been observed in the Arctic and has led to Arctic column ozone losses of up to 40% (winter 2010/2011). In typical, dynamically active warm winters, the estimated chemical ozone loss is rather small.

2 The ClO dimer cycle

The ClO dimer cycle starts with formation of ClOOCl by recombination of two ClO molecules:

$$\mathrm{ClO} + \mathrm{ClO} + \mathrm{M} \underset{k_{\mathrm{diss}}}{\overset{k_{\mathrm{rec}}}{\rightleftharpoons}} \mathrm{ClOOCl} + \mathrm{M} \qquad \text{R18}$$

The formation reaction is favoured by low temperature, high pressure (more collision partners M) and high abundance of ClO. The reverse reaction, dissociation of ClOOCl also benefits from high pressure, but is slowed by low temperatures. In darkness, without available solar radiation, the recombination rate and the dissociation rate govern the relation between ClO and ClOOCl concentrations. The change in concentration of ClO ([ClO]) can then be calculated with the formula:

$$0.5\frac{\mathrm{d[ClO]}}{\mathrm{dt}} = k_{\mathrm{diss}}[\mathrm{M}][\mathrm{ClOOCl}] - k_{\mathrm{rec}}[\mathrm{M}][\mathrm{ClO}]^2 \qquad (2.1)$$

When the thermal equilibrium is established, the concentration of ClO does not change and

$$\frac{\mathrm{d[ClO]}}{\mathrm{dt}} = 0 \qquad (2.2)$$

The situation changes under sunlit conditions, when the short-wave solar radiation reaches the polar stratosphere and ClOOCl, sensitive to wavelengths between 200 – 450 nm gets photolysed:

$$\mathrm{ClOOCl} + h\nu \xrightarrow{J_{\mathrm{ClOOCl}}} \mathrm{Cl} + \mathrm{ClOO} \qquad \text{R19}$$

$$\mathrm{ClOO} + \mathrm{M} \rightarrow \mathrm{Cl} + \mathrm{O_2} + \mathrm{M} \qquad \text{R20}$$

The Cl atoms react with ozone creating new ClO molecules (R21), which restart the ClO

dimer or the ClO-BrO cycle. Photolysis provides a new element in Equation 2.1:

$$0.5\frac{\mathrm{d[ClO]}}{\mathrm{dt}} = k_{\mathrm{diss}}[\mathrm{M}][\mathrm{ClOOCl}] - k_{\mathrm{rec}}[\mathrm{M}][\mathrm{ClO}]^2 + J_{\mathrm{ClOOCl}}[\mathrm{ClOOCl}] \tag{2.3}$$

and results in an additional production term. That makes the photolysis rate of ClOOCl an extremely important parameter for both polar catalytic cycles. It is the rate-limiting step in the ClO dimer cycle under twilight conditions, and also has a major influence on the rate of the ClO-BrO cycle by governing the amount of active chlorine present as ClO.

The kinetic parameters controlling the night-time and day-time ClO dimer cycle are described in the following sections. For each of these parameters, large discrepancies exist that often cannot be explained by the reported uncertainty limits of laboratory measurements. Moreover, studies testing the consistency with atmospheric observations have shown that some of the constants determined in the laboratory cannot be reconciled with atmospheric ClO and ClOOCl measurements (Santee et al., 2003; Stimpfle et al., 2004; von Hobe, 2007; Schofield et al., 2008; Kremser et al., 2011).

2.1 Recombination and dissociation constants

The self reaction of ClO molecules is a reaction of the $\mathrm{A+B \leftrightarrow [AB]^* \xrightarrow{M} AB}$ type ($[\mathrm{AB}]^*$ denotes transition state) and is pressure and temperature dependent. The low-pressure-limiting rate constants are given by NASA Jet Propulsion Laboratory (JPL) recommendation in the form:

$$k_{\mathrm{rec},0} = \mathrm{k}_0^{300}\left(\frac{\mathrm{T}}{300}\right)^{-\mathrm{n}} \mathrm{cm^6 molecule^{-2} s^{-1}} \tag{2.4}$$

(where k_0^{300} is adjusted for air as the third body at temperature equal 300 K). The high-pressure-limiting rate constant is given in a similar form:

$$k_{\mathrm{rec},\infty} = \mathrm{k}_\infty^{300}\left(\frac{\mathrm{T}}{300}\right)^{-\mathrm{m}} \mathrm{cm^3 molecule^{-1} s^{-1}} \tag{2.5}$$

Troe (1977a,b, 1979) has developed a theoretical description of the 'falloff' of termolecular reactions between $k_{\mathrm{rec},0}$ and $k_{\mathrm{rec},\infty}$ limits for given temperature and pressure:

$$k_{\mathrm{rec}}([\mathrm{M}],\mathrm{T}) = \left(\frac{k_{\mathrm{rec},0}[\mathrm{M}]}{1+\frac{k_{\mathrm{rec},0}[\mathrm{M}]}{k_{\mathrm{rec},\infty}}}\right) \times 0.6^{\left\{1+\left[\log_{10}\left(\frac{k_{\mathrm{rec},0}[\mathrm{M}]}{k_{\mathrm{rec},\infty}}\right)\right]\right\}^{-1}} \tag{2.6}$$

The first term is the Lindemann-Hinshelwood factor, which establishes the basic shape of the falloff from $k_{\mathrm{rec},0}$ to $k_{\mathrm{rec},\infty}$. The second term has the effect of broadening the falloff region.

Direct studies of Reaction R18 started first after development of the flash photolysis technique and the subsequent identification of the ultraviolet absorption spectrum of ClO. Since these early studies, rate coefficients for Reaction R18 have been measured using several kinetic techniques such as flash photolysis-ultraviolet absorption, discharge flow-ultraviolet absorption, discharge flow-mass spectrometry, and molecular modulation-ultraviolet absorption and have been obtained by Basco and Hunt (1979), Hayman et al. (1986), Sander et al. (1989), Trolier et al. (1990), Nickolaisen et al. (1994), Bloss et al. (2001) and Boakes et al. (2005). The constants $k_{\mathrm{rec},0}$ and $k_{\mathrm{rec},\infty}$ resulting from these studies are presented in Fig. 2.1 and Fig. 2.2 respectively.

First investigations of the termolecular process of Reaction R18 were made by Basco and Hunt (1979). They estimated $k_{\mathrm{rec},0}$ at 298 K and noticed that the coefficient of Reaction R18 increases with decreasing temperature. Hayman et al. (1986) investigated the kinetics of Reaction R18 between 268 and 338 K in a molecular modulation experiment, monitoring ClO via absorption spectroscopy at 277.3 nm and derived rate constant with N_2 used as the third body. The obtained constant is equated to $k_{\mathrm{rec},0}$, the low-pressure limit for recombination constant and is significantly higher than the values estimated in other measurements. Sander et al. (1989) employed broadband flash photolysis with UV absorption spectroscopy and measured k_{rec} for temperatures between 195 – 247 K, reporting rate coefficients for Reaction R18 in nitrogen, oxygen and argon. These values were considerably smaller than those reported by Hayman et al. Trolier et al. (1990) also used the technique of flash photolysis/UV absorption, monitoring ClO principally through a single wavelength detection at the peak at 282.65 nm, together with a limited number of measurements performed using a diode array detection system to monitor the ClO spectrum between approximately 225 and 300 nm. The measurements were performed between 200 and 298 K. They found also that the falloff curves obtained from fitting Eq. 2.6 to their kinetic data could not be computed, because the measurements of k_{rec} were consistently higher than the fitted curves at low gas

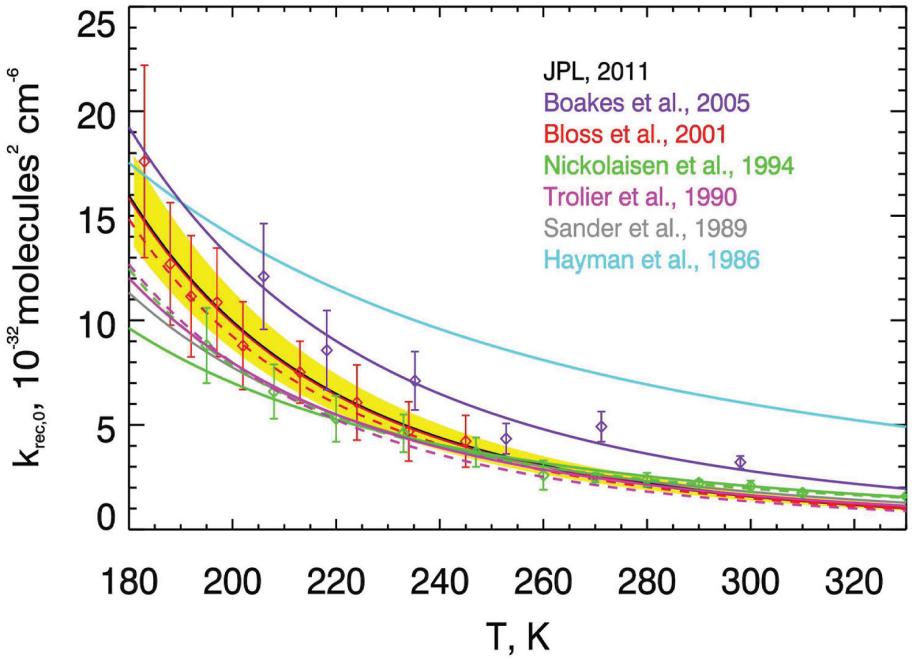

Figure 2.1: Temperature dependence of various $k_{rec,0}$ measurements. For Trolier et al. (1990), the first set of $k_{rec,0}$ values (solid line) gives the data obtained excluding the x-intercept from their analysis, in the second set (dashed line) the x-intercept was included in the falloff fits. In case of Nickolaisen et al. (1994), the solid line represents the treatment from Equation 2.4 with $(\frac{T}{300})^n$, whereas the dashed line the Eq. 2.4 with $e^{-E/T}$. The dashed line of Bloss et al. (2001) represents data corrected to air, the solid line the data corrected to nitrogen. For Boakes et al. (2005), the two points at each temperature corresponds to results with and without incorporating an intercept in the falloff curves. The yellow area corresponds to uncertainty of JPL 2011 (Sander et al., 2011) recommendation.

pressure. As a result, they analysed the data a second time with an arbitrary x-intercept added to Eq. 2.6. In 1994, Nickolaisen et al. obtained $k_{rec,0}$ with He, O_2, Ar, N_2, CF_4, SF_6 and Cl_2 as the third body and indicated, that measured large value of $k_{rec,0}$ for [M]=Cl_2 is due to a mechanism in which a ClO-Cl_2 intermediate catalyses the formation of ClOOCl. This effect is assumed to be responsible for the nonzero intercept observed by Trolier et al. Bloss et al. (2001) measured k_{rec} in nitrogen and air over the range of conditions relevant to the polar stratosphere, the results showed good agreement with the previous studies at the higher temperatures (T>200 K), but at lower temperatures the rate was obtained to be

higher than extrapolation of the previous results. Boakes et al. (2005) studied Reaction R18 over the temperature range 206 – 298 K and the pressure range 1 – 1000 hPa in nitrogen bath gas. Similarly to studies of Trolier et al. (1990), in their results an intercept was observed in falloff curves obtained at low temperatures, but they suggest disregarding their data at less than 130 hPa. $k_{\mathrm{rec},0}$ values published by Boakes et al. (2005) are significantly larger than the previous studies' results suggesting rapid ClO dimerisation.

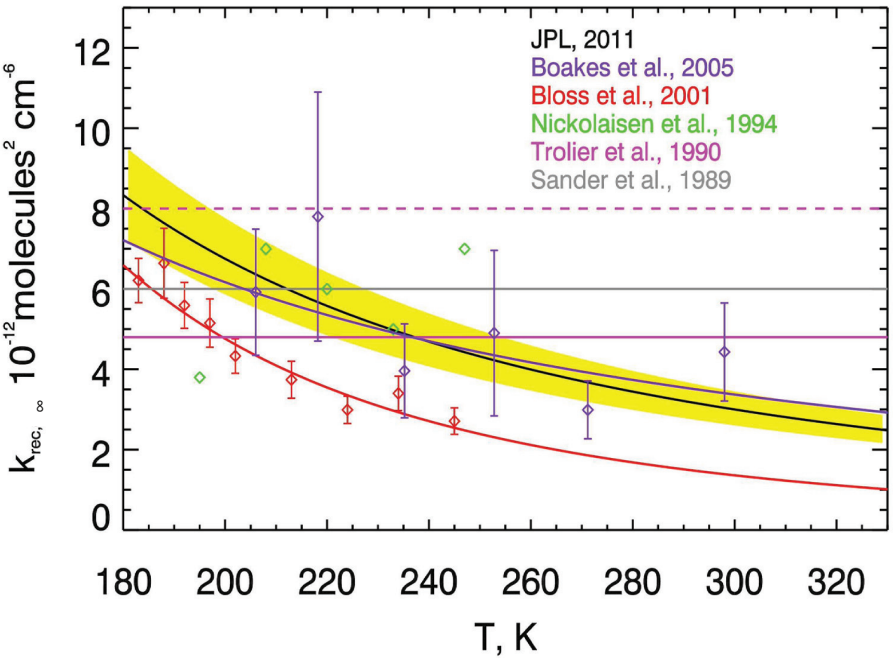

Figure 2.2: Temperature dependence of various $k_{\mathrm{rec},\infty}$ measurements. For Trolier et al. (1990), similarly as in Fig. 2.1, the two lines correspond to the data obtained with excluding (solid line) or including (dashed line) of the intercept in the analysis. JPL 2011 $k_{\mathrm{rec},\infty}$ uncertainty is shown with yellow colour.

The JPL 2011 (Sander et al., 2011) recommendation for $k_{\mathrm{rec},0}$ plotted in Fig. 2.1 is based on a fit to data from Sander et al. (1989) as quoted by Nickolaisen et al. (1994) (260 – 390 K), Bloss et al. (2001) (183 – 245 K), Trolier et al. (1990) (200 – 263 K) and Boakes et al. (2005), whereas the Trolier et al. (1990) data have been corrected for values at the zero pressure intercept as suggested by Trolier et al.. With this adjustment all the data except the Hayman

et al. (1986) and Boakes et al. (2005) values are in reasonable agreement. The recommended values for $k_{\mathrm{rec},0} = 1.6 \times 10^{-32}(\mathrm{T}/300)^{-4.5}$ and fits very well to the results of Bloss et al. (2001) for measurements in nitrogen. $k_{\mathrm{rec},\infty}$ equals $3.0 \times 10^{-12}(\mathrm{T}/300)^{-2}$ (Fig. 2.2) and provides the best agreement with data of Boakes et al. (2005). Error limits (yellow areas in both Figures) represent an attempt to include all the data within the 95% uncertainty.

In the atmosphere, mostly the low pressure limits are observed as a result of the falloff behaviour with increasing pressure. Below 150 hPa, variation of the high pressure limit, $k_{\mathrm{rec},\infty}$, by a factor of two changes the result of k_{rec} (Eq. 2.6) by less than 10% (von Hobe, 2007). The JPL recommendation for $k_{\mathrm{rec},\infty}$ provides a good estimation at stratospheric pressure and is often used for model calculations. The values of $k_{\mathrm{rec},0}$ however is based on the data of Bloss et al. (2001), whereas the best agreement with atmospheric observations and with unimolecular theory shows $k_{\mathrm{rec},0}$ published by Nickolaisen et al., as shown by von Hobe (2007). Therefore, further measurements are necessary to determine the correct values.

The dissociation constant, k_{diss}, indicates the strength of binding between two ClO molecules in terms of how easy it is to separate the complex ClOOCl. Thermal decomposition rate constants of ClOOCl have been deduced mostly from the thermal equilibrium relation $k_{\mathrm{rec}}/k_{\mathrm{diss}} = [\mathrm{ClOOCl}]/[\mathrm{ClO}]^2$. Direct determinations were made by Nickolaisen et al. (1994) and Bröske and Zabel (2006). Nickolaisen et al. (1994) obtained $k_{\mathrm{diss},0}$ from fitting the observed decay of ClO in the temperature range between 260 and 310 K to an overall reaction mechanism. Bröske and Zabel (2006) observed the thermal first-order decay rate of ClOOCl in the temperature range 242 – 261 K at total pressure between 2 and 480 mbar. The decay was then used to determine the $k_{\mathrm{diss},0}$. Neither of the studies extended to stratospheric temperatures, but the data derived by Bröske and Zabel (2006) are easier to interpret and the method used is less sensitive to undesirable ClOOCl loss processes than the method adopted by Nickolaisen et al. (von Hobe, 2007). Comparison with the calculation using the unimolecular rate theory (Troe, 1977a,b, 1979; Patrick and Golden, 1983) shows similar results with $k_{\mathrm{diss},0}$ published by Bröske and Zabel (2006). Von Hobe (2007) combined the theory calculations and the measurements of Bröske and Zabel and proposed the following dissociation con-

stant rate for the stratospheric temperatures:

$$k_{\mathrm{diss},0} = 1.66 \times 10^{-6} \mathrm{e}^{-7821/\mathrm{T}} \tag{2.7}$$

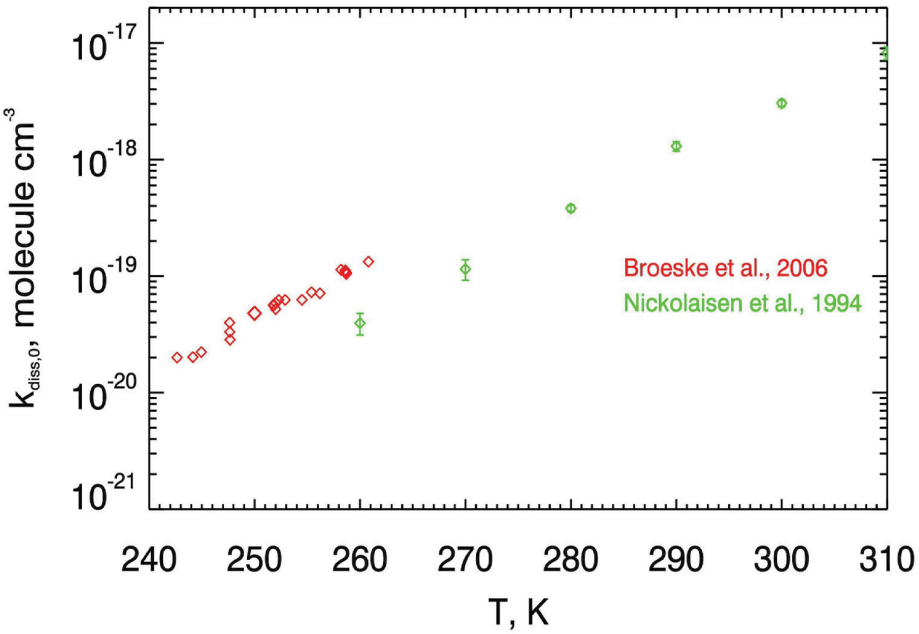

Figure 2.3: Temperature dependence of various $k_{\mathrm{diss},0}$ measurements.

There are no reliable measurement of $k_{\mathrm{diss},\infty}$ and therefore this parameter is calculated from $k_{\mathrm{rec},\infty}$ through relation with equilibrium constant K_{eq}, which is described in the following section.

2.2 Equilibrium constant

The forward and backward reactions (R18) of the ClO dimer cycle i.e. the ClO recombination and the ClO dimer (ClOOCl) thermal dissociation, govern the partitioning between ClO and ClOOCl in darkness with a thermal equilibrium constant

$$K_{\mathrm{eq}} = \frac{k_{\mathrm{rec}}}{k_{\mathrm{diss}}} = \frac{[\mathrm{ClOOCl}]}{[\mathrm{ClO}]^2}. \tag{2.8}$$

K_{eq} is mostly expressed in the form:

$$K_{eq} = A\,e^{(B/T)}\,\text{molecules}\,\text{cm}^{-3} \tag{2.9}$$

where A and B are related to standard reaction enthalpy $\Delta_r H^\circ$ and entropy $\Delta_r S^\circ$:

$$A = \frac{RT}{N_A} e^{\Delta_r S^\circ/R},\ B = -\Delta_r H^\circ/R \tag{2.10}$$

where N_A is the Avogadro constant and R is the universal gas constant. The factor RT/N_A converts K_{eq} into units of molecules^{-1} cm^3. The kinetic laboratory studies on $K_{eq}(T)$ are interpreted either by Third Law analysis or by Second Law analysis.

In the first case $\Delta_r S^\circ$ is calculated from standard entropies using the Third Law of thermodynamics for ClO dimerisation:

$$\Delta_r S^\circ = S^\circ(\text{ClOOCl}) - 2S^\circ(\text{ClO}) \tag{2.11}$$

and $\Delta_r H^\circ$ can then be calculated by rearranging the van't Hoff equation:

$$\Delta_r H^\circ(T) = -RT \ln K_{eq}(T) + T\Delta_r S^\circ(T) \tag{2.12}$$

$S^\circ(\text{ClO})$ and $S^\circ(\text{ClOOCl})$ are calculated as the sum of the contributions to the total molecular standard entropy from the translational, rotational, vibrational and electronic partition functions. If the entropy is known (or can be calculated from molecular properties) as a function of temperature, experimental values of $K_{eq}(T)$ can be used to extract a value for $\Delta_r H^\circ$ and $K_{eq}(T)$ can be calculated over a wide temperature range. The parameters A and B can then be determined from a linear fit.

In the Second Law analysis, $\Delta_r S^\circ$ and $\Delta_r H^\circ$ are obtained from a linear least squares fit to the observed K_{eq} values at different temperatures. The two methods provide significantly different values for the temperature dependence of equilibrium constant and the first method is mostly preferred due to entropies of ClO and ClOOCl, which can be well constrained from spectroscopic data. Available K_{eq} values from various studies are presented in Fig. 2.4.

The first measurements of K_{eq} were described by Basco and Hunt in 1979. They employed

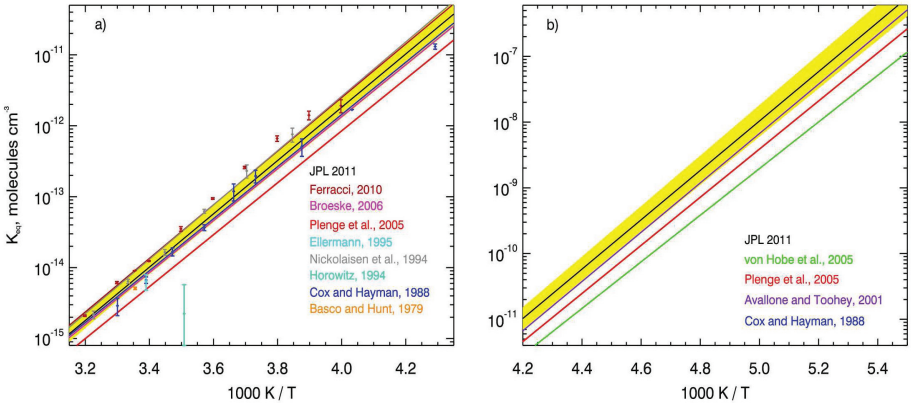

Figure 2.4: Temperature dependence of various K_{eq} measurements. In panel a, the K_{eq} estimated for laboratory temperatures are plotted, in panel b the values valid for stratospheric conditions are shown. The yellow area represents the uncertainty for the JPL 2011 recommendation.

a flash-photolysis apparatus combined with UV spectroscopy to determine the UV ClOOCl spectrum and obtained $K_{eq}(298K) = 5.1 \times 10^{-15}$ cm^{3}molecule^{-1}. In 1988, Cox and Hayman employed modulated photolysis of a static gas mixture to generate ClO radicals and their dimerisation products and with UV absorption spectroscopy they monitored ClO radicals. They determined K_{eq} over the range 233 – 300 K. Horowitz et al. (1994) determined K_{eq} at 285 K. Nickolaisen et al. (1994) used flash photolysis with UV absorption spectroscopy to obtain K_{eq} over a temperature range between 260 and 310 K. In 1995, Ellermann et al. produced ClO by pulse radiolysis Cl_2O/Cl_2 mixed with different bath gases and studied kinetics by monitoring of absorption signals at 277.2 nm. Using the acquired experimental curves and computer modelling, they estimated $K_{eq}(295K) = 6.4 \times 10^{-15}$ cm^{3}molecule^{-1}.

The first derivation of K_{eq} from field measurements was made by Avallone and Toohey (2001) from in-situ aircraft experiments with resulting $K_{eq} = 1.99 \times 10^{-30} \times T \times \exp(8854/T)$. Atmospheric measurements from an airborne platform have also been used by von Hobe et al. (2005), the deduced K_{eq} parameters were $A = 3.61 \times 10^{-27}$ and $B = 8167$.

In 2005, Plenge et al. measured the bond strength of the ClO dimer (the enthalpy change of ClO dimerisation) by photoionisation mass spectrometry and based their parameterisa-

tion of K_{eq}(T) on the value of $\Delta_r H°$ from their own study and Third Law entropies $\Delta_r S°$ from statistical mechanics. Bröske and Zabel (2006) monitored ClOOCl decomposition at four temperatures between 245 and 260 K by means of UV and IR spectroscopy to determine k_{diss} over the range 243 – 261 K and calculated K_{eq} employing the at that time recommended JPL values of k_{rec}. In the most recent study, Ferracci and Rowley (2010) generated ClO radicals via laser flash photolysis of Cl_2/Cl_2O mixtures in synthetic air and monitored the radicals with UV absorption spectroscopy. The equilibrium constant was determined from the ratio of the rate constants of the forward and reverse Reaction R18 over the temperature range 256.55 – 312.65 K. They used the Second Law and Third Law thermodynamic methods to obtain the standard enthalpy and entropy changes of reaction from the estimated K_{eq}(T). The two methods provided significantly different results.

The recommended JPL 2011 values of the equilibrium constant and the thermochemical parameters are from a third-law calculation based on the data from Cox and Hayman (1988) and Nickolaisen et al. (1994). The 95% error limits were chosen to incorporate all the data points in these two studies.

2.3 Photolysis rate

At daylight, reactions R19 - R21 shift the ClO_x (= ClO + 2ClOOCl) partitioning towards the monomer and drive chemical ozone loss (R21). The ClOOCl photodissociation Reaction R19 is the rate-limiting step of the ClO dimer cycle under twilight conditions that prevail throughout most of the winter in the polar stratosphere. By governing the ClO concentration, reaction R19 also limits the rate of reaction R22 in the ClO-BrO cycle, making the ClOOCl photolysis frequency J_{ClOOCl} by far the most critical kinetic parameter for the overall ozone loss rate (von Hobe et al., 2007). The inability to tightly constrain J_{ClOOCl} is one of the key issues preventing full quantitative understanding of the ozone depletion in the winter/early spring polar atmosphere.

J_{ClOOCl} is a product of the ClOOCl photolysis cross section (plotted in Fig. 2.5a) and the actinic flux $I(\lambda)$ (Fig. 2.5b) integrated over wavelengths:

$$J_{ClOOCl} = \int \sigma_{ClOOCl}(\lambda) \cdot \phi(\lambda) \cdot I(\lambda) \cdot d\lambda \tag{2.13}$$

The photolysis cross section in the formula is given as a multiplication of absorption cross section $\sigma_{\mathrm{ClOOCl}}(\lambda)$ and the photolysis quantum yield $\phi(\lambda)$, i.e. the fraction of absorbed photons leading to photodissociation. The factors determining J_{ClOOCl} are introduced below.

2.3.1 Photolysis quantum yield

The measurements of $\phi(\lambda)$ were carried out by Cox and Hayman (1988); Molina et al. (1990); Moore et al. (1999); Plenge et al. (2005) and most recently by Huang et al. (2011). They all have shown, that excited states of ClOOCl are rapidly dissociative, what was also confirmed by theoretical studies (Birk et al., 1989; Kaledin and Morokuma, 2000; Toniolo et al., 2001; Peterson and Francisco, 2004). The determined $\phi(\lambda)$ values are usually between 0.9 and 1. In Figure 2.5a, absorption cross sections and spectra are plotted under the assumption, that the quantum yield $\phi(\lambda) \sim 1$ for the whole wavelength range, i.e. absorption and photolysis cross sections are to be equivalent.

JPL 2011 recommends treatment of photolysis and absorption cross sections as equal shifting the focus to the efficiency of direct formation of ClO via photolysis of ClOOCl, rather than absorption versus photolysis. This focus affects ozone loss but not the partitioning of ClO and ClOOCl.

2.3.2 Absorption/photolysis cross sections

Three kinds of absorption/photolysis data of ClOOCl can be distinguished:

- Photolysis cross sections, which are determined by monitoring the disappearance of ClOOCl (Chen et al., 2009; Lien et al., 2009; Jin et al., 2010) or the appearance of Cl atoms (Wilmouth et al., 2009) in photolysis experiments at discrete wavelengths.

- Absolute absorption cross sections measured by Cox and Hayman (1988), DeMore and Tschuikow-Roux (1990), Burkholder et al. (1990), Bloss et al. (2001), Papanastasiou et al. (2009) for the wavelength range relevant for ClOOCl photolysis in the stratosphere ($\lambda > 310\,\mathrm{nm}$).

- Relative absorption cross spectra as determined by Huder and DeMore (1995), von Hobe et al. (2009), Pope et al. (2007). Those laboratory studies are lacking the knowl-

edge of the amount of ClOOCl present in the absorption cell and have to be scaled to absolute cross sections or photolysis cross sections from the above mentioned studies.

The available absorption spectra, absorption cross sections and photolysis cross sections of ClOOCl from various studies are shown in Fig. 2.5 and summarised in Table 2.1.

The first study on $\sigma_{\mathrm{ClOOCl}}(\lambda)$ was published by Molina and Molina (1987). The derived UV absorption spectrum of ClOOCl was possibly affected by the presence of Cl_2O_3 and other impurities, which significantly influenced the shape of the spectrum. The spectrum is considered as incorrect and hence is not included in Fig. 2.5 and Table 2.1. In 1988, Cox and Hayman reported a UV absorption spectrum of ClOOCl with a strong and broad feature with a maximum at approximately 245 nm and a tail extending to beyond 300 nm. In 1990, Burkholder et al. used three independent ClO source reactions, generated ClOOCl in a flow tube and measured its absorption spectrum in the range between 212 and 410 nm. The results presented by Burkholder et al. (1990) generally produced the best agreement in a number of studies comparing modelled and observed ClO_x partitioning (Stimpfle et al., 2004; von Hobe, 2007; Schofield et al., 2008; Kremser et al., 2011) as well as ozone loss (Santee et al., 2003; Chipperfield et al., 2005; Frieler et al., 2006; Tripathi et al., 2006). In the same year, DeMore and Tschuikow-Roux used a static photolysis cell containing Cl_2/Cl_2O or Cl_2/O_3 mixtures or pure Cl_2O to generate ClOOCl and recorded its absolute absorption spectrum. In 1995, Huder and DeMore revisited the ClOOCl absorption spectrum with a similar static photolysis cell and considered a logarithmic extrapolation as a better estimate of the cross sections than the actual data for λ >310 nm. Bloss et al. (2001) studied the dimerisation kinetics of ClO + ClO + M reaction using the technique of flash photolysis with UV absorption spectroscopy and measured a value for σ_{ClOOCl} at 210 nm.

In 2007, Pope et al. used an innovative method to prepare ClOOCl. They condensed gaseous ClOOCl to a solid form at about 150 K and pumped out the precursor gases, then they let solid ClOOCl sublimate, and measured its spectrum. This method offers a ClOOCl sample of a high concentration and low impurities. During the measurements, significant absorption due to Cl_2, either from the co-condensed reactant or from decomposition of ClOOCl was observed. To subtract the contribution of Cl_2, which varied in concentration

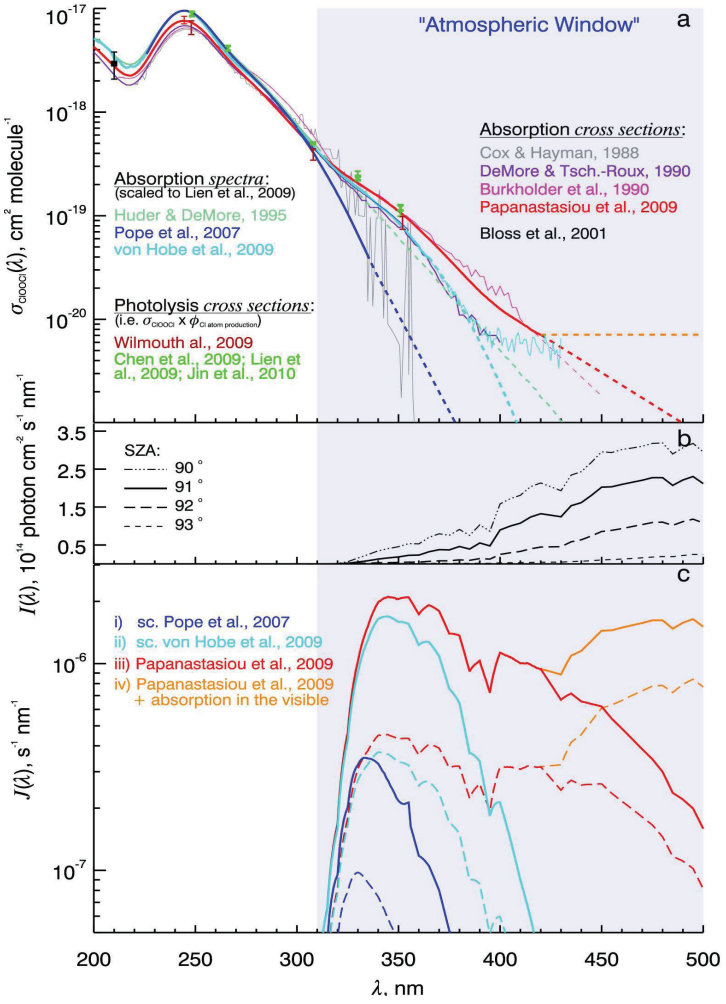

Figure 2.5: The upper panel presents a comparison of UV/Vis absorption spectra, absorption cross sections and photolysis cross sections of ClOOCl from various studies. The dashed extensions show the exponential extrapolation of chosen spectra in the actinic region. The orange line represents an artificial spectrum with ClOOCl absorption band in the visible. The middle panel shows spectral actinic flux $I(\lambda)$ calculated using a HALOE O_3 climatology (Grooß and Russell, 2005) and CLaMS photolysis code (Becker et al., 2000) for four solar zenith angles (SZA) and an altitude of 18.4 km. The photolysis rate constants estimated for chosen absorption cross sections and $I(\lambda)$ at 91° (solid line) and 92° (dashed line) SZA are shown in panel c. The overall J_{ClOOCl} effective in the atmosphere is obtained by integration of the areas under the plotted curves.

during the sublimation process, Pope et al. (2007) used a least-squares fitting procedure that assumed two Gaussian-like expressions representing the ClOOCl spectrum. In the analysis, they overestimated the influence of Cl_2, hence the reported $\sigma_{ClOOCl}(\lambda)$ is much smaller than any published values and would result in unrealistic low ClOOCl values. Although, the study of Pope et al. provided erroneous results, it developed a method for preparing almost pure ClOOCl.

Von Hobe et al. (2009) followed the synthesis method of Pope et al. (2007) and prepared a pure ClOOCl sample isolated in a neon matrix, the impurity of which was checked with IR/Vis matrix spectroscopy and low-temperature Raman spectroscopy. Von Hobe et al. explained the observed differences to previously published spectra and indicated that the earlier measurements of σ_{ClOOCl} at the peak of ≈ 245 nm may be inaccurate. Because of likely loss of chlorine atoms from the matrix during photolysis, absolute cross sections were not estimated. They assumed however, that if there is no loss of Cl from the matrix, an upper limit of σ_{ClOOCl} at 245 nm is placed at about a factor of 3 higher than σ_{ClOOCl} measured by Cox and Hayman (1988).

Papanastasiou et al. (2009) measured ClOOCl absorption cross sections using diode array spectroscopy and laser photolysis to generate ClO radicals. For their spectral analysis they used reaction stoichiometry and three observed isosbestic points to account for chemical species impurities which appear to represent an interference to a greater or lesser degree in all pre-2009 studies. The isosbestic point observed at 408.5 nm shows that ClOOCl absorbs measurably at wavelengths longer than 350 nm. Papanastasiou et al. (2009) confirmed the spectrum measured in the same laboratory by Burkholder et al. (1990), but estimated roughly 20% higher cross sections at the maximum. Results of Papanastasiou et al. (2009) are recommended in JPL 2011.

Wilmouth et al. (2009) used flow-tube and atomic resonance fluorescence techniques to measure Cl atom production during photolyzing of ClOOCl at 248, 308, and 352 nm. They obtained the product of the ClOOCl absorption cross section at the three wavelengths by scaling their signals to the known Cl atom yield in the photolysis of Cl_2 or the literature cross section at the peak of the ClOOCl absorption spectrum. The Cl_2 concentration was

monitored in-situ using fluorescence excited by the resonance lamp. By assuming $\phi(\lambda) = 1$, they obtain the lower limit to the absorption cross section.

Chen et al. (2009), Lien et al. (2009), Jin et al. (2010) measured photolysis cross sections, $\sigma_{\mathrm{ClOOCl}}\phi(\lambda)$, at specific wavelengths by a new experimental method involving pulsed laser photolysis of ClOOCl in a molecular beam combined with mass spectrometric detection. This new method is not sensitive to spectral interference from Cl_2. Lien et al. (2009) carried out the measurements for 248.4 nm at three temperatures and showed that the method is the only one of which the error bars are small enough to reveal the temperature effect. They indicated also a slightly negative temperature effect at 248.4 nm, whereas Chen et al. (2009) and Jin et al. (2010) measured a positive and a quite significant temperature effect of the ClOOCl cross section at 308, 351 and 330 nm (cf. Table 2.1). This Doppler broadening effect is the modification of the perceived frequency of radiation due to the motion of the molecule and may explain, at least in part, the differences between the spectra plotted in Fig. 2.5.

The JPL 2011 recommended ClOOCl absorption cross sections are based on the measurements of Papanastasiou et al. (2009) for the temperature range 190 – 250 K. Data at $\lambda >$ 420 nm are estimated from the following formula $\sigma_{\mathrm{ClOOCl}}(\lambda) = 9.5 \times 10^{-16} \times \exp(-0.0281 \times \lambda)$, where λ is in nm and σ_{ClOOCl} is in units of $\mathrm{cm^2 molecule^{-1}}$. A summary of ClOOCl absorption/photolysis cross sections studies is given in Table 2.1.

The laboratory studies, in which relative absorption spectra have been measured, have to be scaled to one of the presented absolute absorption or photolysis cross sections. In Figure 2.6, the possible scaling points at the absorption peak are plotted. The studies of Cox and Hayman (1988), DeMore and Tschuikow-Roux (1990) and Burkholder et al. (1990) indicated the absorption peak value of ClOOCl at 245 nm between 5.8×10^{-18} and $7.2\times10^{-18}\mathrm{cm^2 molecule^{-1}}$. According to the results of Papanastasiou et al. (2009), the absorption peak is at 244.5 nm and has a value of $7.6\times10^{-18}\mathrm{cm^2 molecule^{-1}}$, Wilmouth et al. (2009) placed the absorption peak to $6.6\times10^{-18}\mathrm{cm^2 molecule^{-1}}$ at 248.0 nm, whereas studies of Lien et al. (2009) showed even higher photolysis cross section ($8.85\times10^{-18}\mathrm{cm^2 molecule^{-1}}$) near to the assumed peak, at 248.4 nm. The relative absorption spectra plotted in Fig. 2.5a

are scaled to peak value reported by Lien et al. (2009) for two reasons:

- The method used by Lien et al. (2009) is insensitive to UV absorption interference by impurities and does not require information on the absolute ClOOCl concentration,
- It seems unreasonable to scale a relative absorption spectrum to an absolute cross section associated with a different spectral shape, because in this case we would approve the shape of the absolute spectrum as the correct one. That is why scaling of e.g. von Hobe et al. (2009) spectrum to cross sections of Papanastasiou et al. (2009) is incorrect.

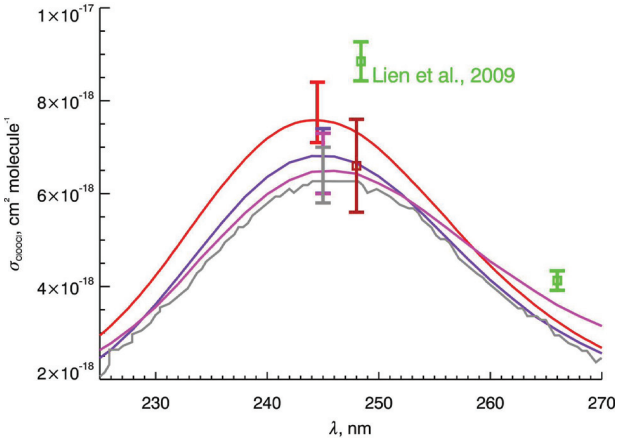

Figure 2.6: Peak close-up for Figure 2.5a. The colours of lines and squares correspond respectively to the absolute cross sections and photolysis cross sections plotted in Figure 2.5a.

The upper panel of Fig. 2.5 shows that the existing laboratory studies on σ_{ClOOCl} agree reasonably well at wavelengths below 310 nm, but display large uncertainties in the long wavelength tail, i.e. in the region of most relevance in the atmosphere. These uncertainties propagate directly into the atmospheric J_{ClOOCl} values derived from the cross section measurements (Fig. 2.5c). Because the incoming sunlight at λ <310 nm is extremely weak due to the absorption of ozone, it is the weak tail of the ClOOCl absorption spectrum at λ >310 nm that is responsible for its photodissociation in the atmosphere.

2.3.3 Actinic flux

Another factor that strongly influences atmospheric J_{ClOOCl} values is the actinic flux $I(\lambda)$, which is equal to the total number of photons incident at a point and is calculated by inte-

Study	Year	Temperature (K)	λ (nm)	$10^{20}\sigma(\lambda)$ (cm^2)	Type of data
Cox and Hayman	1988	200 – 300	220 – 360	640 ± 60	Absolute spectrum
Permien et al.	1988	235	211 – 290	—	Relative spectrum
Burkholder et al.	1990	205 – 250	212 – 410	650 +80/-50	Absolute spectrum
DeMore & Tschuikow-Roux	1990	206	190 – 400	680 ± 80	Absolute spectrum
Vogt & Schindler	1990	230	204 – 350	—	Relative spectrum
Huder & DeMore	1995	195	200 – 310	—	Relative spectrum
Bloss et al.	2001	183 – 245	210	294 ± 86	Absorption cross section
McKeachie et al.	2004	223	235 – 400	—	Relative spectrum
Pope et al.	2008	193	226 – 355	—	Relative spectrum
von Hobe et al.	2009	10	220 – 400	—	Relative spectrum
Chen et al.	2009	200	308	49	Photolysis cross
		250	308	50.9	sections
		200	351	11.2	
		250	351	12.6	
Lien et al.	2009	160	248.4	890	Photolysis cross
		200	248.4	885	sections
		260	248.4	873	
Wilmouth et al.	2009	240 ± 10	248	660 ± 100	Photolysis cross
			308	39.3 ± 4.9	sections
			352	8.6 ± 1.2	
Papanastasiou et al.	2009	200 – 228	200 – 420	760 +80/-50	Absolute spectrum
Jin et al.	2010	200	330	23.1	Photolysis cross
		250	330	24.7	sections

Table 2.1: Summary of ClOOCl absorption/photolysis cross sections studies. The earlier studies by Basco and Hunt (1979) and Molina and Molina (1987) have been shown to have incorrectly identified the UV spectrum of ClOOCl (Burkholder et al., 1990) and are therefore not included in the table. In case of absolute spectra, the values are given at the peak of the spectrum, ~ 245 nm.

grating the solar radiance $L(\lambda,\theta,\phi)$ over the zenith θ and azimuth ϕ angles:

$$I(\lambda) = \int_0^{2\pi} \int_0^{\pi/2} L(\lambda,\theta,\phi) sin(\theta) d\theta \, d\phi = I_{dir}(\lambda) + I_{diff}(\lambda) \tag{2.14}$$

The actinic flux is the suitable radiation quantity for photolysis frequencies determination (Kazadzis et al., 2004). It includes the radiance $L(\lambda,\theta,\phi)$ from all angular directions, however in practice a distinction is often made for the contributions of the direct solar beam ($I_{dir}(\lambda)$), and the diffuse radiation down-welling ($I_{diff}\downarrow(\lambda)$) and up-welling ($I_{diff}\uparrow(\lambda)$) incident respectively from the upper and lower layers. This diffuse radiation arises from molecular (Rayleigh) scattering, reflections at the Earth's surface (the albedo of land or sea surface), and scattering by aerosols and clouds (Palancar et al., 2011). It is therefore dependent on the wavelength, on the altitude and on specific local environmental conditions. Up to now, models and field studies on J_{ClOOCl} did not pay proper attention to the impact of $I(\lambda)$ on ClOOCl chemistry. Here, the influence of ozone, albedo, clouds and aerosols on the ClOOCl photolysis is determined from ClO in-situ measurements in the polar stratosphere (described in Section 6).

Previous studies investigating the consistency of published J_{ClOOCl} with atmospheric observations of ClO and ClOOCl have focused on the photochemical equilibrium between ClOOCl formation and photolysis rate, so called steady state approximation:

$$\frac{J_{\mathrm{ClOOCl}}}{k_{\mathrm{rec}}} \approx \frac{[\mathrm{ClO}]^2}{[\mathrm{ClOOCl}]}. \tag{2.15}$$

Shindell and de Zafra (1995), Avallone and Toohey (2001) and Stimpfle et al. (2004) tested different combinations of J_{ClOOCl} and k_{rec} through comparison of the resulting ClO and ClOOCl with in-situ data. Stimpfle et al. (2004) proposed four possible parameter pairs giving good agreement with the measured data and ruled out photolysis of ClOOCl longwards of 800 nm. Von Hobe (2007) analysed available laboratory and field data and estimated limits for J_{ClOOCl} (JPL 2002, Burkholder et al. 1990), k_{rec} and K_{eq}. The derivation of $J_{\mathrm{ClOOCl}}/k_{\mathrm{rec}}$ from ClO in-situ data was also described by Schofield et al. (2008). Here, the term 'self-match' flight was used for a flight pattern, in which the aircraft encounters

the same air masses twice. The pattern enabled observation of change in ClO mixing ratios due to increasing solar zenith angle during sunset. Schofield et al. (2008) proposed wide range of parameters fitting their data. $J_{\mathrm{ClOOCl}}/k_{\mathrm{rec}}$ ratio depending on assumed K_{eq} was estimated also by Kremser et al. (2011) from ClO microwave radiometer data.

Derivation of J_{ClOOCl} or $J_{\mathrm{ClOOCl}}/k_{\mathrm{rec}}$ from field data is difficult due to changing conditions in the atmosphere and significant measurement uncertainties. An unambiguous determination of kinetic parameters from the data acquired in the stratosphere is therefore impossible and further laboratory measurements are necessary. To emphasise the importance of the issue, Figure 2.7 is presented. It shows ozone loss in the Antarctic winter 2003 along a single trajectory simulated with different values of J_{ClOOCl} and k_{rec} and compared to measured data (von Hobe, 2007). The Figure demonstrates clearly, that the calculations with J_{ClOOCl} basing on cross sections of Pope et al. (2007) cannot reproduce the field data. It shows also the significance of J_{ClOOCl} in model ozone calculations.

In this thesis, in Section 5, an experiment is described, in which the self-match method presented by Schofield et al. (2008) was followed, but the flight started in the night, when the air masses were in thermal equilibrium and the observed change in ClO concentrations was due to decreasing solar zenith angle during sunrise. To ensure that ClO was measured twice in the same air masses, a detailed check of match quality was carried out. In Section 6 an analysis of influence of ozone column, albedo, clouds and aerosols on the actinic flux and hence on the ClOOCl photolysis at the point of measurements is provided. From the observed ClO concentration increase, J_{ClOOCl} was estimated and compared with ClO increases resulting from four sets of ClOOCl absorption cross sections/scaled spectra (Section 7). The results shown in this thesis were published by Sumińska-Ebersoldt et al. (2011).

[4] improved Limb Atmospheric Spectrometer II developed by the Environment Agency of Japan is a sensor to monitor the polar stratospheric ozone

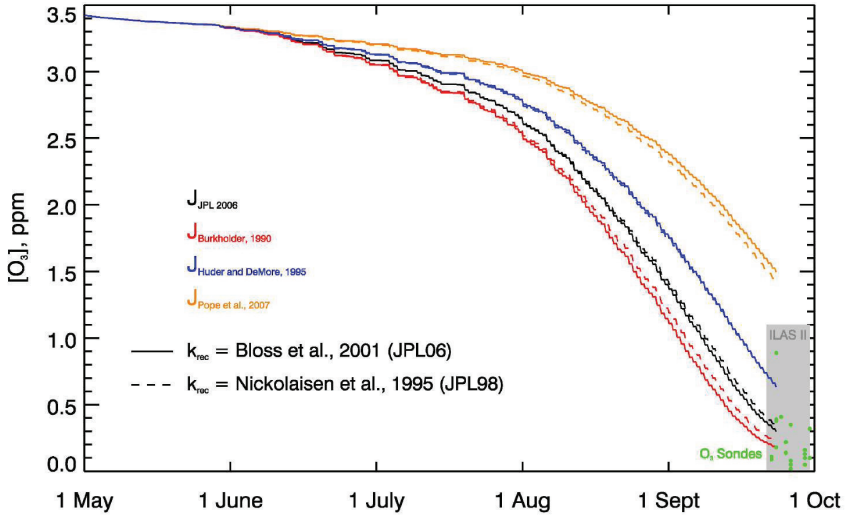

Figure 2.7: J_{ClOOCl} and k_{rec} influence on simulated ozone values for the Antarctic winter 2003. The single trajectory simulation ending on the 450 K isentrope was initialised using satellite observations and tracer correlations. For comparison, ozone sonde data and ILAS-II[4] observations within the Antarctic Vortex at 450 K potential temperature near the end of the simulation are shown. Plot adopted from von Hobe (2007).

3 The HALOX instrument

ClO measurements analysed in this thesis were made with the HALOX (HALOgen OXides) instrument, which employs the chemical conversion resonance fluorescence (CCRF) technique. In this Section, the CCRF technique is described and the instrument set-up and specifications as well as the calibration are presented.

3.1 The CCRF technique in ClO detection

The CCRF method is an adaptation of the fast flow reactor technique, which has found extensive use in conjunction with resonance fluorescence detection for laboratory studies of gas phase reaction kinetics. In experiments carried out by Clyne and Cruse (1972) and Anderson and Kaufman (1972), a flowing gas sample was probed with a collimated beam of radiation. The photons resonantly scattered out of the beam were counted photoelectrically by a detector observing in a direction perpendicular to the source beam. In the 1970', the CCRF technique was adopted for stratospheric balloon-borne measurements of ground state atomic oxygen O(^{3}P) (Anderson, 1975) and hydroxyl radical OH($X^2\Pi$) (Anderson, 1976) concentrations. First in-situ ClO measurements made with CCRF were reported by Anderson et al. (1977). Brune et al. (1989) determined ClO and BrO concentrations in the Antarctic polar vortex using a CCRF instrument employed aboard of ER-2 aircraft.

The CCRF technique is a chemical kinetic-spectroscopic technique in which the oxygen atom is extracted from a radical (in this case ClO) in a reaction with a defined species (here nitric oxide):

$$ClO + NO \rightarrow Cl + NO_2 \qquad \text{R28}$$

providing an atom (here Cl), which is detected by atomic resonance fluorescence.

For the detection of the Cl atoms a rectangular arrangement of an atomic emission lamp

and a photomultiplier detector located downstream of the NO injector is used (Brune et al., 1989, see Fig. 3.1). The Cl-lamp emits the Cl signature at 118.9 nm (energy state diagram in Figure 3.2), which originates from the doublet (118.875 and 118.774 nm) and gives the best possibility for the resonance fluorescence due to its location in an oxygen absorption minimum. To suppress other lines oxygen gas filters flushed with synthetic air are used. A photon emitted from the lamp is absorbed by a Cl atom leading to its excitation. After a delay, the Cl atom returns to its original state re-emitting the light in a random direction. This mechanism is termed resonance fluorescence.

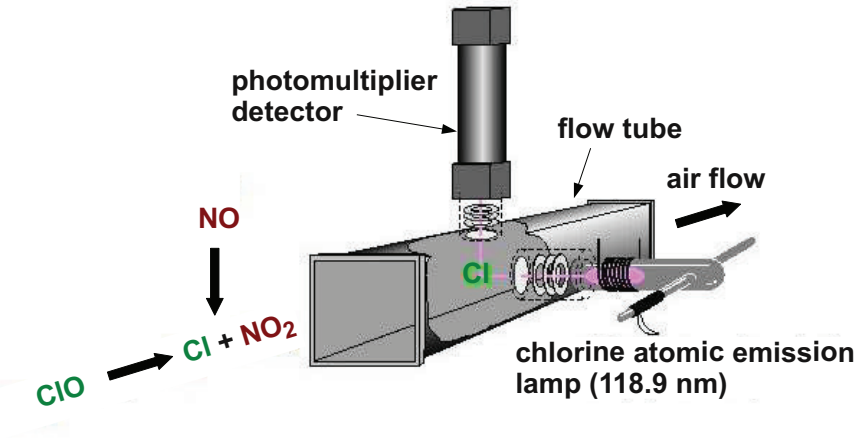

Figure 3.1: HALOX instrument: Chemical conversion resonance fluorescence technique.

The Cl-lamp is a low pressure gas discharge lamp containing trace amounts of chlorine in 5 hPa helium, its body is schematically shown in Fig. 3.1. A source of Cl in the lamp is platinum chloride ($PtCl_2$), which decomposes thermally giving chlorine in the gas phase:

$$PtCl_2 \xrightarrow{T\approx 300^\circ C} Pt + Cl_2 \qquad \text{R29}$$

Via the temperature of the $PtCl_2$ compartment, the partial pressure of chlorine and hence

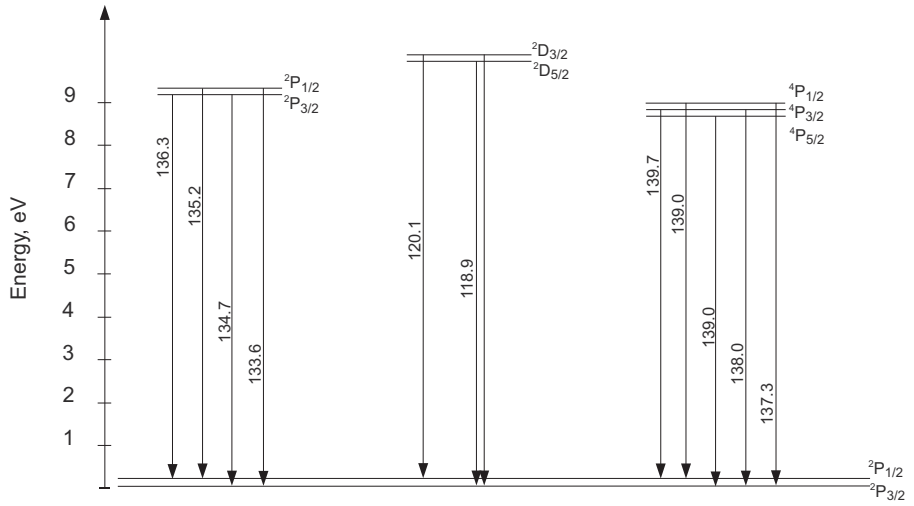

Figure 3.2: Diagram of relevant energy states of the chlorine atom. The wavelengths are given in nm according to Radziemski Jr. and Kaufman (1969).

the emissive power of the lamp can be regulated. In the opposing lamp arm, a barium getter is placed, which reduces the partial pressure of Cl_2 via the following reaction:

$$Ba + Cl_2 \rightarrow BaCl_2 \qquad \text{R30}$$

Barium reacts also with water and oxygen improving the purity of the lamp. The upper panel of Figure 3.3 shows an emission spectrum of a Cl-lamp and provides a list of typical chemical impurities. The contamination lines are absorbed within an air filter placed in front of the lamp window, which is made from magnesium fluoride (MgF_2) and cuts all lines below about 115 nm. In the lower panel of Figure 3.3, the influence of the air filter on the spectrum is presented.

The photomultiplier tube detects the re-emitted photons and the photons coming from scattering of the lamp beam from the chamber walls S_{chamber} and the pressure dependent Rayleigh scatter signal S_{Rayleigh}, so that:

$$S = S_{\text{Cl}} + S_{\text{chamber}} + S_{\text{Rayleigh}} \qquad (3.1)$$

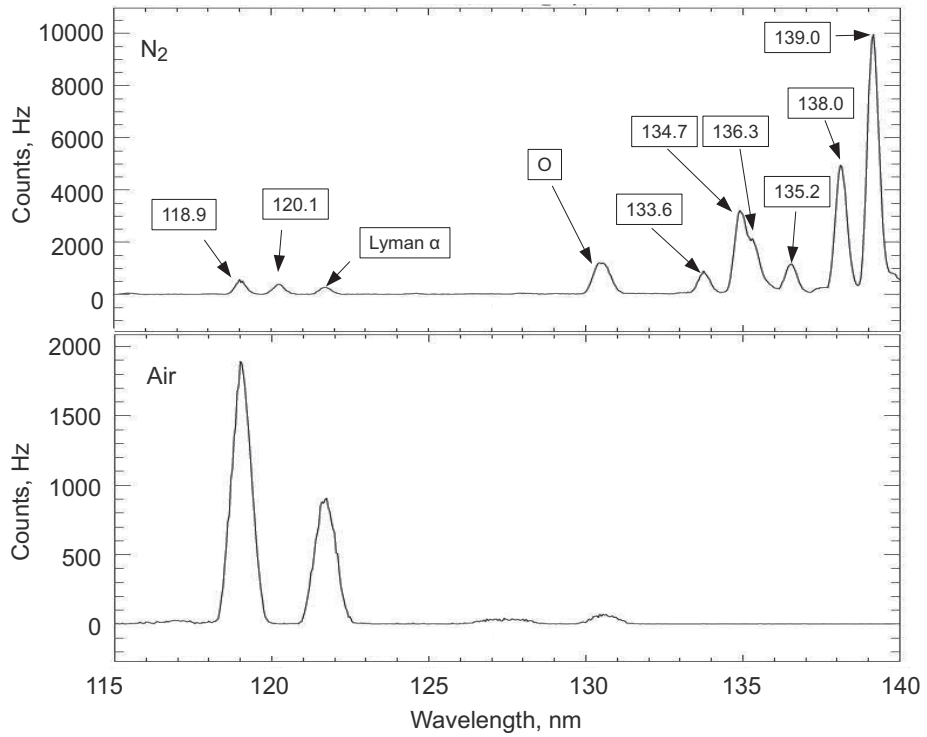

Figure 3.3: Emission spectrum of a chlorine lamp. In the upper panel, the unfiltered emission spectrum is shown. The spectrum measured with an air filter is plotted in the lower panel. Note the two different ordinate scales.

To determine separately the background consisting of Rayleigh and chamber scatter and the resonance fluorescence signal due to the Cl atoms, the NO addition is periodically switched on and off. From the resulting signal difference and the data acquired during measurement calibration (cf. Section 3.2), the Cl atom concentration in the investigated air can be obtained. The efficiency of Reaction R28 in the air mass is calculated with FACSIMILE[5] considering NO and O_3 concentrations, flow rate, temperature and pressure and is typically about 80 to 90%.

[5] a modeling tool designed by MCPA Software Ltd. to efficiently solve differential equations, with the focus on modeling the kinetics of physical and chemical systems

3.2 Calibration

Before and after a field campaign, a calibration of the instrument is necessary, in which a calibration factor C_{cal} is determined and compared with reference values (Avellone, 1993). C_{cal} provides a ratio of the resonance fluorescence signal and the concentration of Cl atoms and can be written as follows:

$$C_{\text{cal}}^{\text{Cl}} := \frac{S_{\text{Cl}}}{[\text{Cl}]} \tag{3.2}$$

As shown by Anderson (1978); Anderson et al. (1980), the resonance fluorescence signal S_{Cl} resulting from the excitation of Cl atoms with a given lamp depends on the photon flux of the lamp at 118.9 nm $F^{118.9}$, concentration of the Cl atoms in the detection volume [Cl], on the effective cross section of Cl $\sigma_{\text{Cl}}^{118.9}$ and the parameters of the lamp and detector setup. The detector setup parameters for the radiation at 118.9 nm (including the geometry of the system and reflectivity of the walls of the flow tube) can be combined and treated as a constant value $K^{118.9}$. The photon flux $F^{118.9}$ changes with the time due to e.g. degradation of the MgF_2 window and the density and has to be characterize by another quantity, that can be easily observed. The photon flux from the lamp is proportional to the background signal seen by the detector S_{bgr}, and therefore the background signal can be used for normalization of the calibration factor.

The background signal S_{bgr} is a sum of S_{chamber} and S_{Rayleigh}. Its change at 118.9 nm due to change of $[N_2]$ is represented by the following equation:

$$\left(\frac{\partial S_{\text{bgr}}}{\partial [\text{N}_2]}\right)_{N_2}^{118.9} = F^{118.9} K^{118.9} \sigma_{\text{N}_2,\text{Ray}}^{118.9}, \tag{3.3}$$

where $\sigma_{\text{N}_2,\text{Ray}}^{118.9}$ is a cross section of N_2 for Rayleigh scattering.

The normalized calibration factor is defined by

$$\left(C_{\text{cal}}^{\text{Cl}}\right)_{\text{N}_2}^{\text{norm}} = \frac{\left(C_{\text{cal}}^{\text{Cl}}\right)_{\text{N}_2}}{\left(\frac{\partial S_{\text{bgr}}}{\partial [\text{N}_2]}\right)_{\text{N}_2}^{118.9}} \tag{3.4}$$

The quantity $\left(\partial S_{bgr}/\partial [N_2]\right)_{N_2}^{118.9}$ is estimated in the laboratory by observation of the signal change with changing pressure of N_2 in the flow tube.

Since not only the 118.9 nm line is emitted from a lamp, but also e.g. Lyman-α (121.6 nm)

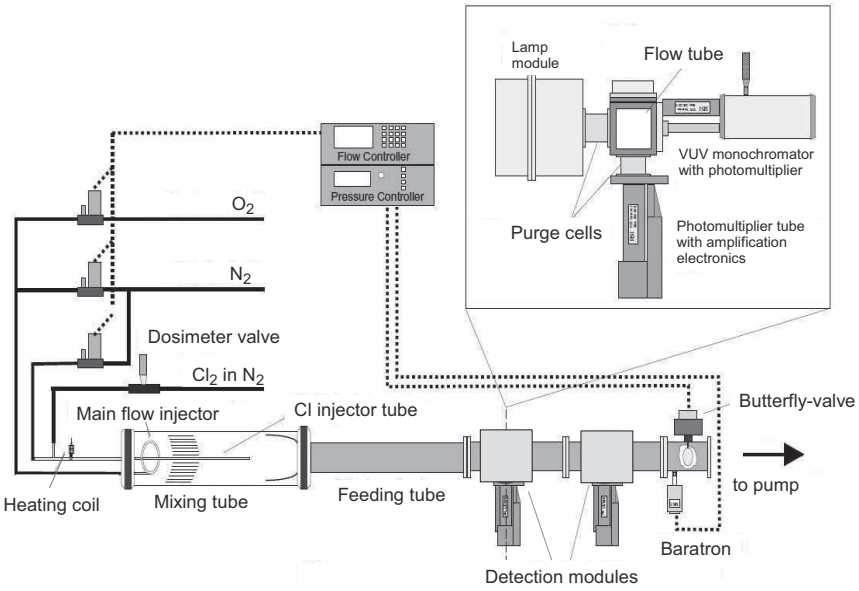

Figure 3.4: Schematic view of the HALOX calibration bench.

line is usually present in the lamp spectrum (see Fig. 3.3), Eq. 3.4 gets the form:

$$\left(C_{\mathrm{cal}}^{\mathrm{Cl}}\right)_{\mathrm{N_2}}^{\mathrm{norm}} = \frac{\left(C_{\mathrm{cal}}^{\mathrm{Cl}}\right)_{\mathrm{N_2}}}{(1-\mathrm{Ly}_\alpha)\left(\frac{\partial S_{\mathrm{bgr}}}{\partial[\mathrm{N_2}]}\right)_{\mathrm{N_2}}^{118.9+121.6}}, \tag{3.5}$$

where Ly_α depends on the intensity of the Lyman-α line and Cl-line and equals to $I_{121.6}/F(I_{118.9}+I_{121.6})$, where F denotes a spectral correction factor for the monochromator and is equal $\approx$1.1.

Figure 3.4 shows schematically a setup used for the calibration. During a calibration, the pressure in the flow tube are adjusted to conditions prevailing during a stratospheric measurement flight. The composition of air is regulated by mass flow controllers and the pressure by a butterfly-valve located just upstream of the vacuum pump.

The calibration starts, when the lamp emission is stable and 118.9 and 121.6 nm line signals, $S_{118.9}$ and $S_{121.6}$, can be estimated with the monochromator/photomultiplier setup

(see Fig. 3.4). From these values Ly$_\alpha$ is calculated.

By observing of the detector signal varying with changing [N_2] in the flow tube, the quantity $(\partial S/\partial p)_{N_2}^{118.9+121.6}$ is obtained. At constant temperature, the pressure p is proportional to the number concentration and therefore (∂S/∂p) is proportional to $(\partial S_{bgr}/\partial[M])$, i.e. to $(\partial S_{bgr}/\partial[N_2])_{N_2}^{118.9+121.6}$.

Afterwards, a defined pressure in the flow tube is set and the monochromator is adjusted to 118.9 nm. Chlorine molecules mixed with nitrogen atoms are injected into a mixing tube and directed over a red-hot tungsten filament, which enables thermal dissociation. The counts of the photomultiplier attached to the monochromator change due to the absorption of the lamp radiation by Cl atoms. The absorption is defined as follows:

$$A = \frac{I_0 - I}{I_0} \tag{3.6}$$

with I_0 and I standing respectively for the counts on the photomultiplier, when the tungsten wire is turned off and on. The absorption A enables calculation of [Cl] in the flow tube as shown by Schwab and Anderson (1982) and Woyke (1997).

Switching the tungsten filament off and on causes also a change in Cl mixing ratio in the feeding tube from 0 up to several ppb and S_0 and S are observed at the photomultiplier placed perpendicular to the lamp. The difference of those two signals gives the resonance fluorescence signal: $S_\Delta = S - S_0$. During a calibration, the Cl concentration is significantly higher than during stratospheric measurements and the resonance fluorescence radiation is reabsorbed. Therefore $S_{Cl} = \frac{\Delta S}{1-A}$.

Knowing Ly$_\alpha$, $(\partial S_{bgr}/\partial[N_2])_{N_2}^{118.9+121.6}$, [Cl] and S_{Cl}, the normalized calibration factor $(C_{cal}^{Cl})_{N_2}^{norm}$ can be estimated (Eq. 3.2 and Eq. 3.5). At the end of the calibration, the values of $(\partial S/\partial p)_{N_2}^{118.9+121.6}$, $S_{118.9}$ and $S_{121.6}$ are measured again to ensure that the lamp flux did not change during the calibration.

The calibration factor changes with pressure. Avellone (1993) estimated following dependence, which here is defined as reference:

$$\text{Ref} := \left(\frac{(C_{cal}^{Cl})_{N_2}}{\left(\frac{\partial S_{bgr}}{\partial p}\right)_{N_2}^{118.9}} \right)^{-1} \left[\frac{10^5 \text{cm}^3}{\text{atoms} \cdot \text{hPa}} \right] = 10.3 + 0.134 \cdot p[\text{hPa}]. \tag{3.7}$$

The results of the calibration for different pressures are compared with the reference to check, if the calibration was correct and if there were any possible wall losses in the feeding tube.

For the measurements in the air, a relation between the calibration factor in nitrogen and air is needed. The pressure dependence of the ratio was estimated by Woyke (1997):

$$\frac{\left(C_{\mathrm{cal}}^{\mathrm{Cl}}\right)_{\mathrm{N_2}}}{\left(C_{\mathrm{cal}}^{\mathrm{Cl}}\right)_{\mathrm{air}}} = 0.00171 \cdot p[\mathrm{hPa}] + 1.094 - 0.094 \cdot exp\left(-0.049 \cdot p[\mathrm{hPa}]\right). \tag{3.8}$$

3.3 The instrument configuration

A schematic setup of the actual HALOX instrument designed for the left wing pod of the M-55 Geophysica aircraft is shown in Fig. 3.5. It consists of two parallel measurement ducts suspended under the instrument base plate and the gas supply and electronics units mounted on top of the plate. The electronics box consists of the instrument power supply units, the instrument control and data acquisition computer, control and interface electronics, and signal distribution panel. The gas supply unit carries two 1 l bottles of synthetic air, one 500 ml bottle of nitric oxide (NO), and several mechanical and electrical valves, gauges, and gas flow controllers (von Hobe et al., 2005). NO is added to the sampled air via needle arrays placed in each measurement duct in order to produce chlorine atoms via Reaction R28.

There are two measurement ducts: one operating at ambient pressure (A) and one operating at reduced pressure (B). Both consist of an air inlet, two thermistor arrays for temperature measurement within the air flow, the NO injector, and two detection modules. The open duct A, in which the flow velocity is regulated in the range $10 - 20\,\mathrm{ms}^{-1}$ by a butterfly valve, enables ClO measurements with a detection limit of 5 ppt and an accuracy of approximately 15%. In measurement duct B, which is pumped to decrease the pressure inside by about 40%, the sum of ClO and ClOOCl can be measured after thermal dissociation of the dimer in a heated (approx. 370 K) inlet nozzle. To extract the ClOOCl concentration measured in duct B, the ClO background has to be subtracted. This is done using the ClO measurement of duct A, which is compared to the signal in duct B at regular intervals with-

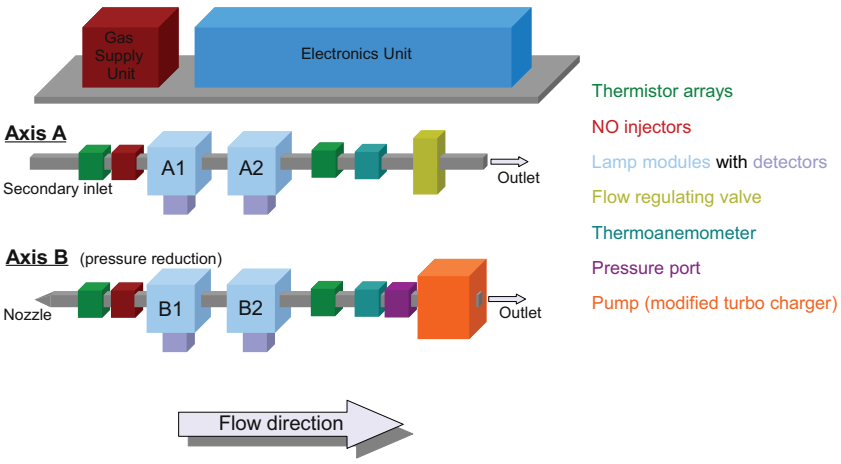

Figure 3.5: HALOX instrument configuration. Power supply, instrument control and data acquisition computer, pressure sensors ect. are placed in the electronics unit. In the B axis, a pressure reducing system was integrated to enable measurements of ClOOCl and $ClONO_2$.

out nozzle heating. The typical accuracy of the ClOOCl measurement is between 20 and 30%. It results from the propagation of the accuracies of A and B ducts and depends to some extent on the relative amounts of ClO, ClOOCl and $ClONO_2$ present. The minimum time resolution of the ClO and ClOOCl measurements is given by the NO addition cycles and is around 20 s or 10 s for the double duct operation (von Hobe et al., 2005).

4 Chemistry transport and radiative transfer models

To obtain the results presented in this thesis three models were used. The Chemical Lagrangian Model of the Stratosphere from Research Centre Jülich was employed for planning of the self-match flight (Section 5) and analysis of the acquired data (Section 7). To estimate the influence of ozone column, albedo, aerosol and clouds on the ClOOCl photolysis, two radiative transfer models were compared and used for the estimation of the actinic flux $I(\lambda)$ on the flight trajectory (Section 6). The first one, libRadtran, is a high resolution model created at Deutsches Zentrum für Luft- und Raumfahrt (DLR) and University of Munich (Mayer and Kylling, 2005). The second one was written by Prather (1981) and Salawitch et al. (1994) and was used in previous research (Salawitch et al., 1993; Stimpfle et al., 2004; Schofield et al., 2008). The model is currently operated at the University of Maryland (UMD) and therefore, in this thesis it is referred to as the UMD model.

4.1 The CLaMS Model

For preparation of the flight trajectory and the analysis presented in Sections 7, the Chemical Lagrangian Model of the Stratosphere (CLaMS) (McKenna et al., 2002a,b; Grooß et al., 2005, 2011) developed at the Research Centre Jülich was used. CLaMS is based on a Lagrangian approach, in which one considers an ensemble of air parcels following the wind and, consequently, forming a time-dependent irregular grid moving with the wind elements. The chemistry taking place can be calculated on this irregular grid. CLaMS enables investigation of small-scale features often observed in stratospheric flows and provides a tool for chemistry calculations in single air parcels along their trajectories. Fig. 4.1 shows the CLaMS model scheme with its most important components.

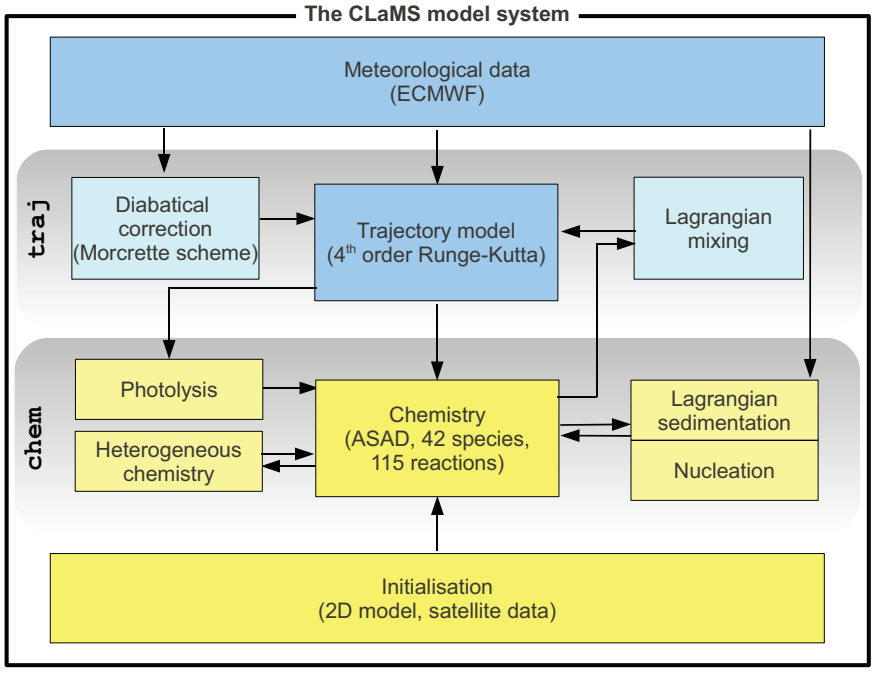

Figure 4.1: Schematic diagram of CLaMS model.

The CLaMS module `traj` enables forward and backward trajectory calculations (i.e. forward and reverse in the time direction) from a particular point or set of points in the stratosphere and upper troposphere. For initialization of a run, coordinates and altitude information is needed. The calculations of the air parcel trajectories are based on meteorological analyses of the European Centre for Medium-Range Weather Forecasts (ECMWF, Simmons et al., 1989). The ECMWF data used in the analysis presented in this thesis have a meridional and zonal resolution of 1°, a temporal resolution of 6 hours and a vertical one of 10 K in potential temperature coordinates. The numerical integration is based on the 4th order Runge-Kutta scheme. The radiative transfer code inherent in CLaMS bases on studies of Lary and Pyle (1991a,b) and Becker et al. (2000).

The vertical coordinate of CLaMS in the stratosphere is the potential temperature Θ, below the tropopause, the model smoothly transforms from the isentropic to the ζ hybrid-

pressure coordinate proportional to pressure (Konopka et al., 2007). In this way, CLaMS takes into account the effect of large-scale convective transport as implemented in the vertical wind of the meteorological analysis. The stratosphere is stably stratified and therefore the vertical winds can be neglected in many applications focusing on short time scales. For polar regions, however, the diabatic descent of the air masses has to be taken into account. For this purpose an improved version (Zhong and Haigh, 1995) of the Morcrette radiation scheme (Morcrette, 1991) is employed in CLaMS.

CLaMS uses a comprehensive set of reactions occurring in the stratosphere including 42 species, 115 reactions and full chlorine chemistry. The chemistry package `chem` is a box model running on multiple trajectories at the same time. It calculates the change of chemical composition along each given trajectory. CLaMS enables usage of different solvers to integrate the system of stiff ordinary differential equations resulting from the chemistry (Carver et al., 1997; McKenna et al., 2002b). The calculations presented in this thesis were carried out with the SVODE solver (Brown et al., 1989). The photolysis rates in CLaMS are calculated in spherical geometry (Meier et al., 1982; Becker et al., 2000) using a climatological ozone profile from HALOE (Grooß and Russell, 2005) or profiles from various satellite data, e.g. from Microwave Limb Sounder (MLS).

Heterogeneous chemistry is based on the code of Carslaw et al. (1995) and is calculated on ice, nitric acid trihydrate (NAT), and liquid ternary $H_2O/H_2SO_4/HNO_3$ (STS) particles. The parameterisations of the uptake coefficient to model heterogeneous chemistry on liquid aerosols and on NAT particles are derived from Hanson (1998) and Hanson and Ravishankara (1993) respectively. Also, a Lagrangian denitrification scheme is implemented into the three-dimensional version of CLaMS to calculate the growth and sedimentation of nitric acid trihydrate particles along individual particle trajectories. NAT formation is assumed to occur at a HNO_3 supersaturation of a factor of 10 (Grooß et al., 2005).

In this thesis, the results of CLaMS box-model-mode runs are shown. This mode enables chemistry calculations in an air parcel moving on a given forward or backward trajectory. The results of such runs are presented in Sections 5 and 7.

4.2 Radiative transfer models

Radiative transfer is one of the most important topics in atmospheric research. Solar radiation drives weather and climate of the Earth, atmospheric dynamics is driven by the differential heating by the sun, caused by the latitudinal gradient of the incident solar irradiance and the rotation of the Earth about its axis. In addition to being the driving force of weather and climate, solar radiation controls atmospheric chemistry. The key reactions in atmospheric chemistry like the photolysis of NO_2, which is the only production mechanism of ozone in the troposphere, and the photolysis of O_3, which causes the formation of the OH radical or the ClOOCl photolysis investigated here are driven by radiation and thus are directly proportional to the available radiation in the ultraviolet spectral region. Therefore, a detailed knowledge of the atmospheric radiative transfer and accurate calculation of the photolysis rates are necessary to evaluate stratospheric models (Becker et al., 2000).

To estimate correct ClOOCl photolysis rates, information about actinic fluxes $I(\lambda)$ in the investigated air masses is necessary. In the analysis described in Section 6, two radiative transfer models were compared and used for calculations of $I(\lambda)$ and J_{ClOOCl} values.

4.2.1 libRadtran software package

The libRadtran software package of Deutsches Zentrum für Luft- und Raumfahrt (DLR) and University of Munich is a free radiative transfer model (RTM) and is available from http://www.libradtran.org. LibRadtran is a library of radiative transfer routines and programs. It is also often referred to as UVSPEC or DISORT, and is widely used and cited (Bais et al., 2005; Bernhard et al., 2005; Antón et al., 2007), e.g. by the satellite communities (Arola et al., 2005, 2007; Bugliaro et al., 2010). It provides transparent input options considering various atmospheric scenarios (haze, clouds, ect.), which can be implemented in calculations in an easy and transparent way.

The central program of the libRadtran package is the radiative transfer tool `uvspec`, which calculates the radiation field in the Earth's atmosphere. A schematic structure of `uvspec` is shown in Figure 4.2. The `uvspec` program includes the full solar and thermal spectrum from 120 nm to 100 μm with a resolution up to 0.05 nm.

The uvspec program reads an input from standard input file containing the time and coordinates as well as atmospheric properties like ozone profile, surface pressure, solar zenith angles, various molecules, aerosol or cloud microphysics (Fig. 4.2). The absorption and scattering properties of these constituents may either be taken from the algorithms and databases provided with libRadtran or be provided by the user. The data are converted into optical parameters with an atmospheric shell. Boundary conditions are the solar spectrum at the top of the atmosphere and the reflecting surface at the bottom. LibRadtran provides several extraterrestrial solar spectra and various surface models. Radiances, irradiances, heating rates for the given optical properties and actinic flux are estimated with one of 10 available radiative transfer equation solvers. The uvspec program gives the user a choice of various radiative transfer solvers, e.g. the widely-used discrete ordinate SDISORT code by Stamnes et al. (1988) and Dahlback and Stamnes (1991) to accurately simulate radiances, a fast two-stream code to calculate approximate irradiance (Kylling et al., 1995), or a polarization-dependent code polRadtran (Evans and Stephens, 1991). Finally, the correction due to extraterrestrial solar irradiance, Earth-Sun distance, convolution with a slit function ect. are computed (Mayer and Kylling, 2005).

In the analysis presented in Section 6 two solvers were used: the DIScrete ORdinate Radiative Transfer solver (SDISORT) and a sophisticated three dimensional solver MYSTIC (Monte Carlo code for the phYSically correct Tracing of photons In Cloudy atmospheres) code (Mayer, 2009; Emde et al., 2010) that cannot be currently downloaded with the free package.

SDISORT

The discrete ordinate SDISORT method was developed by Chandrasekhar (1960), Stamnes et al. (1988) and Dahlback and Stamnes (1991). It solves the radiative transfer in 1-D quasi-spherical geometry and allows accurate calculations of radiance, irradiance, and actinic flux. The standard version of SDISORT, the DISORT solver developed by Stamnes et al. (1988) and Stamnes et al. (2000) is very well-tested and the mostly used 1-D radiative transfer solver, however, at the high zenith angles analysed in this thesis, the 3-D MYSTIC gives much more precise results.

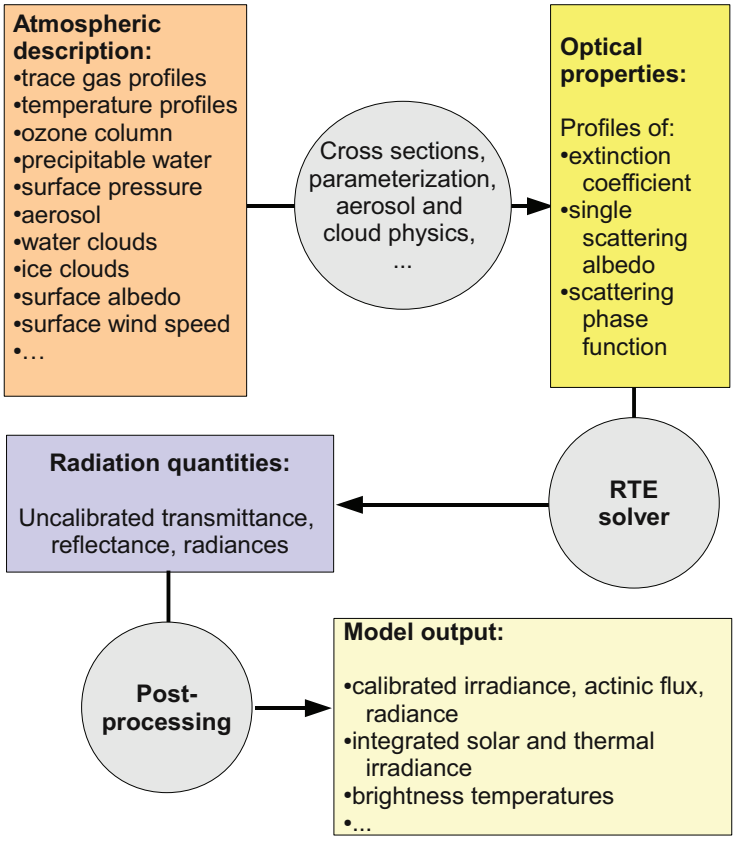

Figure 4.2: Structure of the libRadtran `uvspec` model. Diagram adopted from Mayer et al. (2011)

The SDISORT considers the transfer of monochromatic unpolarized radiation in a scattering, absorbing and pseudo-spheric medium, with a specified bidirectional reflectivity at the lower boundary and is customized for airmass calculations. The medium can be forced by a parallel beam and/or diffuse incidence and/or Planck emission at either boundary. It enables the inclusion of 2-D density profiles of trace gases. Intensities at user-selected angles and levels are the normal output. In addition to intensities, fluxes, flux divergences, and mean intensities are available as byproducts (or, optionally, the only products). Strongly

forward-peaked scattering is treated by the δ–M method (Wiscombe, 1977) with corrections of Nakajima and Tanaka (1988). Due to included thermal (Planck) emission, both internally and as a boundary condition, SDISORT is a suitable solver for thermal infrared and microwave applications in addition to solar-spectrum applications (Stamnes et al., 2000).

MYSTIC

Monte Carlo radiative transfer is a technique where individual photons are traced on their random paths through the atmosphere. The method enables a physically correct tracing of photons in cloudy atmospheres. MYSTIC uses this approach to calculate solar and thermal radiance, irradiance, and actinic flux. It has been used for remote sensing as well as for climate and photochemistry applications. It allows the definition of arbitrarily complex 3-D clouds, inhomogeneous surface albedo as well as topography.

In MYSTIC the photons are traced from a source, which can be either the sun or, in the thermal spectral range, the surface or an atmospheric constituent (molecule, cloud droplet, ice crystal, aerosol particle). The solar source is described by the extraterrestrial irradiance of the sun, while thermal emission is defined by the emission coefficient and the temperature. The end of the photon path is either absorption by an atmospheric constituent, absorption by the surface, or when the photon leaves the atmosphere at the top of the atmosphere.

Each photon is assigned an initial location and direction. For a solar photon the location will be at top of the atmosphere, at a random location in the x-y plane, assuming that the model domain is illuminated homogeneously by the sun. The direction is defined by the solar zenith and azimuth angles. In the thermal spectral range, the photon is emitted somewhere in the atmosphere. The selection of the photon start locations is made according to the emission coefficient and the temperature. The chosen coefficient and temperature values have to ensure that after many photons the distribution of emitted photons will follow the product of the emission coefficient and Planck function.

Photons are traced from scattering to scattering. Absorption is considered implicitly, by

reducing the photon weight by the Lambert-Beer factor:

$$\exp(-\tau_{\text{abs}}) = \exp\left(\sum_{\text{cells}} l_i \cdot k_{\text{abs},i}\right), \tag{4.1}$$

where l_i is the length which the photon travels in cell i – determined by geometry and $k_{\text{abs},i}$ is an absorption coefficient. Interaction with the surface is either treated by actually absorbing the photon if it is not reflected, or by always reflecting the photon in a random direction and reducing the photon weight by multiplying it with the Lambertian albedo or bi-directional reflectance distribution function[6] (Mayer, 2009). The MYSTIC runs can be made for desired amount of photons. Increasing the number of photons results in longer run time, but increases also the accuracy of a simulation.

MYSTIC is a forward/backward Monte Carlo code with model atmosphere consisting of a 1-D background of molecules and aerosol particles and a 3-D grid of cloudy cells. A schematic diagram of the algorithm is shown in Figure 4.3. The involved physics is simulated as closely as possible on the basis of the input atmosphere, without any further simplifying assumptions. MYSTIC as well as SDISORT do not consider refraction of the sun beams in the Earth's atmosphere.

4.2.2 UMD radiative transfer model

The University of Maryland (UMD) Radiative Transfer Model is based on an early version of the FastJX model (Wild et al., 2000; Bian and Prather, 2002) that was used in numerous climate models and publications (Neu et al., 2007; Binkowski et al., 2007; Voulgarakis et al., 2009).

In the UMD model the radiation field is calculated at each time step. The model includes absorption by molecular oxygen, nitric oxide and ozone as well as first-order molecular scattering, but does not consider clouds. The spectral resolution of the model equals 5 nm. The incident light is assumed to be unpolarized. The attenuation of the direct solar flux is calculated by integrating through the atmosphere in the direction of the sun. The calculation takes into account both sphericity and changes in local solar time along the path. Refrac-

[6] a four-dimensional function defined by Nicodemus (1965) that specifies the directional reflectance and emissivity of an opaque surface

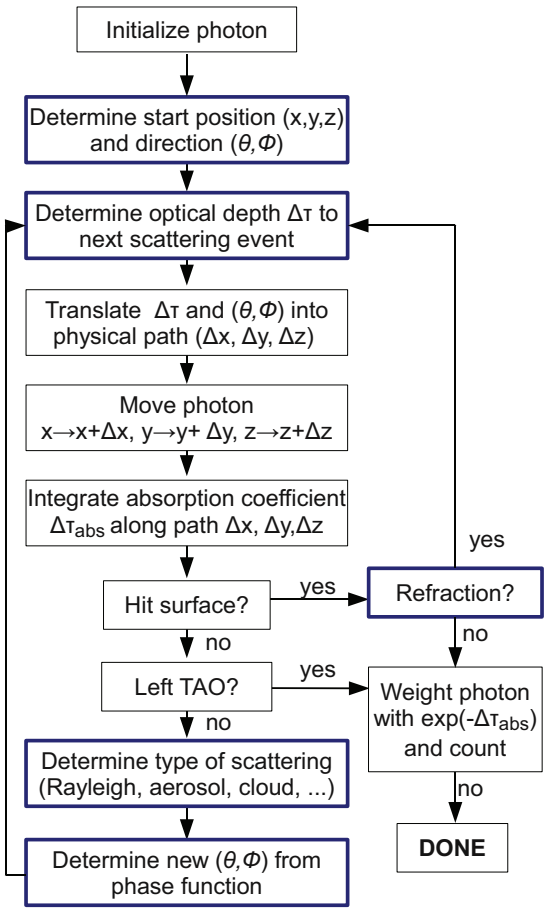

Figure 4.3: Schematic diagram of the basic MYSTIC model for surface irradiance calculation. The blue-framed boxes include a random number. TAO corresponds to 'top of the atmosphere'. Adopted from Mayer (2009).

tion is not included. This direct solar flux is the source function used to calculate the diffuse radiation in an inhomogeneous scattering atmosphere (Prather, 1981; Minschwaner et al., 1993). Due to assumptions made in the routines of this model, the run time is short when comparing with SDISORT and MYSTIC, but the accuracy is lower.

5 The self-match flight

The idea behind a self-match flight is to sample the same air masses twice during outbound and inbound flight legs of the same flight as has been described by Schofield et al. (2008). The analysis of the self-match flight described in this thesis was published by Sumińska-Ebersoldt et al. (2011). Here, additional information (atmospheric conditions on the flight track, temperature and solar zenith angle in the air masses prior to the flight ect.) and more elaborated sensitivity studies (influence of clouds, aerosol, photolysis quantum yield, ect.) are included. The impact of actinic flux on ClOOCl photolysis rates is discussed in Section 6 and constraints on J_{ClOOCl} are investigated in Section 7.

The self-match flight was carried out on 30$^{\mathrm{th}}$ January 2010 from Kiruna (67°49'N, 20°20'E), Sweden, as part of the large aircraft field campaign within the European project RECONCILE, employing the Russian research aircraft M-55 Geophysica with a ceiling altitude of 20 km. 17 partners from 9 different countries took a part in the RECONCILE campaign, information on the measurements and data acquired during the campaign is summarized by von Hobe et al. (2011).

Location and timing of the self-match flight were planned as to direct the aircraft into a region of elevated ClO_x levels. This was identified prior to the flight using the chemistry-transport model CLaMS (see Section 4.1) in the forecast mode. Coordinates and timing of the match points were calculated by Ralph Lehmann from Alfred Wegener Institute for Polar and Marine Research in Potsdam, Germany. Air mass trajectories for the motion of individual air parcels between the two encounters were calculated based on data from the European Centre for Medium-Range Weather Forecasts (ECMWF). Ninety-five match trajectory start points were defined by the one-minute time intervals at which ClO was measured on the outbound flight leg. Forward trajectories were calculated until 12:00 UTC

of 30th January with 1 minute time resolution. The points with the lowest distance to the inbound flight track were then defined as pairing match points. The flight track and match-pair trajectories, as well as solar zenith angle, pressure and potential temperature prevailing on the track are shown in Fig. 5.1.

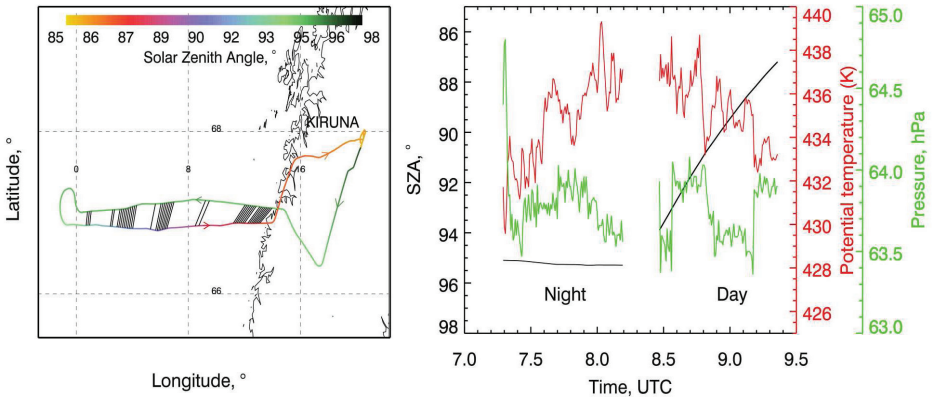

Figure 5.1: On the left hand side the flight path of the RECONCILE self-match flight on 30 January 2010 is plotted. The solar zenith angle on the track is represented by the colour scale. The black lines between outbound and inbound parts of flight represent the trajectories of the match pairs fulfilling the strict match conditions (cf. Section 5.2). Atmospheric parameters (solar zenith angle, pressure and potential temperature) on the outbound and inbound self-match flight legs are plotted on the right hand side.

To enable the analysis of the SZA dependence of J_{ClOOCl} and put limits on the probable J_{ClOOCl} values, the flight was carried out over sunrise, with the first measurements still in darkness (i.e. with no active photolysis reactions and the chemical system expected to be in thermal equilibrium), and the second (matching) measurement in daylight, moving from higher to lower solar zenith angles (i.e. increasing solar radiation and photolysis rates) over the course of the inbound flight leg as is shown in Fig. 5.1. This was achieved by a nearly sun-synchronous flight pattern in westward direction for the outbound flight leg and the inbound flight leg coming back in eastward direction.

5.1 Measurements

ClO was measured by the HALOX instrument (see Section 3) situated in a pod underneath the left wing of the Geophysica aircraft (von Hobe et al., 2005). Nitric oxide (NO), converting ClO to Cl atoms, was added to ambient air flowing through measurement ducts periodically with 10 s cycles. In the study presented here, the differences between ClO measurements on the outbound and inbound flight legs are investigated. Therefore, most critical for the analysis is precision, which varies between 4% and 8% depending on the stability of the light source (helium discharge lamps containing chlorine) and on the observed detector noise. Random noise is reduced and signal-to-noise-ratio increased by integrating the signal over six NO addition cycles, yielding a time resolution of 1 minute.

In the analysis below, the combined systematic (accuracy) and random (precision) error were used and fully propagated into calculations of differences between data from the outbound and inbound flight legs. This is a conservative estimate, because some of the systematic errors will cancel out. However, there are parameters leading to such errors that can potentially change over the course of a flight (e.g. lamp output and contribution from different spectral lines), and the full consideration of all errors ensures the significance of the results demonstrated in Section 7.

Temperature and pressure plotted in Fig. 5.1 were measured using commercial Rosemount sensors and geolocation data were provided by the Geophysica avionic system.

To examine the accuracy of matches (cf. Section 5.2), measurements of nitrous oxide (N_2O) were used. This trace gas is expected to be unaffected by chemical processes on the time scale of the self-match flight and thus should show conserved mixing ratios. Nitrous oxide was measured by the 2-channel gas chromatograph HAGAR (High Altitude Gas Analyser, Volk et al., 2000) with a time resolution of 90 s. Mean precision and accuracy are better than 1% and 2% of the tropospheric background value, respectively.

Additionally, the data of COPAS (COndensation PArticle Counting System, Weigel et al., 2009) enabled an identification on exhaust particles from the Geophysica engines on the inbound flight leg. COPAS consists of an aerosol inlet and two dual-channel continuous flow Condensation Particle Counters (CPCs) and enables measurements of number concentra-

tions of the particles with diameters of 6 nm, 11 nm and 15 nm. The particles are detected in three channels operated with distinct temperature differences between the saturator and the condenser block. An other channel is operated with an aerosol heating line for a determination of the number of non-volatile particles. In the COPAS data, the exhaust gases of Geophysica were observed several times on the inbound flight leg confirming the good performance of the self-match flight.

The ascent and descent data from the modified Forward Scattering SpectrometerProbe (FSSP, with newer electronics; Dye and Baumgardner, 1984) and a Cloud Imaging Probe (CIP, Baumgardner et al., 2001) from University of Mainz enabled the parameterisation of the clouds layer below the flight track and thus the estimation of the actinic flux.

5.2 Matches

Match points on the inbound flight leg corresponding to those on the outbound leg were found by minimising the horizontal radius around the coordinates of the Geophysica track and finding the coordinates fitting in time on the CLaMS forward trajectories. As shown in Fig. 5.2, the match radii R_{match} were always smaller than 8.5 km. To define a successful match pair, the vertical difference, in terms of potential temperature (Θ) was also considered. Here, $\Delta\Theta$ is defined as a difference between Θ measured in the matching locations of observations on the out- and inbound flight legs and successful matches are considered for $\Delta\Theta < 2.0$ K. The vertical ClO gradient measured during descent was 15 ppt K^{-1} resulting in a ClO gradient smaller than the measurement uncertainty for a 2 K change in potential temperature.

To ensure good quality of the matches, observations of the long-lived tracer N_2O by the HAGAR instrument were used. Match pairs, with differences between N_2O measured on the outbound and inbound flight legs larger than the precision of HAGAR for the relevant data points (~1.6 part per billion by volume, ppb), were rejected. With few exceptions, the tracer measurements confirm an excellent match performance (Fig. 5.2, lower panel), as do several encounters of the Geophysica exhaust on the inbound flight leg identified by COPAS observations on the inbound flight leg.

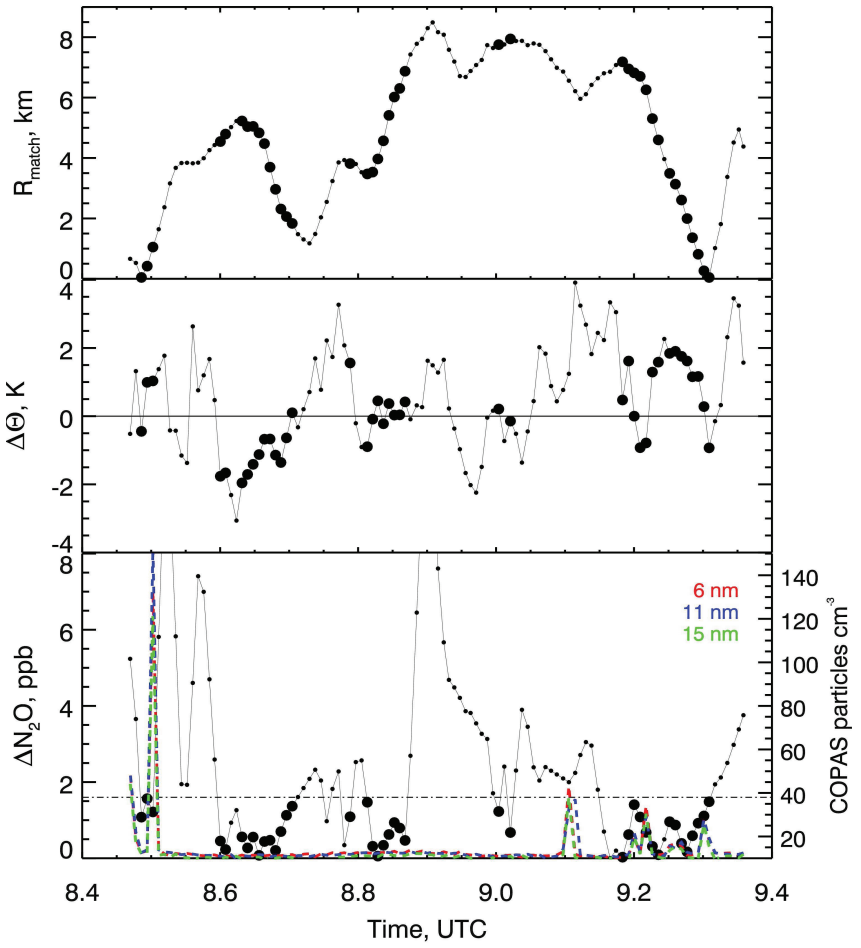

Figure 5.2: Performance of the match-flight. The upper panel and the middle panels show the horizontal and the vertical match accuracy in form of match radii R_{match} (in km) and potential temperature difference $\Delta\Theta$ (in K), respectively. Differences in the mixing ratios of N_2O are shown in the lower panel. The dashed horizontal line corresponds to the HAGAR N_2O measurement precision of 1.6 ppb. The red, blue and green lines represent the COPAS measurements. The increase of particle number concentrations indicates the Geophysica exhaust trail encounters.

Forty-one out from 95 match pairs fulfilled the location ($R_{\mathrm{match}} < 8.5$ km, $\Delta\Theta < 2$ K) and trace gas ($\Delta N_2O < 1.6$ ppb) conditions. Those are marked by large black circles in Fig. 5.2.

5.3 Equilibrium constant estimation

J_{ClOOCl} gives information on the rate of change of ClOOCl/ClO due to photolysis of ClOOCl. Therefore, to estimate this parameter, ClO and ClOOCl concentrations have to be known. Since during the self-match flight, the ClOOCl concentration ([ClOOCl]) was not measured, it has to be estimated from the equilibrium constant K_{eq}, which equals the ratio of [ClOOCl]/[ClO]^2. However, as shown in Section 2.2, there exist large discrepancies in published values of K_{eq}.

The estimation of K_{eq} from ClO measurements and Cl_y information is made in Section 5.3.2. In the following Section, the history of the investigated air masses is discussed to identify the probability of the thermal equilibrium on the outbound flight leg.

5.3.1 Backward trajectories analysis

A state of equilibrium exists when the rate of the forward process equals the rate of the reverse process. It means, when the [ClO] and [ClOOCl] at given conditions do not change significantly. To reach this state, no heterogeneous chlorine activation and no photolysis should occur in the investigated air mass for defined time. The relaxation time of the system depends on the concentrations of ClO_x(=ClO+2ClOOCl). Figures 5.3 and 5.4 show temperatures and solar zenith angles calculated on the backward trajectories of the outbound flight points. The simulation was made with CLaMS (Section 4.1), as input information, the coordinates and atmospheric parameters measured aboard Geophysica were used. Air mass trajectories for the motion of individual air parcels were calculated based on ECMWF data.

Figures 5.3 and 5.4 reveal that the investigated air masses had been in darkness longer than 15 hours prior to the flight and during the 15 hours temperature did not fall below 196.6 K on any of the trajectories. This finding rules out significant contributions to ClO rise from photolysis of Cl_2 released during very recent heterogeneous activation (see Section 1.2.2).

To asses if the time spend in the darkness is sufficient for the system to reach equilibrium, one has to consider the relaxation time of the system depending on the reactive

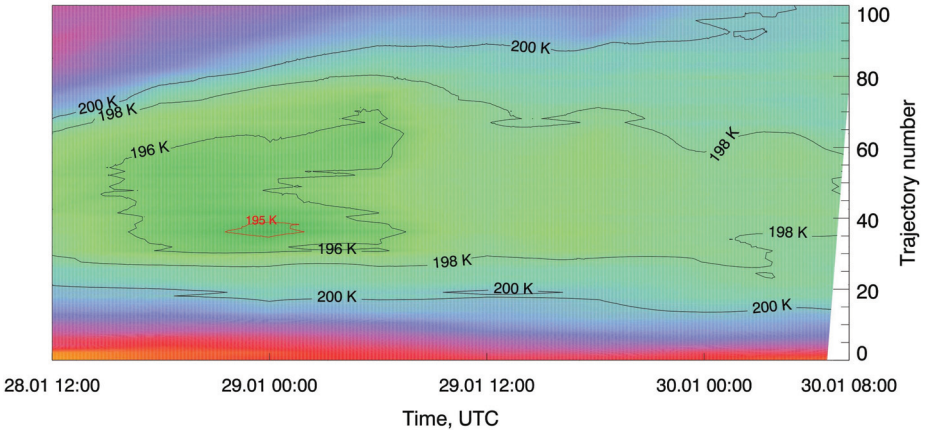

Figure 5.3: Temperature history of the air masses sampled on the outbound flight leg.

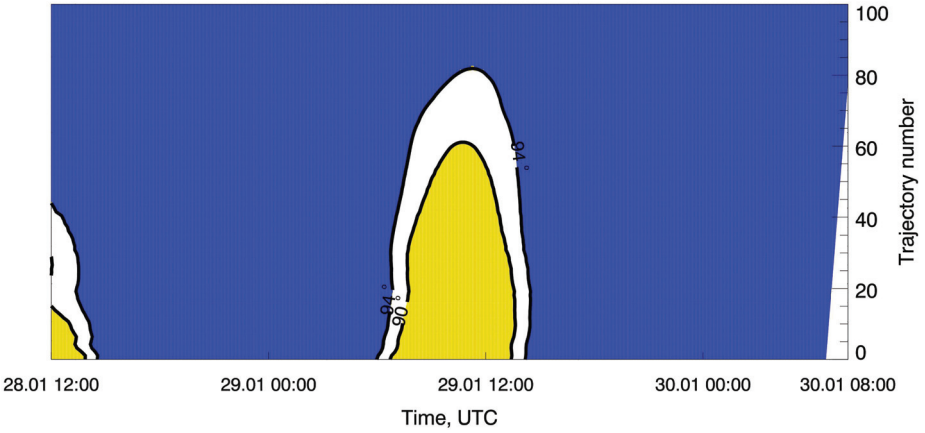

Figure 5.4: SZA history of the air masses sampled on the outbound flight leg.

chlorine ClO_x mixing ratios. From the night-time ClO measurements and different K_{eq}, possible values of ClO_x mixing ratios were estimated between 1500 and 2500 ppt. For three ClO_x values within those limits and pressure and temperature in the air masses on their backward trajectories, the relaxation time was calculated. Figure 5.5 shows results of the calculations and indicates that 15 hours are enough for the studied system to reach its equilibrium state. This result justifies the assumption of thermal equilibrium for the outbound flight leg (von Hobe et al., 2005).

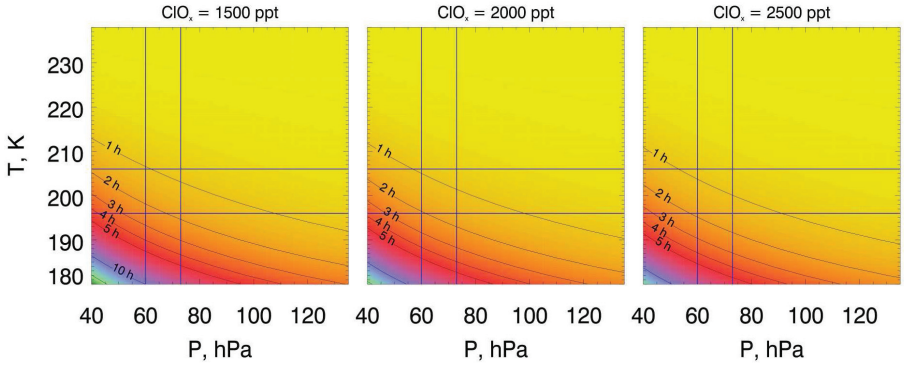

Figure 5.5: Relaxation time of the ClO/ClOOCl system into thermal equilibrium ($ClOOCl/[ClO]^2 > 0.8\,K_{eq}$) for ClO_x equal 1500, 2000, 2500 ppt. The blue lines show minima and maxima of the pressure and temperature values observed on the backward trajectories. The idea of the plot is taken from von Hobe et al. (2005).

5.3.2 Night-time ClOx chemistry

As shown above, the air masses on the outbound flight leg can almost certain be assumed to be in thermal equilibrium state. Therefore, to estimate the ClO increase due to ClOOCl photolysis, the concentration of ClOOCl during the night can be obtained using Eq. 2.8. Figure 5.6 shows ClO_x mixing ratios calculated from the night-time HALOX ClO measurements and K_{eq} by Plenge et al. (2005), Ferracci and Rowley (2010) and JPL 2011. An upper limit for ClO_x is given by the total inorganic chlorine Cl_y, which was obtained from the tracer-tracer correlation with N_2O valid for the year 2000 and published by Grooß et al. (2002).

The N_2O increase of 2.4% over the past 10 years was taken into account while no significant change in stratospheric Cl_y was assumed. With this assumption, the formula was estimated

$$\begin{aligned} Cl_y &= 3.394 + 0.001648 * N_2O - 7.659 \times 10^{-5} * N_2O^2 \\ &\quad + 2.646 \times 10^{-7} * N_2O^3 - 4.469 \times 10^{-10} * N_2O^4 \end{aligned} \tag{5.1}$$

N_2O and Cl_y are given in ppb and the relation is valid for N_2O values between 17 – 320 ppb.

For the observed night-time ClO, only K_{eq} from Plenge et al. (2005) seems plausible. Values of K_{eq} taken from studies of Ferracci and Rowley (2010) and JPL 2011 would result in ClO_x exceeding Cl_y. Therefore, in this study, K_{eq} from Plenge et al. (2005) is used to estimate ClOOCl (green circles in Fig. 5.6) for the further analysis described in Section 7.

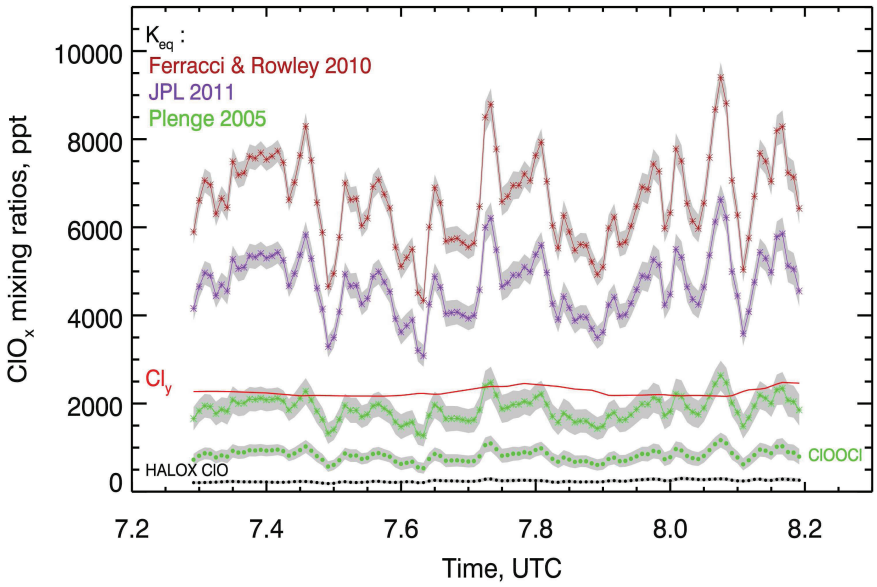

Figure 5.6: ClO_x mixing ratios derived from HALOX ClO night measurements (black circles) in combination with three chosen K_{eq}. ClOOCl mixing ratios calculated with HALOX ClO and K_{eq} from Plenge et al. (2005) are represented by green circles. Grey areas show the uncertainties propagated from the HALOX ClO observations. The red line corresponds to Cl_y calculated from the correlation with N_2O (Eq. 5.1) measured by HAGAR.

6 Actinic flux in the lower stratosphere

Solar radiation is the driving force for many atmospheric processes. To obtain the photolysis rate constant J_{ClOOCl} (Fig. 2.5c), the ClOOCl photolysis cross sections are multiplied by the spectrally resolved actinic flux (Eq. 2.13). The actinic flux defines the total number of photons incident at a given point of the atmosphere and is the sum of the direct flux $I_{\mathrm{dir}}(\lambda)$ and the diffuse flux $I_{\mathrm{diff}}(\lambda)$ (cf. Eq. 2.14). At very high solar zenith angles, the former is often dominated by the latter (Zhang et al., 2010). Both of them depend on the atmospheric radiation field, which changes with wavelength.

The radiation field is affected by scattering and absorption by molecules, aerosol particles, cloud droplets and particles, and surface albedo. To assess, which of the photolysis cross sections are realistic, it is crucial to minimise uncertainties in the actinic flux determined for the RECONCILE self-match flight. In this Chapter, the sensitivity of the actinic flux as function towards various atmospheric parameters is described (Sections 6.2.1-6.2.4).

First, however, the results of calculations for clear sky conditions made with libRadtran/MYSTIC and the UMD radiative transfer models described in Section 4.2 are compared (Section 6.1). The UMD model was used by Stimpfle et al. (2004) and Schofield et al. (2008) for estimation of the kinetic parameters of ClO dimer cycle (Section 2) from their in-situ measurements. To be able to compare our result with those of previous studies, the actinic flux has to be calculated in a similar way. The UMD model, however, does not take into account cloud and aerosol particles and therefore, the more sophisticated libRadtran model is used for further analysis.

6.1 Model comparison for clear sky conditions

For the comparison, the same input data were used in both models according to the atmospheric conditions on the flight track of Geophysica on 30 January 2010 (Figure 5.1). Since not the whole flight was considered in the analysis, only the self-match part of the flight data was used for the calculation of the actinic flux. The runs were made for a pressure of 63.75 hPa corresponding to the mean flight altitude of ≈ 18 km, the mean temperature at the flight track of 198 K and solar zenith angles (SZA) between 88° and 94°. The albedo was set to 0.2, which seems to be a good approximation for a sea surface below the flight track (Jin et al., 2004).

The models were also constrained using temperature and ozone profiles taken from Microwave Limb Sounder (MLS) satellite observations from 30 Jan 2010 and averaged for the area between 60° and 68° N and 0° and 20° E. Both profiles are plotted in Figure 6.1.

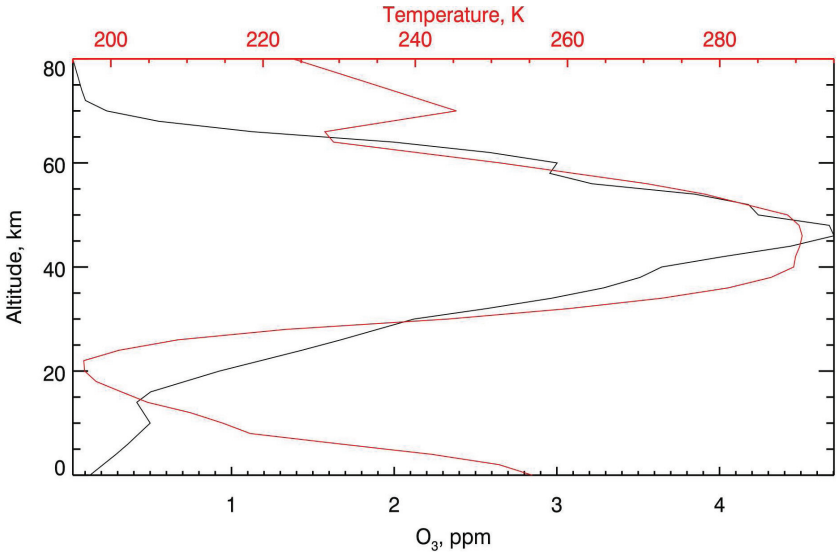

Figure 6.1: Temperature and ozone Microwave Limb Sounder (MLS) profiles from 30 Jan 2010 used for actinic flux calculations.

The UMD and libRadtran models determine the irradiance at the top of the atmosphere using different sources, hence differences occur when calculating photon fluxes. Figure 6.2

shows a comparison of photon fluxes at the top of the atmosphere employed in the two models. The extraterrestrial irradiance of libRadtran has a very high resolution and is a combination of Atlas[7] 3 (200 – 407.8 nm, Woods et al. 1996), Atlas 2 (407.8 – 419.9 nm, Woods et al. 1996), and Modtran 3.5 (419.9 – 800 nm, Christian and Gueymard 2004) spectra. The spectrum used in UMD is taken from the WMO (1985) Assessment Report. The discrepancies in photon flux are relatively small and result from the different spectral resolutions of 0.05 nm and 5 nm for UMD and libRadtran, respectively. When considering differences in the models, like spectral resolution, integral equations or geometry used for calculations in MYSTIC and UMD (cf. Section 4), the differences in the photon fluxes can be neglected.

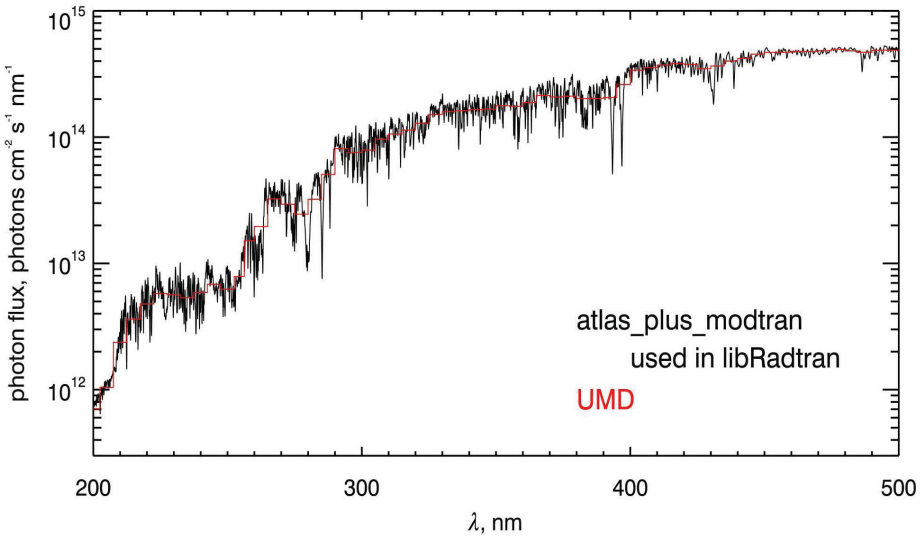

Figure 6.2: Photon flux at the top of the atmosphere in the UMD and libRadtran model. In libRadtran the combined ATLAS 3, ATLAS 2 and Modtran spectra are employed. UMD model uses the spectrum recommended in the WMO (1985) Assessment Report.

The most important part of all radiative transfer models is the procedure calculating the radiation field for a given distribution of optical properties. This procedure ranges from a variety of parametrisations and approximations to sophisticated and accurate solutions of

[7] stands for ATmospheric Laboratory for Applications and Science shuttle mission, the cyphers give the missions numbers, 2 corresponds to the mission from April 1993, and 3 to the mission from November 1994

the full three-dimensional radiative transfer equation. Once the radiative transfer equation is solved, a number of radiative quantities like actinic fluxes can be calculated. The detailed mathematical description of the derivation was described by e.g. Chandrasekhar (1960), Meier et al. (1982) and Lary and Pyle (1991a,b).

The radiation quantities are scalar. Most of the solvers use plane-parallel atmospheres, which means, that they neglect the Earth's curvature and assume parallel homogeneous atmospheric layers. For solar zenith angles less than about 70° this is a good approximation (Dahlback and Stamnes, 1991), but for higher SZA, a so-called pseudo-spherical correction, which treats the direct solar beam in spherical geometry and the multiple scattering in plane-parallel geometry is needed. SDISORT and UMD model both include pseudo-spherical corrections. The corrections, however, do not improve the results at sunset/sunrise conditions significantly. Therefore, for the calculations at SZA 88° – 94° a fully-spherical 3-D solver is required as implemented in MYSTIC .

Figure 6.3 shows the actinic fluxes obtained for the flight track of Geophysica on 30 January 2010 with the UMD and libRadtran/MYSTIC model. For the runs the temperature and ozone MLS profiles (cf. Fig. 6.1), albedo equal 0.2 and surface pressure of 1000 hPa were used. No aerosol and clouds were taken into account. The figure shows that despite differences in photon fluxes and molecular scattering implementation (first-order in UMD and multiple in libRadtran/MYSTIC), at solar zenith angles between 92° and 88° the two radiative transfer models give very similar results. However, at higher solar zenith angles, significant differences appear and at SZA of 93° and 94°, the actinic fluxes calculated with UMD are considerably lower than those from libRadtran reaching 30% difference at 500 nm at 94°. During sunrise, only diffuse radiation reaches the air masses. That implies that the discrepancies in models do not concern the direct actinic flux $I_{\mathrm{dir}}(\lambda)$, but the diffuse flux $I_{\mathrm{diff}}(\lambda)$, which depends on the molecular scattering.

To compare the influence of those differences on $J_{\mathrm{ClOOCl}}(\lambda)$, as an example, σ_{ClOOCl} published by Papanastasiou et al. (2009) was extrapolated to 500 nm (recommended in JPL 2011) and implemented into the two models. The spectra adopted for the UMD and libRadtran models are plotted in Figure 6.4. The curves represent the same data set, the only

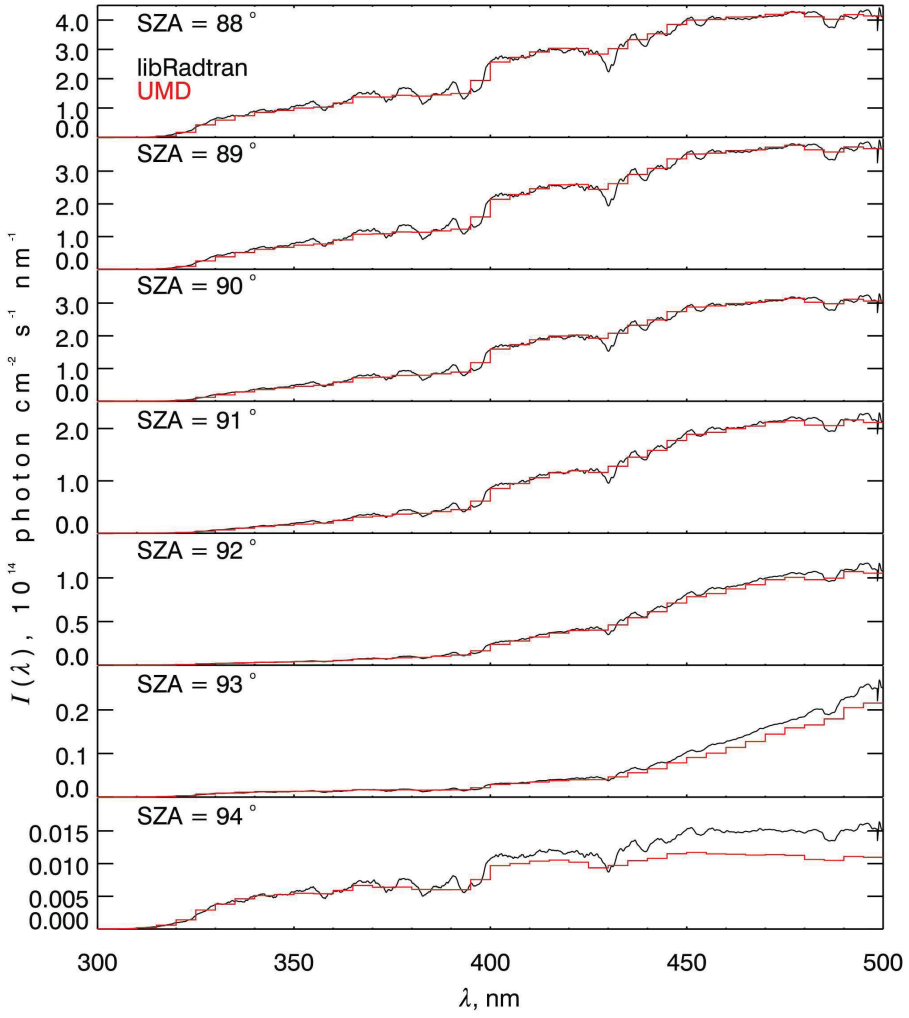

Figure 6.3: Actinic fluxes $I(\lambda)$ at solar zenith angles between 88° and 94° obtained from UMD (red lines) and libRadtran/MYSTIC (black lines) model runs.

difference is the spectral resolution.

The partial $J_{\mathrm{ClOOCl}}(\lambda)$ values presented in Figure 6.5 were calculated by multiplying the actinic fluxes plotted in Figure 6.3 and the $\sigma_{\mathrm{ClOOCl}}(\lambda)$ plotted in Figure 6.4 (Eq. 2.13 without integration). The quantum yield was assumed to be $\phi = 1$ independent of wavelength.

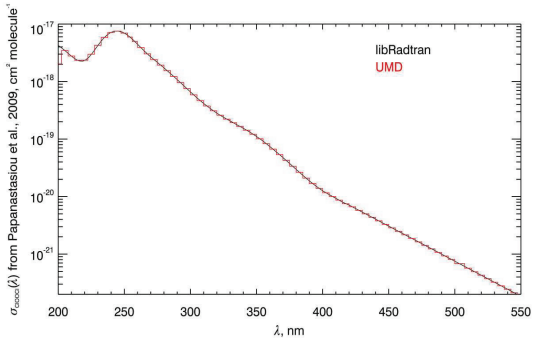

Figure 6.4: $\sigma_{ClOOCl}(\lambda)$ spectrum taken from Papanastasiou et al. (2009), extrapolated as recommended by JPL 2011 and adopted for UMD and libRadtran/MYSTIC calculations. The resolution of spectra is 5 nm in case of UMD and 0.05 nm for libRadtran/MYSTIC.

Figure 6.5 shows that at SZA of 88° – 91° the UMD model values are lower than those from MYSTIC in all spectral regions, except in the range between 350 and 430 nm. The discrepancies at $\lambda < 350$ nm are relatively small and disappear completely at higher solar zenith angles. In this spectral region the relatively small differences are probably resulting from the resolution of wavelengths. At SZA 93° and 94°, discrepancies of approximately 6% occur at wavelengths greater than 400 nm. Those are propagating directly from the discrepancies in actinic flux observed in Figure 6.3 and are due to the molecular scattering representation in the models.

To estimate the effective J_{ClOOCl} in the atmosphere, the partial $J_{ClOOCl}(\lambda)$ plotted in Figure 6.5 has to be integrated over the atmospherically relevant wavelength region between 300 and 500 nm (Eq. 2.13). In Figure 6.6 J_{ClOOCl} is plotted versus solar zenith angles equal 88° – 94°. The figure indicates that due to the discrepancies in partial photolysis rates, the effective photolysis rate is lower for UMD at investigated solar zenith angles. This would result in slower ClO concentration increase during sunrise, when using the UMD values.

The calculations show that the choice of radiative transfer model may influence the results of chemistry model simulations. The inconsistency between UMD and libRadtran models at high solar zenith angles are of similar significance as the impact of the implementation of aerosols (maritime clean atmosphere from the Online Public Access Catalog (OPAC) database (Hess et al., 1998)) and low clouds (2.5 km) prevailing during the flight into the calculations. The influence of those factors is significant especially at 93° and 94° (cf. Fig. 6.6).

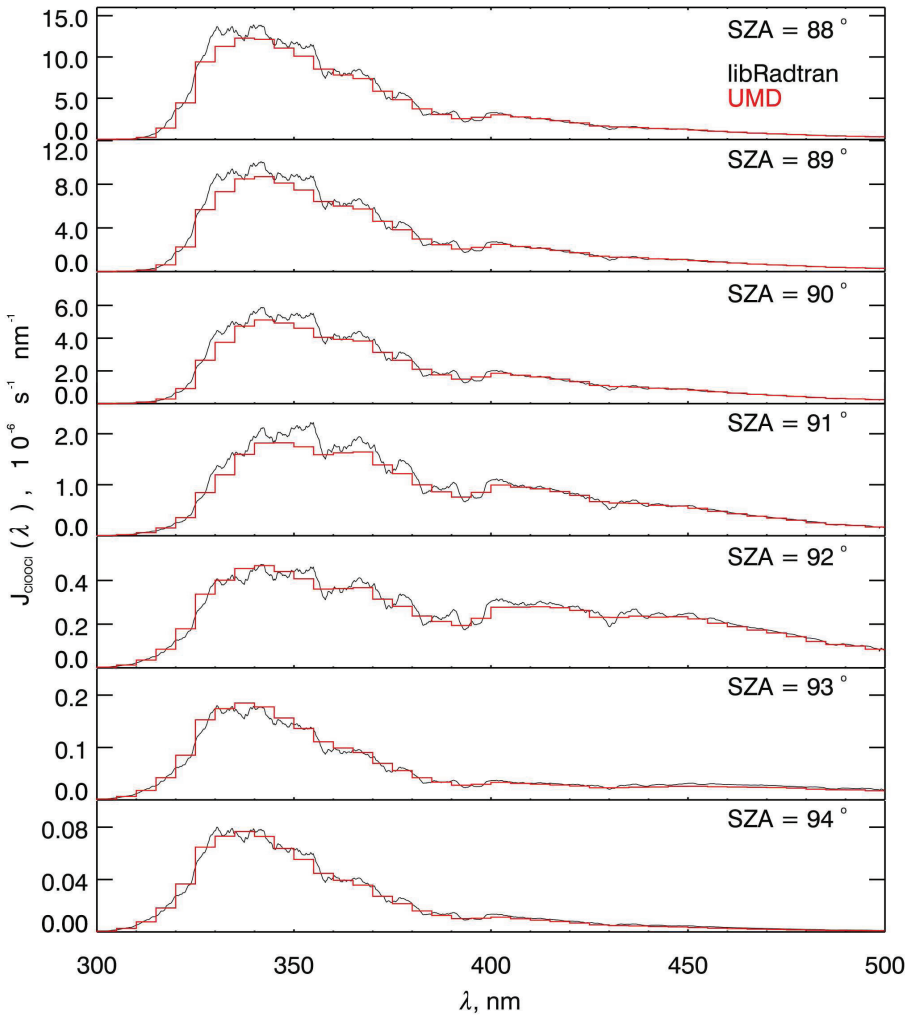

Figure 6.5: Partial $J_{ClOOCl}(\lambda)$ values resulting from UMD and libRadtran/MYSTIC runs for SZA between 88° and 94°.

6.2 Sensitivity studies

In the following sections, the influence of albedo, ozone column, clouds and aerosol on the actinic flux is investigated and the impact of refraction is discussed. Results were computed with the libRadtran model (cf. Section 4.2.1) with the 3-D radiative transfer equation solver

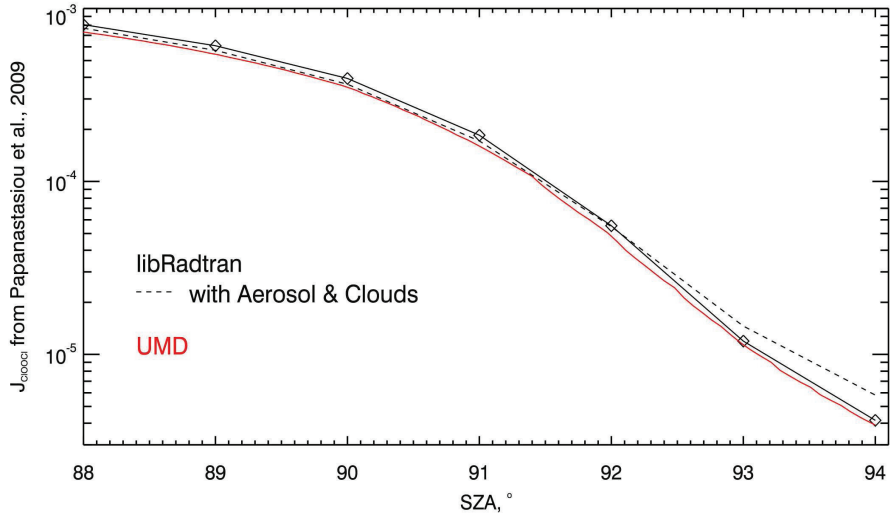

Figure 6.6: J_{ClOOCl} versus SZA estimated with UMD and libRadtran/MYSTIC. In the runs plotted with solid lines, no clouds and aerosol were considered. The dashed line shows results of MYSTIC run with considered cloud at 2.5 km and a maritime clean atmosphere from the Online Public Access Catalog (OPAC) database (Hess et al., 1998).

MYSTIC with full spherical geometry (Emde and Mayer, 2007) and the ALIS (Absorption Lines Importance Sampling) method to minimise the noise in high spectral resolution calculations (Emde et al., 2011). As shown above (Fig. 6.5), libRadtran provides better spectral resolution and the scattering routine is more sophisticated. Furthermore, the UMD model does not enable studies including clouds and aerosols.

For calculations of the actinic fluxes and corresponding partial $J_{\mathrm{ClOOCl}}(\lambda)$ values, a 'most realistic case' (MRC) was defined with:

- ozone profile taken from Microwave Limb Sounder (MLS) from 30$^{\mathrm{th}}$ January 2010 and averaged for the area between 60° and 68° N and 0° and 20° E (see Fig. 6.1)
- albedo fixed at 0.2 (seawater),
- a cloud layer at 2.5 km,
- a maritime clean atmosphere from the OPAC database (Hess et al., 1998) for the aerosol loading.

Additionally, for each of these atmospheric properties, upper and lower limits were estimated. That gives 3 cases of 4 atmospheric properties (ozone, albedo, clouds, aerosol) and thus 81 combinations. $J_{\mathrm{ClOOCl}}(\lambda)$ values were calculated with absorption cross sections published by Papanastasiou et al. (2009) and quantum yield of unity. Figures 6.7, 6.8, 6.11 and 6.12 showing the sensitivity of actinic flux $I(\lambda)$ and $J_{\mathrm{ClOOCl}}(\lambda)$ are plotted on the same scales.

6.2.1 Ozone

The total number density of molecules in the middle atmosphere is significantly lower than in the troposphere and the molecular scattering which occurs is strongly dependent of the wavelength. Therefore, the diffuse radiation field at short wavelengths is important, even if there are only a small number of scatterers in the stratosphere.

The MRC run was performed using the ozone profile plotted in Figure 6.1 and sensitivity runs were carried out with the same profile scaled to 200 and 500 DU respectively. While these values are unrealistically low and high, the results show that the sensitivity of the actinic flux towards ozone at studied zenith angles is low in the relevant wavelength region (Figure 6.7). The influence is visible only between 310 and 350 nm (Hartley and Huggins bands) and above 450 nm (Chappuis bands), giving rise to a spectral window with essentially no ozone absorption over a significant part of the ClOOCl spectrum.

The sensitivity propagates into $J_{\mathrm{ClOOCl}}(\lambda)$ providing a minor impact below 90° SZA due to the Hartley and Huggins ozone bands and above this angle also due to the Chappuis bands. The influence of ozone on J_{ClOOCl} at high solar zenith angles can therefore be neglected.

6.2.2 Albedo

The self-match portion of the flight was entirely over seawater, so the albedo was fixed at 0.2 for the MRC run (described at the beginning of Section 6.2). Again, extreme values of 0.05 and 0.8 were taken as lower and upper limits, and again, the sensitivity is very low at the zenith angles considered here. Under these conditions, the bulk of the actinic flux stands from diffuse downward radiation unaffected by the Earth surface. The sensitivity toward albedo shown in Fig. 6.8 is calculated for clear sky conditions, since clouds would

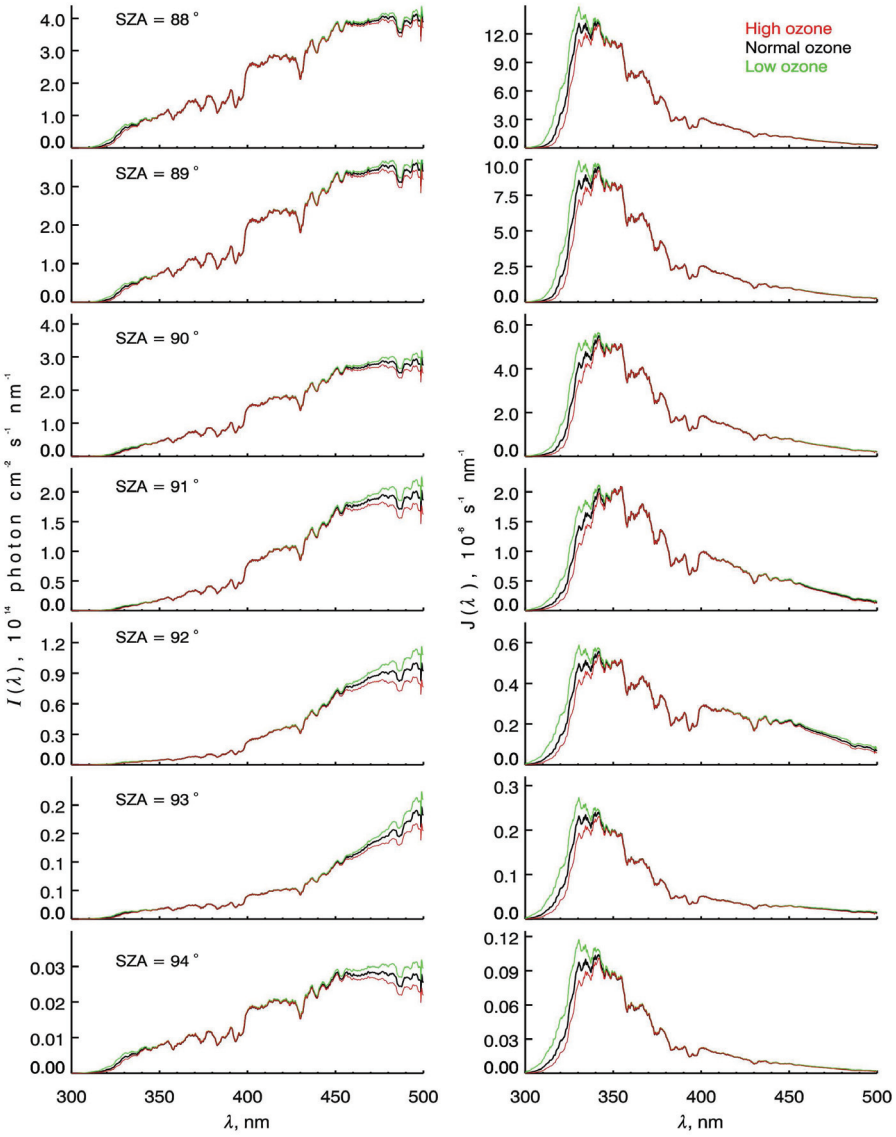

Figure 6.7: Actinic fluxes (left) and corresponding $J_{\mathrm{ClOOCl}}(\lambda)$ values (right) with ozone sensitivity for seven different solar zenith angles.

significantly reduce the albedo influence.

Considering how unrealistic the chosen albedo limits for the presented runs are, it be-

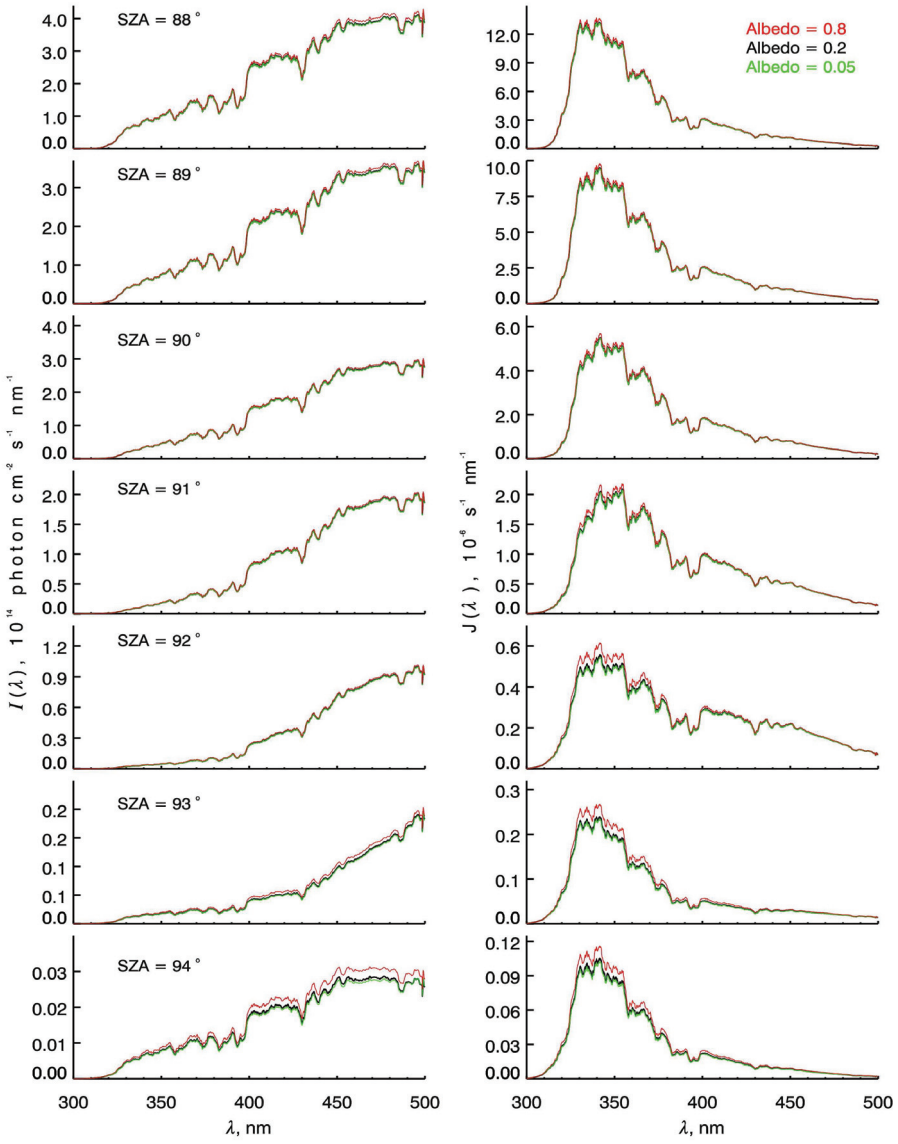

Figure 6.8: Actinic fluxes (left) and corresponding $J_{\mathrm{ClOOCl}}(\lambda)$ values (right) with albedo sensitivity for seven different solar zenith angles. To avoid influence of the cloud coverage, the sensitivity is calculated for clear sky conditions.

comes obvious, that the changes $I(\lambda)$ and $J_{\mathrm{ClOOCl}}(\lambda)$ due to increase in albedo of 0.1 are insignificant, at least at the altitudes between 17 and 18 km, where the measurements were carried out. The results confirm the studies of Anderson and Lloyd (1990), who wrote *'surface albedo variation can be important at solar zenith angles less than 60°, while in twilight virtually no direct solar flux reaches the surface, so that its importance is diminished.'*

6.2.3 Clouds

Numerical transfer of radiative transfer in clouds is a challenging task, due to their high spatial and temporal variability. In a cloud-free atmosphere (Section 6.1) daytime photolysis rates remain high down to the ground. Below optically thin clouds, photolysis rates are mostly enhanced, but in the lower part of thick clouds and beneath them, photolysis rates can be reduced several fold due to absorption. Above optically thick cloud decks, and even within the upper part of these clouds, photolysis rates can be twice as large as the corresponding clear-sky rates due to scattering (Chang et al., 1987; Madronich, 1987; Wild et al., 2000; Kylling et al., 2005).

During the self-match flight the downward looking lidar instrument MAL aboard the Geophysica indicated the presence of patchy clouds at altitudes up to 7 km. MODIS (Moderate Resolution Imaging Spectroradiometer) satellite images (http://www.sat.dundee.ac.uk) show that this cloud layer extended over a rather large region around the flight track (see Figure 6.9). To estimate the characteristic of this cloud, observations of FSSP and CIP (Section 5.1) from a flight on 2$^{\mathrm{nd}}$ February were used, because there are no CIP data available from the self-match flight.

On 2 February, two clouds at 2.5 and 6.5 km altitude were observed. They were parameterised based on FSSP and CIP observations. The cloud layer seen during the self-match flight at 7 km altitude was patchy and broken and therefore for the MRC the compact lower cloud at 2.5 km from 2 February was computed. The two clouds at 2.5 and 6.5 km were considered as an upper limit case in the sensitivity calculation and a cloud free atmosphere marked the lower limit case. The ice water content (IWC) and effective radius (R_{eff}) of cloud particles are listed in Table 6.1, the particle number size distributions $dN/dlogD$ versus their diameter in micrometers are plotted in Figure 6.10.

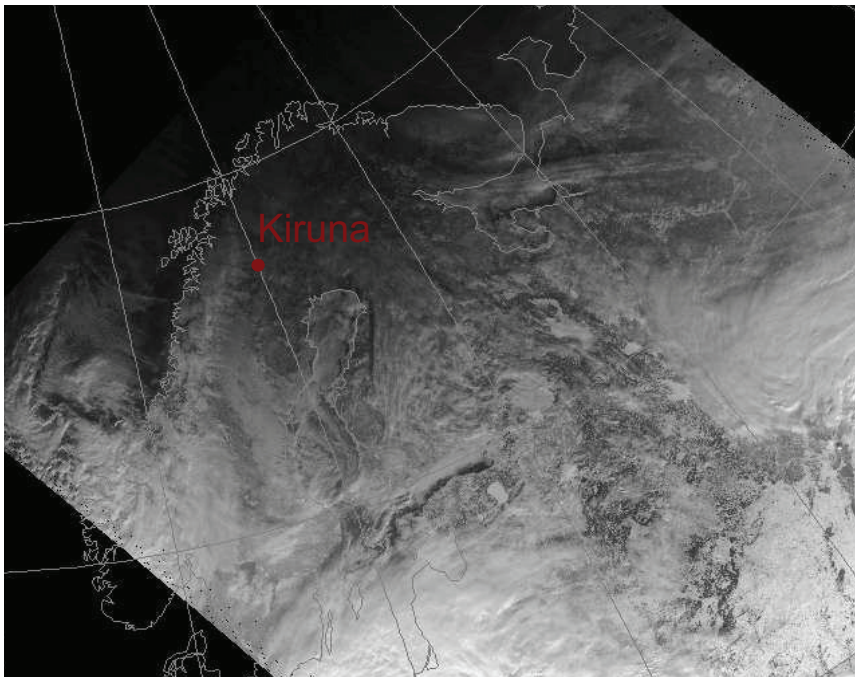

Figure 6.9: Satellite Aqua image of northern Europe from 30th January 2010: cloud conditions during the self-match flight. Photo from NERC Satellite Receiving Station, University of Dundee, Channel 3.

Results of the sensitivity studies are shown in Figure 6.11. The actinic fluxes and ClOOCl photolysis rates are not significantly affected at the altitude, zenith angles and wavelength relevant to this study. The cloud influence is even smaller than the effect of albedo and ozone.

6.2.4 Aerosol

The effect of aerosols on the Earth's climate is considered as one of the largest uncertainties in our understanding of climate change (IPCC, 2007). Aerosols scatter and absorb solar and terrestrial radiation and alter cloud properties. To quantify the aerosol impact, precise information is needed on aerosol microphysical properties such as size distribution, particle shape, refractive index, and chemical composition and on the resulting optical properties

Altitude, km	IWC, g/m^3	R_{eff}, μm
7.000	0	0
6.500	0.000769	113.55
6.000	0.000769	113.55
3.000	0	0
2.500	0.00814	218.76
2.000	0.00814	218.76
1.000	0	0

Table 6.1: Clouds characteristics used in sensitivity calculations. IWC corresponds to ice water content and R_{eff} effective radius of cloud particles.

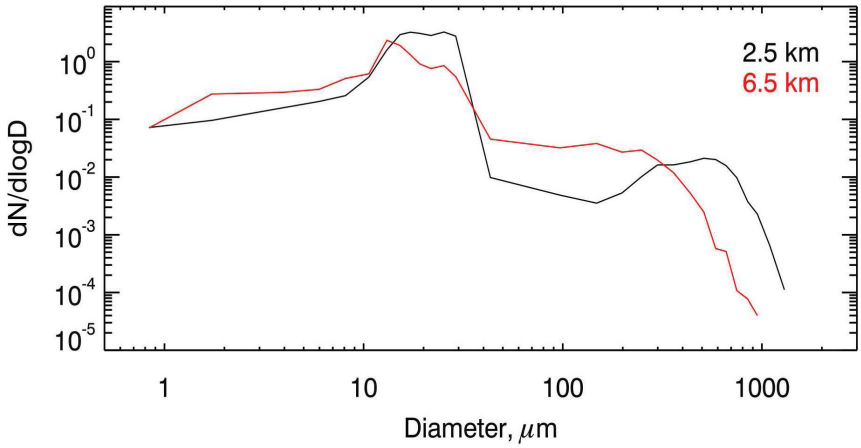

Figure 6.10: Particle number size distributions of the 2.5 and 6.5 km clouds taken from FSSP and CIP observations respectively and used in the sensitivity studies with libRadtran/MYSTIC.

(Emde et al., 2010). Therefore, for the atmospheric aerosol loading in the MRC, a default mixture of aerosol for a maritime clean atmosphere from the OPAC database (Hess et al., 1998) provided with libRadtran was used for the MRC case (Emde et al., 2010). Sensitivity runs were carried out with an aerosol free atmosphere and an aerosol profile with a higher optical thickness from an aerosol model by Shettle (1990).

The results of this study indicate that at $\lambda < 400$ nm aerosol plays a role at SZA above 91°. The influence is however very small. Above 400 nm, the influence is more significant and increases with increasing SZA. Starting at 91° SZA, the change in actinic flux becomes

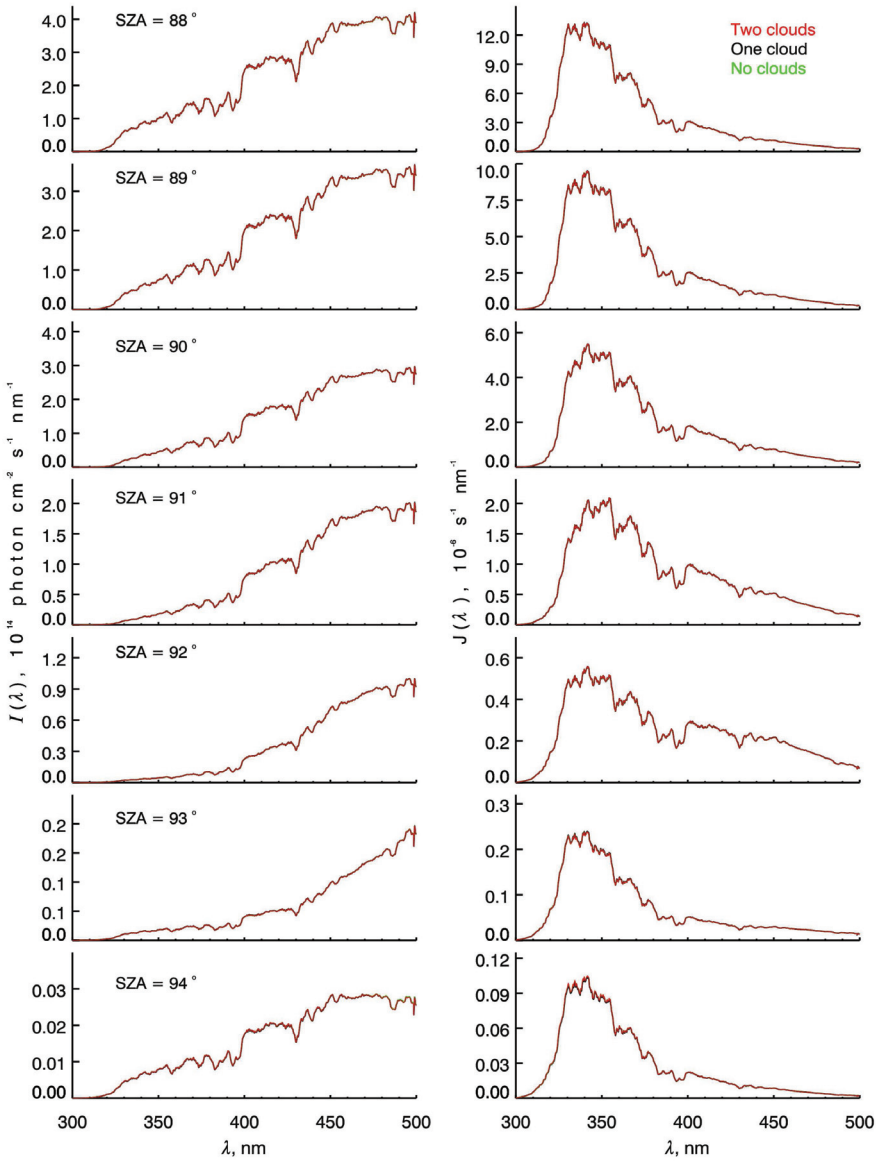

Figure 6.11: Actinic fluxes (left) and corresponding $J_{\mathrm{ClOOCl}}(\lambda)$ values (right) with clouds sensitivity for seven different solar zenith angles. The MRC run was made with one cloud at 2.5 km altitude. The 'two clouds' corresponds to the run with clouds at 2.5 km and 6.5 km altitude.

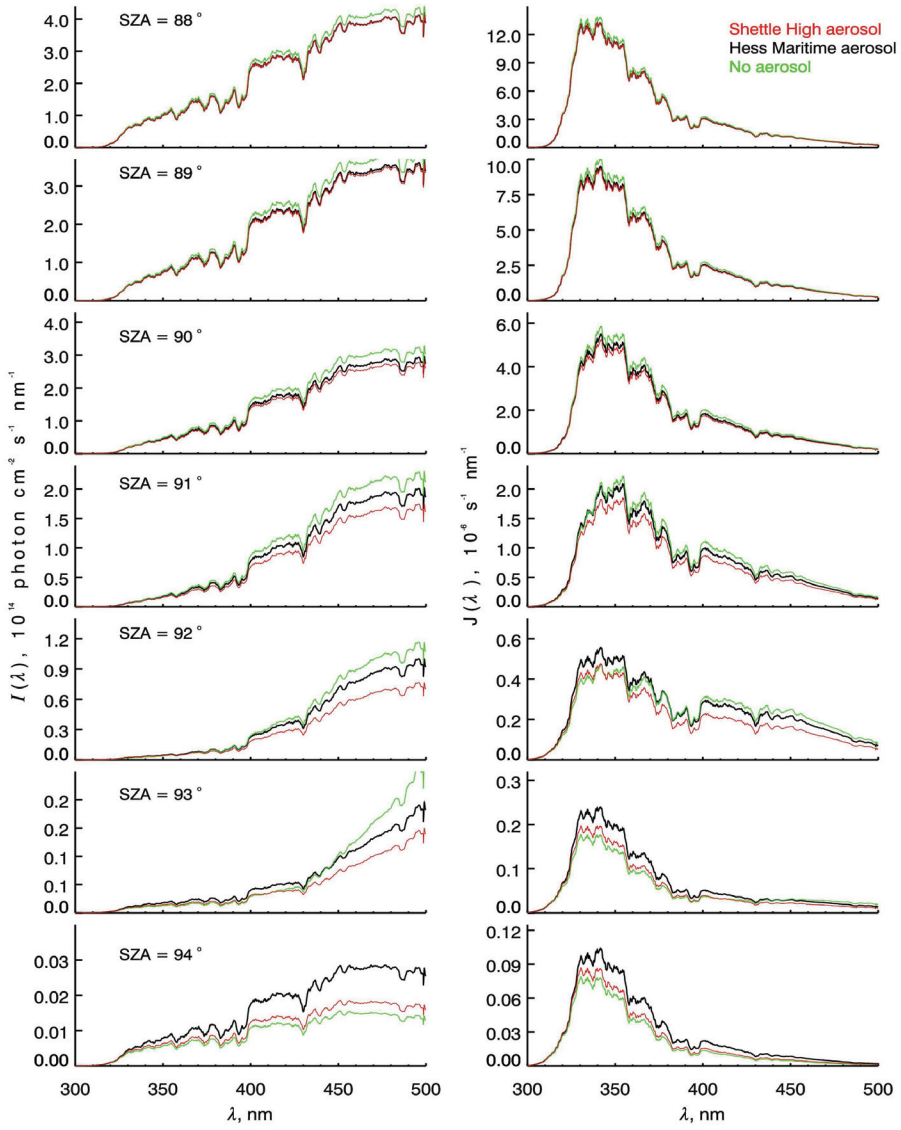

Figure 6.12: Actinic fluxes (left) and corresponding $J_{\mathrm{ClOOCl}}(\lambda)$ values (right) with aerosol sensitivity for seven different solar zenith angles.

important, for $J_{\mathrm{ClOOCl}}(\lambda)$, however, the impact causes only a minor difference.

The sensitivity studies showed that clouds and albedo had hardly any effect on $I(\lambda)$ and $J_{ClOOCl}(\lambda)$ during the self-match flight. Ozone and aerosol influence is also not very significant. The last factor that has to be investigated is refraction. None of the introduced models implements refraction and only an approximate estimation of its impact can be discussed.

6.2.5 Refraction

Refraction in the atmosphere is the bending of a light ray as it passes through the atmosphere due to the increase in the atmospheric density as the light ray travels downward toward the observer (Figure 6.13). Refraction affects atmospheric photochemistry by modifying the solar radiation field, i.e. is the amount of sunlight available in a given volume. The overall effect of refraction is to decrease the optical path and thus increase the amount of direct solar radiation for a given solar zenith angle (DeMajistre et al., 1995). Another very important effect of refraction is the extension of the sunlit day. DeMajistre et al. (1995) showed, that at 20 km, in the absence of refraction, the Sun rises at a solar zenith angle of ~94.5°, if refraction is considered the Sun is still visible when it is below the true horizon and rises at about 95.3°.

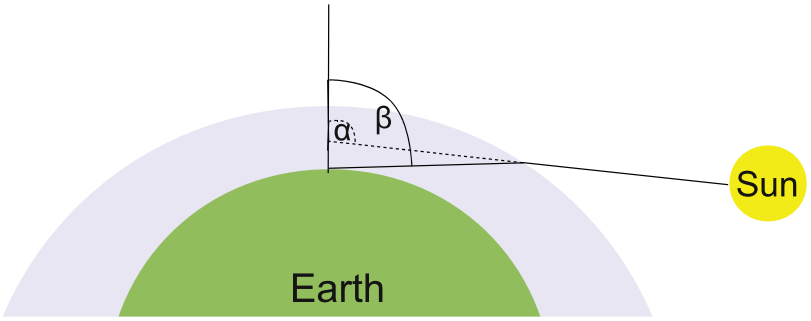

Figure 6.13: Refraction in the atmosphere. A refracted solar beam is drawn with solid black line, the dashed line shows the path for the same position of the sun without considering of the refraction. The solar zenith angle α (no refraction) is larger than β (with refraction).

Since in none of the libRadtran radiative solvers the refraction is implemented, the presented $I(\lambda)$ and therefore also $J_{ClOOCl}(\lambda)$ values are underestimated for SZA > 91°. DeMa-

jistre et al. (1995) and Trentmann et al. (2003) showed, that if refraction is included in a model, J_{ClOOCl} values will increase by 10 to 30% between 92° and 94° SZA.

7 Constraints on the ClOOCl photolysis rate

7.1 Investigated ClOOCl cross sections/spectra

In the analysis we compare the measured increase in [ClO] with the simulated increases resulting from J_{ClOOCl} based on the following four σ_{ClOOCl} data sets:

i) Pope et al. (2007) presented a ClOOCl spectrum giving the lowest absorption in the atmospherically relevant wavelength region (when scaled to any of the absorption peak cross sections plotted in Fig. 2.6) resulting in relatively small J_{ClOOCl} values. Pope et al. (2007) carried out an innovative experiment purifying ClOOCl prior to the absorption measurement, thus removing all impurities other than Cl_2. However, in their spectral analysis they probably overcorrected for the Cl_2 impurity as has been shown by von Hobe et al. (2009) (see below). The spectrum is scaled to measurements of Lien et al. (2009) to obtain cross sections (see Section 2.3.2).

ii) von Hobe et al. (2009) used the technique proposed by Pope et al. (2007) to prepare and purify ClOOCl, but measured the spectrum of a sample isolated in a neon matrix. In the atmospherically relevant region, their spectrum lies considerably higher than the Pope et al. (2007) spectrum but compares rather well to a Pope et al. (2007) gas phase spectrum uncorrected for Cl_2. The von Hobe et al. (2009) spectrum is also scaled to cross section obtained by Lien et al. (2009).

iii) Papanastasiou et al. (2009) measured absolute cross sections over a wavelength range from 220 nm into the visible. The new measurement improves an earlier study from the same laboratory (Burkholder et al., 1990). The two spectra have slightly different shapes but yield similar atmospheric J_{ClOOCl} values. The results presented by Burkholder et al. (1990) generally produced the best agreement in a number of studies

comparing modelled and observed ClO_x partitioning (Stimpfle et al., 2004; von Hobe et al., 2007; Schofield et al., 2008; Kremser et al., 2011) as well as ozone loss (Santee et al., 2003; Chipperfield et al., 2005; Frieler et al., 2006; Tripathi et al., 2006; von Hobe et al., 2007). Results of Papanastasiou et al. (2009) are recommended in JPL 2011 (Sander et al., 2011).

iv) An artificial spectrum based on Papanastasiou et al. (2009), but with a simulated σ_{ClOOCl} set constant to $7.12\times10^{-21}\mathrm{cm}^2\mathrm{molecule}^{-1}$ (measurement by Papanastasiou et al., 2009 at 420 nm) between 420 and 500 nm is used to test the possible existence of an additional ClOOCl absorption band in the visible.

From the four cross sections/spectra and the actinic fluxes $I(\lambda)$ taken from the calculations presented in Section 6, $J_{\mathrm{ClOOCl}}(\lambda)$ values are calculated and plotted in Figure 7.1. The solid lines show calculations made with quantum yield $\phi(\lambda) = 1$ and the dashed lines with $\phi(\lambda) = 0.9$. The differences between those lines are smaller than the uncertainty ranges due to ozone, albedo, clouds, aerosol and refraction impact on the actinic fluxes. In the following analysis, the highest possible $\phi(\lambda) = 1$ is used.

7.2 Constraints on ClOOCl photolysis from the observed increase in ClO

To compare the ClO mixing ratios resulting from the considered J_{ClOOCl} values with ClO mixing ratios observed during the self-match flight, the integrated ClOOCl photolysis rate constants effective in the atmosphere obtained by applying Eq. 2.13 with $I(\lambda)$ calculated for the MRC are used (cf. Section 6). The effective J_{ClOOCl} values with uncertainty resulting from the presented actinic flux investigation are plotted in Fig. 7.2 versus SZA. Clearly the differences resulting from the four different ClOOCl cross sections investigated in this study are greater than the uncertainty propagating from the actinic flux calculations.

The overall rate of change in ClO concentration resulting from reactions R1 - R4 is given by:

$$0.5\frac{d[\mathrm{ClO}]}{dt} = J_{\mathrm{ClOOCl}}[\mathrm{ClOOCl}] + k_{\mathrm{diss}}[\mathrm{M}][\mathrm{ClOOCl}] - k_{\mathrm{rec}}[\mathrm{M}][\mathrm{ClO}]^2 \qquad (7.1)$$

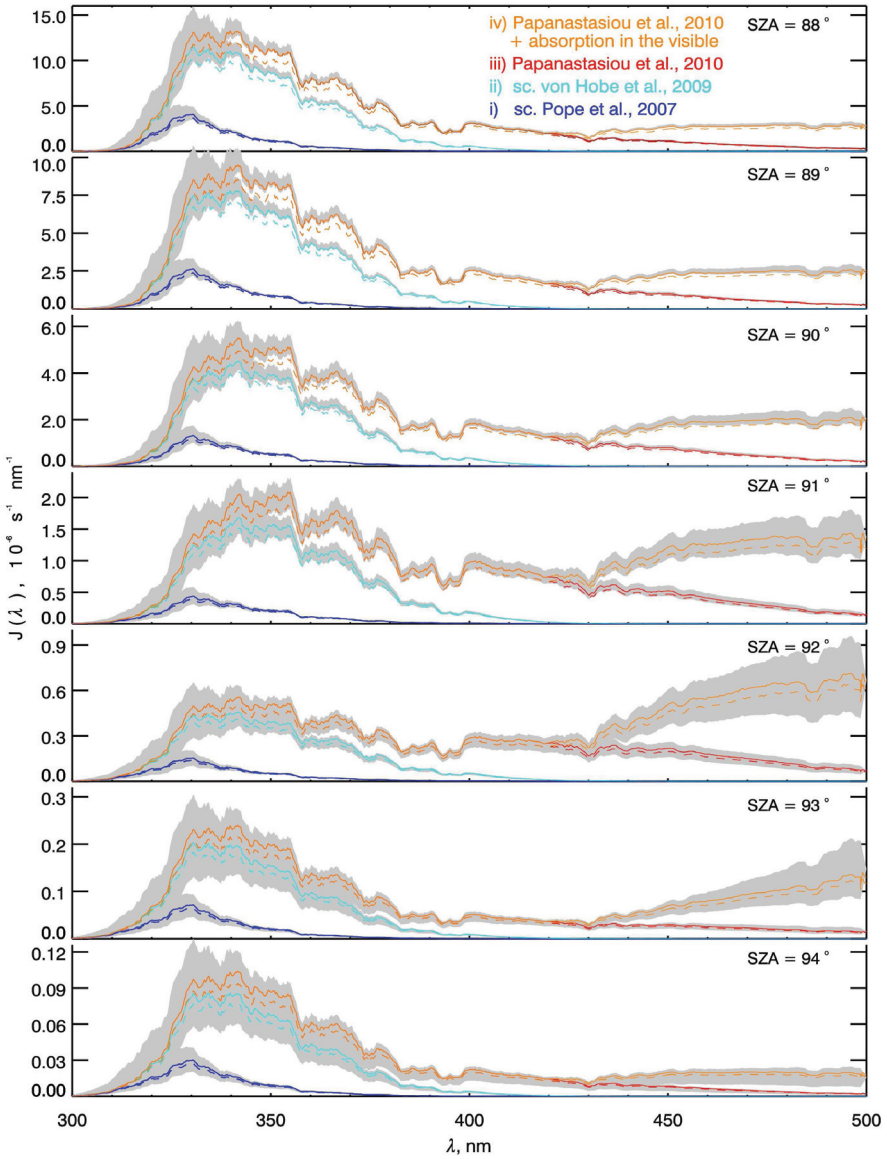

Figure 7.1: Partial ClOOCl photolysis rate constants calculated for four examined σ_{ClOOCl} with actinic fluxes from Section 6 and $\phi(\lambda) = 1$ (solid line) and 0.9 (dashed line). The grey area present a sum of uncertainties propagating from the $I(\lambda)$ uncertainties discussed in Section 6.2.

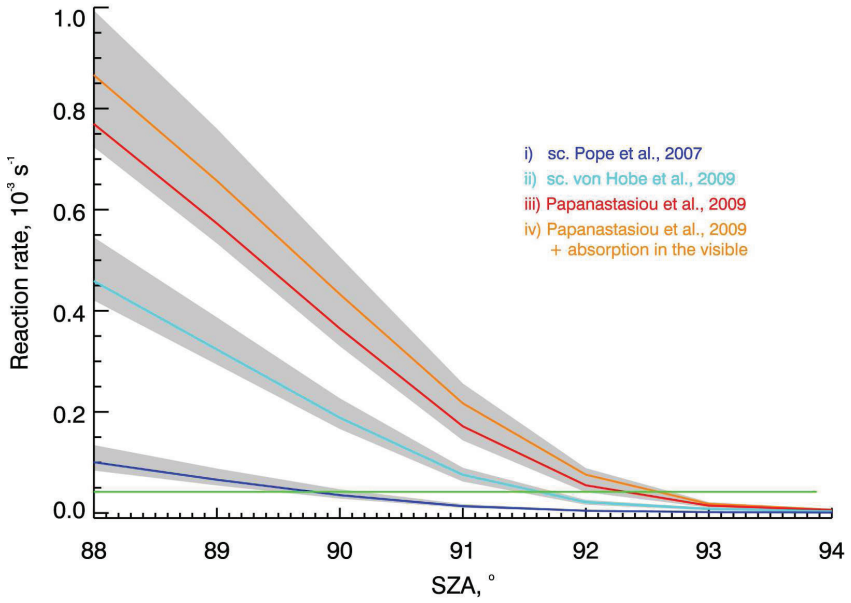

Figure 7.2: Photolysis rate constants based on cross sections i-iv versus solar zenith angle. The green line shows the thermal dissociation rate $k_{\mathrm{diss}}[M]$ for comparison. The constant k_{diss} was determined from the recombination constant taken from JPL 2011 and thermal equilibrium constant of Plenge et al. (2005). The number density $[M]$ was calculated for the mean temperatures and pressure on the track of the Geophysica during the self-match flight. The grey areas show uncertainties in J_{ClOOCl} resulting from uncertainties in the actinic flux.

Fig. 7.2 illustrates the SZA dependence of J_{ClOOCl} for the σ_{ClOOCl} i-iv for the conditions encountered during the RECONCILE self-match flight. The ClOOCl photolysis term is zero in darkness and rises more or less sharply, depending on the choice of σ_{ClOOCl}, as SZA decreases. Also shown is the ClOOCl thermal decomposition rate constant $k_{\mathrm{diss}}[M]$ for the mean temperature and pressure observed during the flight. In thermal equilibrium, the rate of ClO production from thermal decomposition of ClOOCl is expected to equal the removal rate via the ClO self-reaction, i.e. $k_{\mathrm{diss}}[\mathrm{M}][\mathrm{ClOOCl}] = k_{\mathrm{rec}}[\mathrm{M}][\mathrm{ClO}]^2$ and $d[\mathrm{ClO}]/dt = 0$. Thus, when the sun rises, ClO mixing ratios are expected to increase as soon as J_{ClOOCl} becomes large enough so that the photolysis reaction presents a significant additional ClO production term compared to the ClOOCl thermal decomposition. The photolysis

becomes more significant than the decomposition at different SZA for the different σ_{ClOOCl} tested and can be compared to the SZA when a significant rise of ClO concentrations is actually observed.

Fig. 7.3 shows that observed ClO starts to rise close to a SZA of 92°. Also shown is the simulated rise in ClO expected for the photolysis rates i-iv. It was calculated using

$$\Delta[\mathrm{ClO}] = 2 \times \int_{t(95^\circ)}^{t(\mathrm{SZA})} J_{\mathrm{ClOOCl}} \cdot [\mathrm{ClOOCl}]_{\mathrm{outbound}} \cdot dt \tag{7.2}$$

under the assumption that the ClO removal from the self-reaction (R18) is ignored. Strictly, this assumption holds true only at sunrise, i.e. when the first ClOOCl molecule is photolysed. $[\mathrm{ClOOCl}]_{\mathrm{outbound}}$ was calculated from observed night-time [ClO] and K_{eq} according to Plenge et al., 2005 (cf. Section 5.3.2 and Fig. 5.6). As SZA decreases, [ClOOCl] will become smaller and ClO removal via the self-reaction faster, both leading to a reduced overall rate of [ClO] increase. Thus, at the threshold SZA (Fig. 7.2), the observed [ClO] is expected to start rising simultaneously with the expected integrated [ClO] from ClOOCl photolysis and then falling more and more below the calculated [ClO] rise as SZA decreases.

For the scaled cross sections of Pope et al. (2007) i), [ClO] starts to increase much later and rises much slower than observed [ClO]. On the other hand, a significant ClOOCl absorption band in the visible (case iv, Papanastasiou et al., 2009 with Vis) would lead to an even earlier increase in [ClO] and is not supported by our observations. J_{ClOOCl} values based on scaled spectrum of von Hobe (2007) and spectrum of Papanastasiou et al., 2009 produce a reasonably good agreement between observed and expected [ClO] rise within the given uncertainties. They can probably be regarded as maximum and minimum of plausible photolysis cross sections effective in the atmosphere.

7.3 Chemistry simulations along match trajectories

For this analysis, CLaMS box model runs with full chemistry calculations were initialised with the species taken from the Mainz 2-D model (Grooß et al., 1998) and measurements

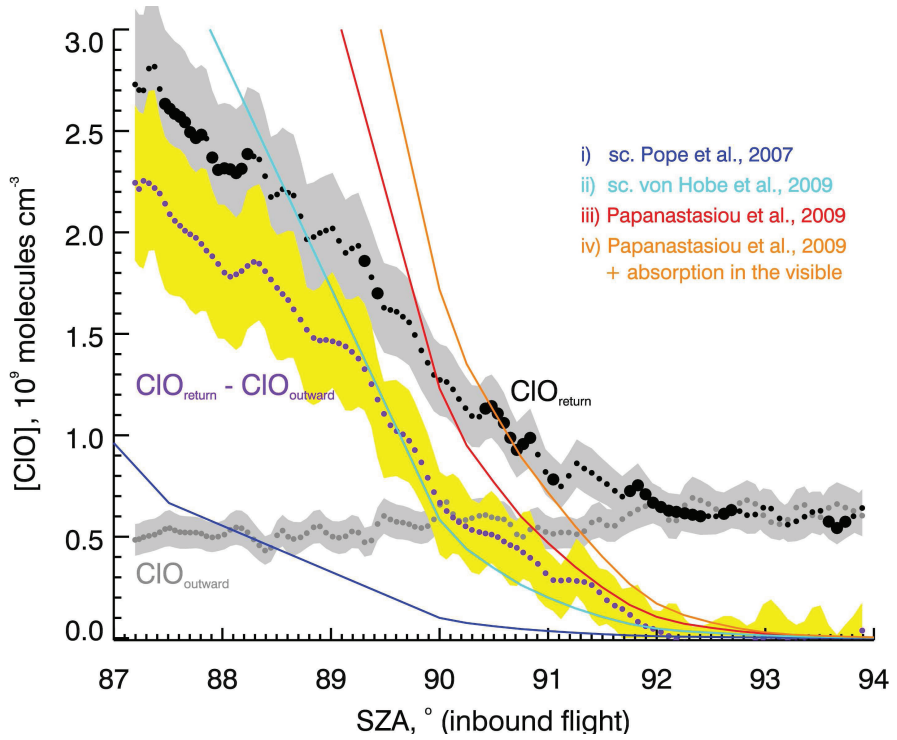

Figure 7.3: Comparison of the observed rise of ClO concentrations (marked by the purple symbols) with SZA to the integrated ClO produced by simulations employing photolysis rates J_{ClOOCl} based on i-iv. The measured rise results from the subtraction of ClO measured on the outbound flight leg (grey symbols) from ClO measured on the inbound flight leg (shown as black symbols with the thicker ones representing strict match pairs). Grey and yellow areas show the measurement uncertainties.

made on the outbound flight leg (von Hobe et al., 2011). For the calculation of the ClOOCl mixing ratios, HALOX ClO and K_{eq} from the publication of Plenge et al. (2005) were used (cf. Section 5.3.2). The ClO mixing ratios resulting from the chemistry simulation runs along the trajectories between the points on the outbound and the inbound flight leg are here compared with values observed on the inbound flight leg. The results are shown in Fig. 7.4.

Simulations were carried out for combinations of the four J_{ClOOCl} parameterisations discussed above and two parameterisations of k_{rec}: JPL 2011 and Nickolaisen et al., 1994. JPL

2011 k_{rec} was chosen as the current recommendation of the scientific community, whereas k_{rec} published by Nickolaisen et al., 1994 due to its good agreement with both atmospheric observations and unimolecular theory as shown by von Hobe et al. (2009).

Irrespective of the agreement between modelled and observed ClO, Fig. 7.4 illustrates the point made earlier, that immediately after sunrise, ClO mixing ratios are much more sensitive to J_{ClOOCl} than to k_{rec}. Only as the sun rises higher and ClO builds up, the influence of k_{rec} becomes important. Clearly, at higher SZA at sunrise, the steady state approximation $J_{ClOOCl}/k_{rec} \approx [ClO]^2/[ClOOCl]$ is not valid.

In agreement with the results presented in Section 7.2, for the scaled spectrum of Pope et al. (2007), simulated ClO falls below observed mixing ratios as soon as they start to rise. In case of scaled spectrum of von Hobe et al. (2009), the model consistently follows the observations at very high SZA over sunrise, but predicts significantly smaller ClO mixing ratios than observed as SZA decreases further and photochemical steady state is approached. At SZA<89°, both simulations (iii and iv) using spectrum of Papanastasiou et al. (2009) show relatively good agreement with the observations, but they overestimate ClO earlier, especially the spectrum with the artificial absorption band in the visible.

Provided that there are no additional reactions other than R18 - R21 governing the ClO dimer cycle, the differences between model and observations for cases i) and iv) are too large for the underlying cross sections to be realistic in the atmosphere. For cases ii) and iii), the behaviour of the scaled von Hobe et al. (2009) parameterisation underestimating observed ClO at SZA < 90° and Papanastasiou et al. (2009) overestimating ClO at SZA > 90°, suggests ClOOCl cross sections within the range between those two. The HALOX measurements indicate an SZA threshold of significant ClO increase due to ClOOCl photolysis near 92° (cf. Fig. 7.3). The spectrum fully fitting our observed data is supposed to have the steep slope and shape of the von Hobe et al. (2009) spectrum, but the scaling should be higher providing larger photolysis at λ <350 nm.

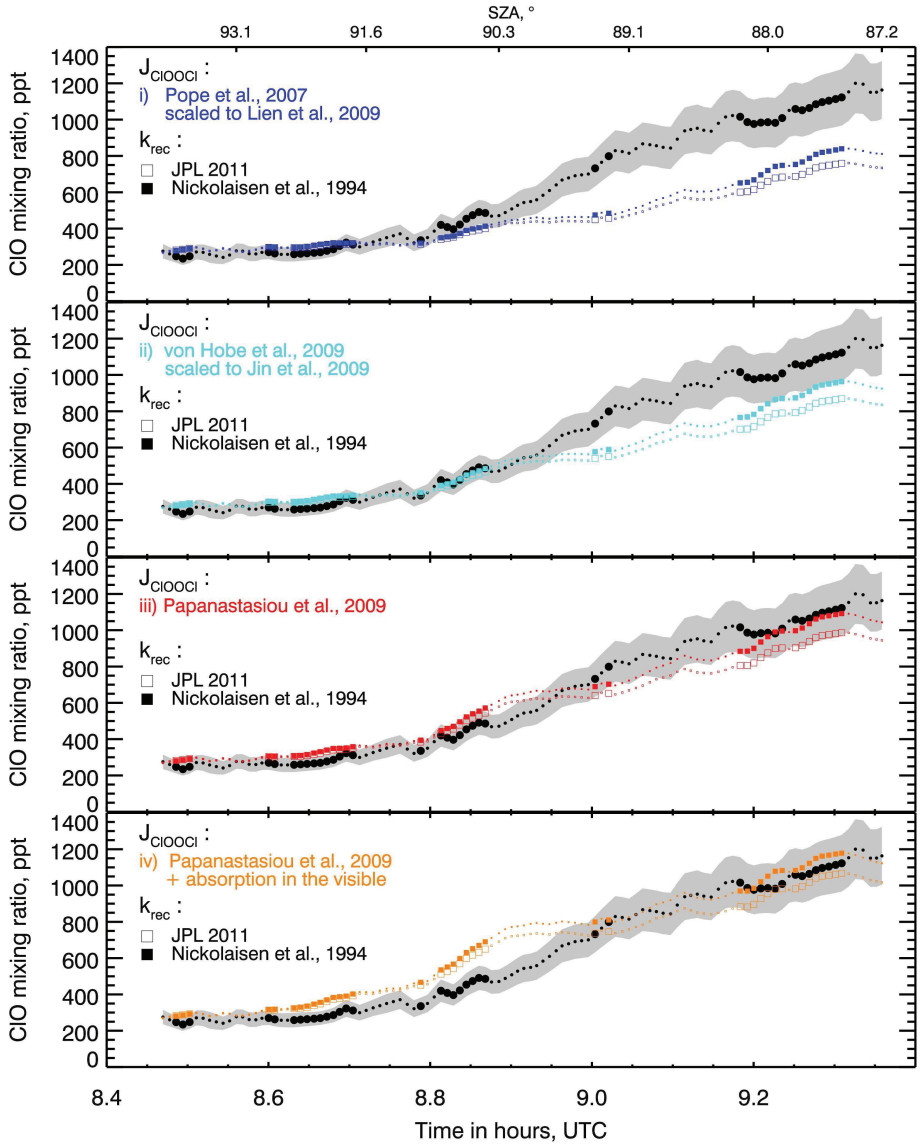

Figure 7.4: Comparison of HALOX ClO mixing ratio with the results of CLaMS simulations using various combinations of kinetic parameters. The black points show the data measured on the inbound flight leg, the 'good matches' are marked with big black circles. The grey areas represent the uncertainty of measurements. For the initialization of the simulations, we used the HALOX data sampled on the outbound flight leg and calculated the ClOOCl mixing ratios with K_{eq} from the publication of Plenge et al. (2005). The used rate constants k_{rec} were taken from JPL 2009 and from the studies of Nickolaisen et al. (1994). Plotted data sets result from the chemistry simulation runs along the trajectories between the points on the outbound and the inbound flight leg.

8 Summary and outlook

ClO measurements during the RECONCILE self-match flight on 30th January 2010 were used to examine the plausibility of published ClOOCl absorption cross sections measured in the laboratory and to test the hypothesis of an additional ClOOCl absorption in the visible. Ninety-five match pairs of dark measurements on the outbound leg and sunlit measurements on the inbound leg were found. Forty-one of them passed the quality threshold based on ECMWF data and tracer observations. ClO concentrations measured at matching outbound and inbound points were used to calculate the ClO increase due to ClOOCl photolysis. The observed increase was compared to the increase expected for four different absorption cross sections or spectra from laboratory measurements.

The second important factor for the atmospheric photolysis rate J_{ClOOCl}, the actinic flux, was investigated with two radiative transfer models (UMD and libRadtran/MYSTIC). The models were compared and sensitivity studies were carried out for ozone, albedo, clouds and aerosol, and the influence of refraction was discussed.

8.1 Conclusions

From this work, the following conclusions are drawn:

1. HALOX ClO observations at nigh time are inconsistent with an equilibrium constant higher than the K_{eq} published by Plenge et al. (2005). This is in agreement with results of e.g. Stimpfle et al. (2004), von Hobe et al. (2007) and Schofield et al. (2008).

2. The observed ClO concentration increase over sunrise is consistent with J_{ClOOCl} in the range resulting from absorption cross sections published by Papanastasiou et al. (2009) and a spectrum from von Hobe et al. (2009) scaled to Lien et al. (2009). The

spectrum published by Pope et al. (2007) and scaled to Lien et al. (2009) is clearly inconsistent with HALOX self-match observations unless there are additional unknown processes converting ClOOCl to ClO in the atmosphere. The observation that ClO mixing ratios only start to increase at SZA below 92° does not support an additional absorption band of ClOOCl at wavelengths > 420 nm.

3. The results agree with previous studies based on ClO observations (e.g. Stimpfle et al., 2004; von Hobe et al., 2007; Schofield et al., 2008; Kremser et al., 2011). While these studies could only draw conclusions on the ratio $J_{\mathrm{ClOOCl}}/k_{\mathrm{rec}}$, the analysis of data over sunrise makes our results independent of k_{rec}. The full chemistry simulations revealed that at high SZA at sunrise, the steady state approximation $J_{\mathrm{ClOOCl}}/k_{\mathrm{rec}} \approx [\mathrm{ClO}]^2/[\mathrm{ClOOCl}]$ is not valid.

4. The range of J_{ClOOCl} values consistent with this analysis would yield ozone loss in stratospheric models consistent with observations (Santee et al., 2003; Chipperfield et al., 2005; Frieler et al., 2006; Tripathi et al., 2006; von Hobe et al., 2007).

5. At high solar zenith angles observed during the self-match flight and prevailing in January in most of the Arctic stratosphere, the albedo as well as tropospheric clouds do not influence $I(\lambda)$ and thus J_{ClOOCl} significantly. The impact of ozone and aerosol is also moderate, so that the uncertainties in $I(\lambda)$ propagating into J_{ClOOCl} are smaller than the uncertainties resulting from different σ_{ClOOCl} measured in the laboratory.

8.2 Outlook

The results of this thesis suggest that a further sunrise self-match flight would enable to estimate K_{eq} directly from the ClO and ClOOCl data. To estimate k_{rec} independently of J_{ClOOCl}, a self-match flight pattern with the outbound flight leg starting directly after sunset would be helpful.

Another improvement is related to more detailed transfer model calculations. Sensitivity studies on the actinic flux should be extended to lower zenith angles, and to a wider range of atmospheric conditions including for example polar stratospheric clouds. None of the mod-

els used for the calculations presented in this thesis includes refraction. DeMajistre et al. (1995) noticed that refraction has the effect of increasing the amount of solar flux available for photodissociation in the atmosphere due to both the reduction of the optical path of the direct solar beam and a significant lengthening of the sunlit day. The J_{ClOOCl} values examined in this thesis would rise, if refraction was included in the models. Unfortunately, there is currently no suitable radiative transfer model that has refraction fully implemented for both, the direct solar beam and diffuse radiation.

As shown here and in numerous other publications, none of the investigated σ_{ClOOCl} is unambiguously consistent with stratospheric observations, therefore further laboratory experiments are necessary to determine the correct σ_{ClOOCl} values, as well as k_{rec}, k_{diss} and K_{eq}. In 2012 results of new σ_{ClOOCl} measurements are expected to be published by Young et al. using an innovative method to monitor Cl_2 impurities (Young et al., 2011). The ClO self-match data should be compared with an expected ClO concentration increase due to the new absorption spectrum.

List of Figures

List of Tables

Bibliography

Anderson, D. E. J. and Lloyd, S. A.: Solar Twilight UV-Visible Radiation Field: Perturbations due to Multiple Scattering, Ozone Depletion, Stratospheric Clouds, and Surface Albedo, Journal of Geophysical Research, 95, 7429–7434, doi:10.1029/JD095iD06p07429, URL http://dx.doi.org/10.1029/JD095iD06p07429, 1990.

Anderson, J. and Kaufman, F.: Kinetics of the reaction OH + NO2 + M → HNO3 + M, Chemical Physics Letters, 16, 375–379, doi:10.1016/0009-2614(72)80296-3, URL http://www.sciencedirect.com/science/article/pii/0009261472802963, 1972.

Anderson, J. G.: The absolute concentration of O(^{3}P) in the earth's stratosphere, Geophysical Research Letters, 2, 231–234, doi:10.1029/GL002i006p00231, 1975.

Anderson, J. G.: The absolute concentration of OH/X 2 Pi/ in the earth's stratosphere, Geophysical Research Letters, 3, 165–168, doi:10.1029/GL003i003p00165, 1976.

Anderson, J. G.: The measurement of atomic and diatomic radicals in the earth's stratosphere, Atmospheric Technology, pp. 55–68, 1978.

Anderson, J. G., Margitan, J. J., and Stedman, D. H.: Atomic Chlorine and the Chlorine Monoxide Radical in the Stratosphere: Three in situ Observations, Science, 198, 501–503, doi:10.1126/science.198.4316.501, URL http://www.sciencemag.org/content/198/4316/501.abstract, 1977.

Anderson, J. G., Grassl, H. J., Shetter, R. E., and Margitan, J. J.: Stratospheric free chlorine measured by balloon-borne in situ resonance fluorescence, Journal of Geophysical Research, 85, 2869–2887, doi:10.1029/JC085iC05p02869, 1980.

Antón, M., Cachorro, V. E., Vilaplana, J. M., Krotkov, N. A., Serrano, A., Toledano, C., de la Morena, B., and Herman, J. R.: Total ozone mapping spectrometer retrievals of noon erythemal-CIE ultraviolet irradiance compared with Brewer ground-based measurements at El Arenosillo (southwestern Spain), Journal of Geophysical Research, 112, doi:10.1029/2006JD007254, URL http://dx.doi.org/10.1029/2006JD007254, 2007.

Arola, A., Kazadzis, S., Krotkov, N. A., Bais, A. F., Gröbner, J., and Herman, J. R.: Assessment of TOMS UV bias due to absorbing aerosols, Journal of Geophysical Research, 110, 2005.

Arola, A., Lindfors, A., Natunen, A., and Lehtinen, K. E. J.: A case study on biomass burning aerosols: effects on aerosol optical properties and surface radiation levels, Atmospheric Chemistry and Physics, 7, 4257–4266, doi:10.5194/acp-7-4257-2007, URL http://www.atmos-chem-phys.net/7/4257/2007/, 2007.

Avallone, L. M. and Toohey, D. W.: Tests of halogen photochemistry using in situ measurements of ClO and BrO in the lower polar stratosphere, Journal of Geophysical Research, 106, 0148–0227, doi:10.1029/2000JD900831, URL http://dx.doi.org/10.1029/2000JD900831, 2001.

Avellone, L.: In situ measurements of ClO and implications for the chemistry of inorganic chlorine in the lower stratosphere, Ph.D. thesis, Dapartment of Chemistry, Harvard University, Cambridge, 1993.

Bais, A., Kazantzidis, A., Kazadzis, S., Balis, D., Zerefos, C., and Meleti, C.: Deriving an effective aerosol single scattering albedo from spectral surface UV irradiance measurements, Atmospheric Environment, 39, 1093–1102, doi:10.1016/j.atmosenv.2004.09.080, URL http://www.sciencedirect.com/science/article/pii/S1352231004010246, 2005.

Basco, N. and Hunt, J. E.: Mutual combination of ClO radicals, International Journal of Chemical Kinetics, 11, 649–664, doi:10.1002/kin.550110611, URL http://dx.doi.org/10.1002/kin.550110611, 1979.

Baumgardner, D., Jonsson, H., Dawson, W., O'Connor, D., and Newton, R.: The cloud, aerosol and precipitation spectrometer: a new instrument for cloud investigations, Atmospheric Research, 59-60, 251–264, doi:10.1016/S0169-8095(01)00119-3, URL http://www.sciencedirect.com/science/article/pii/S0169809501001193, 2001.

Becker, G., Grooß, J.-U., McKenna, D. S., and Müller, R.: Stratospheric photolysis frequencies: Impact of an improved numerical solution of the radiative transfer equation, Journal of Atmospheric Chemistry, 37, 217–229, 2000.

Benson, S. and Axworthy, A. E. J.: Mechanism of the Gas Phase, Thermal Decomposition of Ozone, Journal of Chemical Physics, 26, 1718–1726, doi:10.1063/1.1743610, URL http://link.aip.org/link/?JCP/26/1718/1, 1957.

Bernhard, G., Evans, R. D., Labow, G. J., and Oltmans, S. J.: Bias in Dobson total ozone measurements at high latitudes due to approximations in calculations of ozone absorption coefficients and air mass, Journal of Geophysical Research, 110, D10 305+, doi:10.1029/2004JD005559, URL http://dx.doi.org/10.1029/2004JD005559, 2005.

Bian, H. and Prather, M. J.: Fast-J2: Accurate simulation of stratospheric photolysis in global chemical models, Journal of Atmospheric Chemistry, 41, 281–296, doi:10.1023/A:1014980619462, 2002.

Binkowski, F. S., Arunachalam, S., Adelman, Z., and Pinto, J. P.: Examining Photolysis Rates with a Prototype Online Photolysis Module in CMAQ, Journal of Applied Meteorology and Climatology, 46, 1252–1256, doi:10.1175/JAM2531.1, URL http://dx.doi.org/10.1175/JAM2531.1, 2007.

Birk, M., Friedl, R. R., Cohen, E. A., Pickett, H. M., and Sander, S. P.: The Rotational Spectrum and Structure of Chlorine Peroxide, Journal of Chemical Physics, 91, 6588–6597, doi:10.1063/1.457377, 1989.

Bloss, W. J., Nickolaisen, S. L., Salawitch, R. J., Friedl, R. R., and Sander, S. P.: Kinetics of the ClO self-reaction and 210 nm absorption cross section of the ClO dimer, Journal of Physical Chemistry A, 105, 11 226–11 239, doi:10.1021/jp012429y, 2001.

Boakes, G., Mok, W. H. H., and Rowley, D. M.: Kinetic studies of the ClO + ClO association reaction as a function of temperature and pressure, Physical Chemistry Chemical Physics, 7, 4102–4113, doi:10.1039/B510308H, URL http://dx.doi.org/10.1039/B510308H, 2005.

Bröske, R. and Zabel, F.: Thermal Decomposition of ClOOCl, The Journal of Physical Chemistry A, 110, 3280–3288, doi:10.1021/jp0550053, URL http://pubs.acs.org/doi/abs/10.1021/jp0550053, pMID: 16509654, 2006.

Brown, P. N., Byrne, G. D., and Hindmarsh, A. C.: VODE: A Variable-Coefficient ODE Solver, SIAM Journal on Scientific and Statistical Computing, 10, 1038–1051, doi:10.1137/0910062, URL http://link.aip.org/link/?SCE/10/1038/1, 1989.

Brune, W. H., Anderson, J. G., and Chan, K. R.: In Situ Observations of ClO in the Antarctic: ER-2 Aircraft Results From 54°S to 72°S Latitude, Journal of Geophysical Research, 94, 16 649–16 663, doi:10.1029/JD094iD14p16649, URL http://dx.doi.org/10.1029/JD094iD14p16649, 1989.

Bugliaro, L., Zinner, T., Keil, C., Mayer, B., Hollmann, R., Reuter, M., and Thomas, W.: Validation of cloud property retrievals with simulated satellite radiances: a case study for SEVIRI, Atmospheric Chemistry and Physics Discussions, 10, 21 931–21 988, doi:10.5194/acpd-10-21931-2010, URL http://www.atmos-chem-phys-discuss.net/10/21931/2010/, 2010.

Burkholder, J. B., Orlando, J. J., and Howard, C. J.: Ultraviolet-Absorption Cross-Sections of Cl2O2 Between 210 and 410 nm, Journal of Physical Chemistry, 94, 687–695, doi:10.1021/j100365a033, 1990.

Cadle, R. D., Crutzen, P., and Ehhalt, D.: Heterogeneous Chemical Reactions in the Stratosphere, Journal of Geophysical Research, 80, 3381–3385, doi:10.1029/JC080i024p03381, 1975.

Carslaw, K. S., Clegg, S. L., and Brimblecombe, P.: A Thermodynamic Model of the System HCl-HNO3-H2S04-H20, Including Solubilities of HBr, from <200 to 328 K, The Journal

of Physical Chemistry, 99, 11 557–11 574, doi:10.1021/j100029a039, URL http://pubs.acs.org/doi/abs/10.1021/j100029a039, 1995.

Carver, G. D., Brown, P. D., and Wild, O.: The ASAD atmospheric chemistry integration package and chemical reaction database, Computer Physics Communications, 105, 197–215, doi:10.1016/S0010-4655(97)00056-8, 1997.

Chandrasekhar, S.: Radiative Transfer, Dover, New York, 1960.

Chang, J. S., Rost, R. A., Isaken, I. S. A., Madronich, S., Stockwell, W. R., and Walcek, C. J.: A Three-Dimensional Eulerian Acid Deposition Model: Physical Concepts and Formulation, Journal of Geophysical Research, pp. 14 681–14 700, doi:10.1029/JD092iD12p14681, URL http://dx.doi.org/10.1029/JD092iD12p14681, 1987.

Chapman, S.: A Theory of the Upper Atmospheric Ozone Layer, Memoirs of the Royal Meteorological Society, 3, 103–125, 1930.

Chen, H. Y., Lien, C. Y., Lin, W. Y., Lee, Y. T., and Lin, J. J.: UV Absorption Cross Sections of ClOOCl are Consistent with Ozone Degradation Models, Science, 324, 781–784, doi:10.1126/science.1171305, 2009.

Chipperfield, M. P., Feng, W., and Rex, M.: Arctic ozone loss and climate sensitivity: Updated three-dimensional model study, Geophysical Research Letters, 32, L11 813, doi:10.1029/2005GL022674, 2005.

Christian, A. and Gueymard: The sun's total and spectral irradiance for solar energy applications and solar radiation models, Solar Energy, 76, 423–453, doi:10.1016/j.solener.2003.08.039, URL http://www.sciencedirect.com/science/article/pii/S0038092X03003967, 2004.

Clyne, M. A. A. and Cruse, H. W.: Atomic resonance fluorescence spectrometry for the rate constants of rapid bimolecular reactions. Part 2.-Reactions Cl + BrCl, Cl + Br2, Cl + ICl, Br + IBr, Br + ICl, Journal of Chemical Society , Faraday Trans. 2, 68, 1377–1387, doi:10.1039/F29726801377, URL http://dx.doi.org/10.1039/F29726801377, 1972.

Cox, R. A. and Hayman, G. D.: The Stability and Photochemistry of Dimers of the ClO Radical and Implications for Antarctic Ozone Depletion, Nature, 332, 796–800, doi:10.1038/332796a0, 1988.

Crutzen, P. J.: The influence of nitrogen oxides on the atmospheric ozone content, Quarterly Journal of the Royal Meteorological Society, 96, 320–325, doi:10.1002/qj.49709640815, URL http://dx.doi.org/10.1002/qj.49709640815, 1970.

Crutzen, P. J.: Ozone Production Rates in an Oxygen-Hydrogen-Nitrogen Oxide Atmosphere, Journal of Geophysical Researches, 76, 7311–7327, doi:10.1029/JC076i030p07311, 1971.

Crutzen, P. J.: Estimates of possible future ozone reductions from continued use of fluoro-chloro-methanes (CF2Cl2, CFCl3), Geophysical Research Latters, 1, 205–208, 1974.

Dahlback, A. and Stamnes, K.: A new spherical model for computing the radiation field available for photolysis and heating at twilight, Planetary and Space Science, 39, 671–683, doi:10.1016/0032-0633(91)90061-E, 1991.

DeMajistre, R., Anderson, D. E., Lloyd, S., Swaminathan, P. K., and Zasadil, S.: Effects of refraction on photochemical calculations, Journal of Geophysical Research, 100, 18 817–18 822, doi:10.1029/95JD01836, 1995.

DeMore, W. B. and Tschuikow-Roux, E.: Ultraviolet Spectrum and Chemical Reactivity of the ClO Dimer, Journal of Physical Chemistry, 94, 5856–5860, doi:10.1021/j100378a046, 1990.

Dobson, G. M. B. and Harrison, D. N.: Measurements of the Amount of Ozone in the Earth's Atmosphere and Its Relation to Other Geophysical Conditions, Proceedings of the Royal Society A: Mathematical, Physical and Engineering Sciences, 110, 660–693, doi:10.1098/rspa.1926.0040, 1926.

Drdla, K. and Müller, R.: Temperature thresholds for polar stratospheric ozone loss, Atmospheric Chemistry and Physics Discussions, 10, 28 687–28 720, doi:10.5194/acpd-10-28687-2010, 2010.

Dye, J. E. and Baumgardner, D.: Evaluation of the Forward Scattering Spectrometer Probe. Part I: Electronic and Optical Studies, Journal of Atmospheric and Oceanic Technology, 1, 329–344, doi:10.1175/1520-0426(1984)001<0329:EOTFSS>2.0.CO;2, 1984.

Ellermann, T., Johnsson, K., Lund, A., and Pagsberg, P.: Kinetics and Equilibrium Constant of the Reversible Reaction ClO + ClO + M <=> Cl2O2 + M at 295 K, Acta Chemica Scandinavica, 49, 28–35, doi:10.3891/acta.chem.scand.49-0028, 1995.

Emde, C. and Mayer, B.: Simulation of solar radiation during a total eclipse: a challenge for radiative transfer, Atmospheric Chemistry and Physics, 7, 2259–2270, doi:10.5194/acp-7-2259-2007, URL http://www.atmos-chem-phys.net/7/2259/2007/, 2007.

Emde, C., Buras, R., Mayer, B., and Blumthaler, M.: The impact of aerosols on polarized sky radiance: model development, validation, and applications, Atmospheric Chemistry and Physics, 10, 383–396, doi:10.5194/acp-10-383-2010, URL http://www.atmos-chem-phys.net/10/383/2010/, 2010.

Emde, C., Buras, R., and Mayer, B.: ALIS: An efficient method to compute high spectral resolution polarized solar radiances using the Monte Carlo approach, Journal of Quantitative Spectroscopy and Radiative Transfer, 112, 1622–1631, doi:10.1016/j.jqsrt.2011.03.018, URL http://www.sciencedirect.com/science/article/pii/S0022407311001373, 2011.

Evans, K. F. and Stephens, G. L.: A new polarized atmospheric radiative transfer model, Journal of Quantitative Spectroscopy and Radiative Transfer, 46, 413–423, doi:10.1016/0022-4073(91)90043-P, 1991.

Farman, J. C., Gardiner, B. G., and Shanklin, J. D.: Large losses of total ozone in Antarctica reveal seasonal ClOx/NOx interaction, Nature, 315, 207–210, doi:10.1038/315207a, 1985.

Ferracci, V. and Rowley, M.: Kinetic and thermochemical studies of the ClO + ClO + M <=> Cl2O2 + M reaction, Physical Chemistry Chemical Physics, 12, 11 596–11 608, doi:10.1039/C0CP00308E, 2010.

Frieler, K., Rex, M., Salawitch, R. J., Canty, T., Streibel, M., Stimpfle, R. M., Pfeilsticker, K., Dorf, M., Weisenstein, D. K., and Godin-Beekmann, S.: Toward a better quantitative understanding of polar stratospheric ozone loss, Geophysical Research Letters, 33, L10 812, doi:10.1029/2005GL025466, 2006.

Gillett, N. P. and Thompson, D. W. J.: Simulation of Recent Southern Hemisphere Climate Change, Science, 302, 273–275, doi:10.1126/science.1087440, URL `http://www.sciencemag.org/content/302/5643/273.abstract`, 2003.

Grooß, J. U. and Russell, J. M.: Technical note: A stratospheric climatology for O-3, H2O, CH4, NOx, HCl and HF derived from HALOE measurements, Atmospheric Chemistry and Physics, 5, 2797–2807, 2005.

Grooß, J.-U., Brühl, C., and Peter, T.: Impact of aircraft emissions on tropospheric and stratospheric ozone. Part I: chemistry and 2-D model results, Atmospheric Environment, 32, 3173–3184, doi:10.1016/S1352-2310(98)00016-8, URL `http://www.sciencedirect.com/science/article/pii/S1352231098000168`, 1998.

Grooß, J.-U., Günther, G., Konopka, P., Müller, R., McKenna, D. S., Stroh, F., Vogel, B., Engel, A., Müller, M., Hoppel, K., Bevilacqua, R., Richard, E., Webster, C. R., Elkins, J. W., Hurst, D. F., Romashkin, P. A., and Baumgardner, D. G.: Simulation of ozone depletion in spring 2000 with the Chemical Lagrangian Model of the Stratosphere (CLaMS), Journal of Geophysical Research (Atmospheres), 107, 8295, doi:10.1029/2001JD000456, 2002.

Grooß, J.-U., Günther, G., Müller, R., Konopka, P., Bausch, S., Schlager, H., Voigt, C., Volk, C. M., and Toon, G. C.: Simulation of denitrification and ozone loss for the Arctic winter 2002/2003, Atmospheric Chemistry and Physics, 5, 1437–1448, 2005.

Grooß, J.-U., Brautzsch, K., Pommrich, R., Solomon, S., and Müller, R.: Stratospheric ozone chemistry in the Antarctic: what controls the lowest values that can be reached and their recovery?, Atmospheric Chemistry and Physics Discussions, 11, 22 173–22 198, doi:10.5194/acpd-11-22173-2011, URL `http://www.atmos-chem-phys-discuss.net/11/22173/2011/`, 2011.

Hampson, J.: Photochemical behaviour of the ozone layer., Tech. rep., Canadian Armament Research and Development Establishment, CARDE technical note 1627, 1964.

Hanson, D. R.: Reaction of ClONO2 with H2O and HCl in Sulfuric Acid and HNO3/H2SO4/H2O Mixtures, The Journal of Physical Chemistry A, 102, 4794–4807, doi: 10.1021/jp972767s, URL http://pubs.acs.org/doi/abs/10.1021/jp972767s, 1998.

Hanson, D. R. and Ravishankara, A. R.: Reaction of ClONO2 with HCl on NAT, NAD, and frozen sulfuric acid and hydrolysis of N2O5 and ClONO2 on frozen sulfuric acid, Journal of Geophysical Research, 982, 22 931–22 936, doi:10.1029/93JD01929, 1993.

Hartley, W. N.: On the absorption spectrum of ozone, Journal of Chemical Society, 39, 57–60, doi:10.1039/CT8813900057, 1881.

Hayman, G. D., Davies, J. M., and Cox, R. A.: Kinetics of the reaction ClO+ClO&;products and its potential relevance to Antarctic ozone, Geophysical Research Letters., 13, 1347–1350, doi:10.1029/GL013i012p01347, 1986.

Hess, M., Koepke, P., and Schult, I.: Optical Properties of Aerosols and Clouds: The Software Package OPAC, Bulletin of the American Meteorological Society, 79, 831–844, doi: 10.1175/1520-0477(1998)079<0831:OPOAAC>2.0.CO;2, 1998.

Horowitz, A., Crowley, J. N., and Moortgat, G. K.: Temperature Dependence of the Product Branching Ratios of the ClO Self-Reaction in Oxygen, The Journal of Physical Chemistry, 98, 11 924–11 930, doi:10.1021/j100097a019, URL http://pubs.acs.org/doi/abs/10.1021/j100097a019, 1994.

Huang, W.-T., Chen, A. F., Chen, I.-C., Tsai, C.-H., and Lin, J. J.-M.: Photodissociation dynamics of ClOOCl at 248.4 and 308.4 nm, Physical Chemistry Chemical Physics, 13, 8195–8203, doi:10.1039/C0CP02453H, URL http://dx.doi.org/10.1039/C0CP02453H, 2011.

Huder, K. J. and DeMore, W. B.: Absorption Cross Sections of the ClO Dimer, Journal of Physical Chemistry, 99, 3905–3908, doi:10.1021/j100012a007, 1995.

Hunt, B. G.: The Need for a Modified Photochemical Theory of the Ozonosphere, Journal of Atmospheric Science, 23, 88–95, doi:10.1175/1520-0469(1966)023<0088:TNFAMP>2.0.CO;2, 1966.

IPCC: Climate change 2007: The scientific basis, Tech. rep., Panel on Climate Change (IPCC), IPCC Secretariat, c/o World Meteorological Organization, Geneva, Switzerland, 2007.

Jin, B., Chen, I. C., Huang, W. T., Lien, C. Y., Guchhait, N., and Lin, J. J.: Photodissociation Cross Section of ClOOCl at 330 nm, Journal of Physical Chemistry A, 114, 4791–4797, doi:10.1021/jp909374k, 2010.

Jin, Z., Charlock, T. P., Smith, W. L. J., and utledge utledge utledge utledge, K.: A parameterization of ocean surface albedo, Geophysical Research Letters, 31, doi:10.1029/2004GL021180, URL http://dx.doi.org/10.1029/2004GL021180, 2004.

Johnston, H.: Reduction of Stratospheric Ozone by Nitrogen Oxide Catalysts from Supersonic Transport Exhaust, Science, 173, 517–522, doi:10.1126/science.173.3996.517, URL http://www.sciencemag.org/content/173/3996/517.abstract, 1971.

Jones, W. M. and Davidson, N.: The Thermal Decomposition of Ozone in a Shock Tube, Journal of the American Chemical Society, 84, 2868–2878, doi:10.1021/ja00874a005, URL http://pubs.acs.org/doi/abs/10.1021/ja00874a005, 1962.

Kaledin, A. L. and Morokuma, K.: An ab initio direct-trajectory study of the photodissociation of ClOOCl, Journal of Chemical Physics, 113, 5750–5762, doi:10.1063/1.1290606, 2000.

Kazadzis, S., Topaloglou, C., Bais, A. F., Blumthaler, M., Balis, D., Kazantzidis, A., and Schallhart, B.: Actinic flux and O1D photolysis frequencies retrieved from spectral measurements of irradiance at Thessaloniki, Greece, Atmospheric Chemistry and Physics Discussions, 4, 4191–4225, doi:10.5194/acpd-4-4191-2004, URL http://www.atmos-chem-phys-discuss.net/4/4191/2004/, 2004.

Kettle, A. J., Kuhn, U., von Hobe, M., Kesselmeier, J., and Andreae, M. O.: Global budget of atmospheric carbonyl sulfide: Temporal and spatial variations of the dominant sources and sinks, Geophysical Research Letters, 107, 4658–4674, doi:10.1029/2002JD002187, 2002.

Khosrawi, F., Urban, J., Pitts, M. C., Voelger, P., Achtert, P., Kaphlanov, M., Murtagh, D., and Fricke, K.-H.: Denitrification and polar stratospheric cloud formation during the Arctic winter 2009/2010, Atmospheric Chemistry and Physics Discussions, 11, 11 379–11 415, doi:10.5194/acpd-11-11379-2011, URL http://www.atmos-chem-phys-discuss.net/11/11379/2011/, 2011.

Konopka, P., Günther, G., Müller, R., dos Santos, F. H. S., Schiller, C., Ravegnani, F., Ulanovsky, A., Schlager, H., Volk, C. M., Viciani, S., Pan, L. L., McKenna, D.-S., and Riese, M.: Contribution of mixing to upward transport across the tropical tropopause layer (TTL), Atmospheric Chemistry and Physics, 7, 3285–3308, doi:10.5194/acp-7-3285-2007, URL http://www.atmos-chem-phys.net/7/3285/2007/, 2007.

Kremser, S., Schofield, R., Bodeker, G. E., Connor, B. J., Rex, M., Barret, J., Mooney, T., Salawitch, R. J., Canty, T., Frieler, K., Chipperfield, M. P., Langematz, U., and Feng, W.: Retrievals of chlorine chemistry kinetic parameters from Antarctic ClO microwave radiometer measurements, Atmospheric Chemistry and Physics, 11, 5183–5193, doi:10.5194/acp-11-5183-2011, URL http://www.atmos-chem-phys.net/11/5183/2011/, 2011.

Kylling, A., Stamnes, K., and Tsay, S.-C.: A reliable and efficient two-stream algorithm for spherical radiative transfer: Documentation of accuracy in realistic layered media, Journal of Atmospheric Chemistry, 21, 115–150, doi:10.1007/BF00696577, URL http://www.springerlink.com/content/x7166235748427m4, 1995.

Kylling, A., Webb, A. R., Kift, R., Gobbi, G. P., Ammannato, L., Barnaba, F., Bais, A., Kazadzis, S., Wendisch, M., Jäkel, E., Schmidt, S., Kniffka, A., Thiel, S., Junkermann, W., Blumthaler, M., Silbernagl, R., Schallhart, B., Schmitt, R., Kjeldstad, B., Thorseth,

T. M., Scheirer, R., and Mayer, B.: Spectral actinic flux in the lower troposphere: measurement and 1-D simulations for cloudless, broken cloud and overcast situations, Atmospheric Chemistry and Physics, 5, 1975–1997, doi:10.5194/acp-5-1975-2005, URL http://www.atmos-chem-phys.net/5/1975/2005/, 2005.

Lary, D. J. and Pyle, J. A.: Diffuse radiation, twilight, and photochemistry — I, Journal of Atmospheric Chemistry, 13, 373–392, doi:10.1007/BF00057753, URL http://dx.doi.org/10.1007/BF00057753, 1991a.

Lary, D. J. and Pyle, J. A.: Diffuse radiation, twilight, and photochemistry — II, Journal of Atmospheric Chemistry, 13, 393–406, doi:10.1007/BF00057754, URL http://dx.doi.org/10.1007/BF00057754, 1991b.

Lien, C. Y., Lin, W. Y., Chen, H. Y., Huang, W. T., Jin, B., Chen, I. C., and Lin, J. J.: Photodissociation cross sections of ClOOCl at 248.4 and 266 nm, Journal of Chemical Physics, 131, 174 301, doi:10.1063/1.3257682, 2009.

Madronich, S.: Photodissociation in the Atmosphere 1. Actinic Flux and the Effects of Ground Reflections and Clouds, Journal of Geophysical Research, 92, 9740–9752, doi:10.1029/JD092iD08p09740, URL http://dx.doi.org/10.1029/JD092iD08p09740, 1987.

Mayer, B.: Radiative transfer in the cloudy atmosphere, European Physical Journal Conferences, pp. 75–99, doi:10.1140/epjconf/e2009-00912-1, URL http://www.atmos-chem-phys.net/5/1855/2005/, 2009.

Mayer, B. and Kylling, A.: Technical note: The libRadtran software package for radiative transfer calculations - description and examples of use, Atmospheric Chemistry and Physics, 5, 1855–1877, doi:10.5194/acp-5-1855-2005, URL http://www.atmos-chem-phys.net/5/1855/2005/, 2005.

Mayer, B., Kylling, A., Emde, C., Hamann, U., and Buras, R.: libRadtran user's guide, URL http://www.libradtran.org/doc/libRadtran.pdf, edition for libRatran version 1.6-beta, 2011.

McElroy, M. B., Salawitch, R. J., Wofsy, S. C., and Logan, J. A.: Reductions Of Antarctic Ozone Due To Synergistic Interactions Of Chlorine And Bromine, Nature, 321, 759–762, doi:10.1038/321759a0, 1986.

McKenna, D. S., Grooß, J. U., Günther, G., Konopka, P., Müller, R., Carver, G., and Sasano, Y.: A new Chemical Lagrangian Model of the Stratosphere (CLaMS) - 2. Formulation of chemistry scheme and initialization, Journal of Geophysical Research (Atmospheres), 107, 4256, doi:10.1029/2000JD000114, 2002a.

McKenna, D. S., Konopka, P., Grooß, J. U., Günther, G., Müller, R., Spang, R., Offermann, D., and Orsolini, Y.: A new Chemical Lagrangian Model of the Stratosphere (CLaMS) - 1. Formulation of advection and mixing, Journal of Geophysical Research (Atmospheres), 107, 4309, doi:10.1029/2000JD000113, 2002b.

Meier, R. R., Anderson, J. D. E., and Nicolet, M.: Radiation field in the troposphere and stratosphere from 240-1000 NM. I - General analysis. II - Numerical analysis, Planetary and Space Science, 30, 923–933, doi:10.1016/0032-0633(82)90134-9, 1982.

Minschwaner, K., Salawitch, R. J., and McElroy, M. B.: Absorption of Solar Radiation by O2: Implications for O3 and Lifetimes of N2O, CFCl3, and CF2Cl2, Journal of Geophysical Research, 98, 10 543–10 561, doi:10.1029/93JD00223, URL http://dx.doi.org/10.1029/93JD00223, 1993.

Molina, L. T. and Molina, M. J.: Production of Cl2O2 from the Self-Reaction of the ClO Radical, Journal of Physical Chemistry, 91, 433–436, 1987.

Molina, L. T. and Rowland, F. S.: Stratospheric sink for chlorofluoromethanes: chlorine atomc-atalysed destruction of ozone, Nature, 249, 810–812, doi:10.1038/249810a0, 1974.

Molina, M., Colussi, A., Molina, L., Schindler, R., and Tso, T.-L.: Quantum yield of chlorine-atom formation in the photodissociation of chlorine peroxide (ClOOCl) at 308 nm, Chemical Physics Letters, 173, 310–315, doi:10.1016/0009-2614(90)85275-H, URL http://www.sciencedirect.com/science/article/pii/000926149085275H, 1990.

Moore, T. A., Okumura, M., Seale, J. W., and Minton, T. K.: UV Photolysis of ClOOCl, The Journal of Physical Chemistry A, 103, 1691–1695, doi:10.1021/jp984410+, URL http://pubs.acs.org/doi/abs/10.1021/jp984410%2B, 1999.

Morcrette, J.-J.: Radiation and Cloud Radiative Properties in the European Centre for Medium Range Weather Forecasts Forecasting System, Journal of Geophysical Research, 96, 9121–9132, doi:10.1029/89JD01597, URL http://dx.doi.org/10.1029/89JD01597, 1991.

Müller, R.: A brief history of stratospheric ozone research, Meteorologische Zeitschrift, 18, 003–024, 2009.

Müller, R.: Tracer-tracer Relations as a Tool for Research on Polar Ozone Loss, vol. 58, Forschungszentrum Jülich GmbH, Jülich, Germany, 2010.

Müller, R., Grooß, J.-U., Lemmen, C., Heinze, D., Dameris, M., and Bodeker, G.: Simple measures of ozone depletion in the polar stratosphere, Atmospheric Chemistry and Physics, 8, 251–264, doi:10.5194/acp-8-251-2008, URL http://www.atmos-chem-phys.net/8/251/2008/, 2008.

Nakajima, T. and Tanaka, M.: Algorithms for radiative intensity calculations in moderately thick atmospheres using a truncation approximation, Journal of Quantitative Spectroscopy and Radiative Transfer, 40, 51–69, doi:10.1016/0022-4073(88)90031-3, URL http://adsabs.harvard.edu/abs/1988JQSRT..40...51N, 1988.

Neu, J. L., Prather, M. J., and Penner, J. E.: Global atmospheric chemistry: Integrating over fractional cloud cover, Journal of Geophysical Research, 112, doi:10.1029/2006JD008007, URL http://dx.doi.org/10.1029/2006JD008007, 2007.

Nickolaisen, S. L., Friedl, R. R., and Sander, S. P.: Kinetics And Mechanism Of The ClO+ClO Reaction - Pressure And Temperature Dependences Of The Bimolecular And Termolecular Channels And Thermal-Decomposition Of Chlorine Peroxide, Journal of Physical Chemistry, 98, 155–169, doi:10.1021/j100052a027, 1994.

Nicodemus, F. E.: Directional Reflectance and Emissivity of an Opaque Surface, Applied Optics, 4, 767–773, doi:10.1364/AO.4.000767, URL http://ao.osa.org/abstract.cfm?URI=ao-4-7-767, 1965.

Palancar, G. G., Shetter, R. E., Hall, S. R., Toselli, B. M., and Madronich, S.: Ultraviolet actinic flux in clear and cloudy atmospheres: model calculations and aircraft-based measurements, Atmospheric Chemistry and Physics, 11, 5457–5469, doi:10.5194/acp-11-5457-2011, URL http://www.atmos-chem-phys.net/11/5457/2011/, 2011.

Papanastasiou, D. K., Papadimitriou, V. C., Fahey, D. W., and Burkholder, J. B.: UV Absorption Spectrum of the ClO Dimer (Cl2O2) between 200 and 420 nm, Journal of Physical Chemistry A, 113, 13 711–13 726, doi:10.1021/jp9065345, 2009.

Patrick, R. and Golden, D. M.: Third-order rate constants of atmospheric importance, International Journal of Chemical Kinetics, 15, 1189–1227, doi:10.1002/kin.550151107, 1983.

Peterson, K. A. and Francisco, J. S.: Does chlorine peroxide absorb below 250 nm?, Journal of Chemical Physics, 121, 2611–2616, doi:10.1063/1.1766012, 2004.

Plenge, J., Kuhl, S., Vogel, B., Müller, R., Stroh, F., von Hobe, M., Flesch, R., and Ruhl, E.: Bond strength of chlorine peroxide, Journal of Physical Chemistry A, 109, 6730–6734, doi:10.1021/jp044142h, 2005.

Pope, F. D., Hansen, J. C., Bayes, K. D., Friedl, R. R., and Sander, S. P.: Ultraviolet absorption spectrum of chlorine peroxide, ClOOCl, Journal of Physical Chemistry A, 111, 4322–4332, doi:10.1021/jp067660w, 2007.

Prather, M. J.: Ozone in the Upper Stratosphere and Mesosphere, Journal of Geophysical Research, 86, 5325–5338, doi:10.1029/JC086iC06p05325, URL http://dx.doi.org/10.1029/JC086iC06p05325, 1981.

Radziemski Jr., L. J. and Kaufman, V.: Wavelengths, Energy Levels, and Analysis of Neutral Atomic Chlorine (Cl I), Journal of the Optical Society of America, 59, 424–442, doi:10.1364/JOSA.59.000424, URL http://www.opticsinfobase.org/abstract.cfm?URI=josa-59-4-424, 1969.

Rosenlof, K. H.: How Water Enters the Stratosphere, Science, 302, 1691–1692, doi:10.1126/science.1092703, URL http://www.sciencemag.org/content/302/5651/1691.short, 2003.

Rowland, F. S. and Molina, M. J.: Chlorofluoromethanes in the enviroment, Reviews of Geophysics and Space Physics, 13, 1–35, 1975.

Salawitch, R. J., Wofsy, S. C., Gottlieb, E. W., Lait, L. R., Newman, P. A., Schoeberl, M. R., Loewenstein, M., Podolske, J. R., Strahan, S. E., Proffitt, M. H., Webster, C. R., May, R. D., Fahey, D. W., Baumgardner, D., Dye, J. E., Wilson, J. C., Kelly, K. K., Elkins, J. W., Chan, K. R., and Anderson, J. G.: Chemical Loss of Ozone in the Arctic Polar Vortex in the Winter of 1991-1992, Science, 261, 1146–1149, doi:10.1126/science.261.5125.1146, URL http://www.sciencemag.org/content/261/5125/1146.abstract, 1993.

Salawitch, R. J., Wofsy, S. C., Wennberg, P. O., Cohen, R. C., Anderson, J. G., Fahey, D. W., Gao, R. S., Keim, E. R., , Woodbridge, E. L., Stimpfle, R. M., Koplow, J. P., Kohn, D. W., Webster, C. R., May, R. D., Pfister, L., Gottlieb, E. W., Michelsen, H. A., Yue, G. K., Wilson, J. C., Brock, C. A., Jonsson, H. H., Dye, J. E., Baumgardner, D., Proffitt, M. H., Loewenstein, M., Podolske, J. R., Elkins, J. W., Dutton, G. S., Hintsa, E. J., Dessler, A. E., Weinstock, E. M., Kelly, K. K., Boering, K. A., Daube, B. C., Chan, K. R., and Bowen, S. W.: The distribution of hydrogen, nitrogen, and chlorine radicals in the lower stratosphere: Implications for changes in O3 due to emission of NOy from supersonic aircraft, Geophysical Research Letters, 21, 2547–2550, doi:10.1029/94GL02781, URL http://dx.doi.org/10.1029/94GL02781, 1994.

Sander, S. P., Friedl, R. R., and Yung, Y. L.: Rate of formation of the ClO dimer in the polar stratosphere: implications for ozone loss, Science, 245, 1095–1098, doi:10.1126/science.245.4922.1095, URL http://www.sciencemag.org/content/245/4922/1095.abstract, 1989.

Sander, S. P., Friedl, R. R., Barker, J. R., Golden, D. M., Kurylo, M. J., Wine, P. H., Abbatt, J., Burkholder, J. B., Kolb, C. E., Moortgat, G. K., Huie, R. E., and Orkin, V. L.: Chemical

kinetics and photochemical data for use in atmospheric studies Evaluation Number 17, Jet Propulsion Laboratory, Pasadena, CA, 2011.

Santee, M. L., Manney, G. L., Waters, J. W., and Livesey, N. J.: Variations and climatology of ClO in the polar lower stratosphere from UARS Microwave Limb Sounder measurements - art. no. 4454, Journal of Geophysical Research (Atmospheres), 108, 4454–4454, doi: 10.1029/2002JD003335, 2003.

Schiff, H. I.: Neutral reactions involving oxygen and nitrogen, Canadian Journal of Chemistry, 47, 1903–1916, doi:10.1139/v69-309, URL http://www.nrcresearchpress.com/doi/abs/10.1139/v69-309, 1969.

Schofield, R., Frieler, K., Wohltmann, I., Rex, M., von Hobe, M., Stroh, F., Koch, G., Peter, T., Canty, T., Salawitch, R., and Volk, C. M.: Polar stratospheric chlorine kinetics from a self-match flight during SOLVE-II/EUPLEX, Geophysical Research Letters, 35, L01 807, doi:10.1029/2007GL031740, 2008.

Schwab, J. J. and Anderson, J. G.: Oscillator strengths of Cl(I) in the vacuum ultraviolet: The 2D-2P transitions, Journal of Quantitative Spectroscopy and Radiative Transfer, 27, 445–457, doi:10.1016/0022-4073(82)90079-6, URL http://www.sciencedirect.com/science/article/pii/0022407382900796, 1982.

Shaw, T. A. and Shepherd, T. G.: Atmospheric science: Raising the roof, Nature Geoscience, 1, 12–13, doi:10.1038/ngeo.2007.53, 2008.

Shettle, E. P., ed.: Models of aerosols, clouds, and precipitation for atmospheric propagation studies, 1990.

Shindell, D. T. and de Zafra, R. L.: The chlorine budget of the lower polar stratosphere: Upper limits on ClO, and Implications of new Cl2O2 photolysis cross sections, Geophysical Research Letters, 22, 3215–3218, doi:10.1029/95GL03262, URL http://dx.doi.org/10.1029/95GL03262, 1995.

Simmons, A. J., Burridge, D. M., Jarraud, M., Girard, C., and Wergen, W.: The ECMWF medium-range prediction models development of the numerical formulations and the

impact of increased resolution, Meteorology and Atmospheric Physics, 40, 28–60, URL http://dx.doi.org/10.1007/BF01027467, 10.1007/BF01027467, 1989.

Solomon, S., Garcia, R. R., Rowland, F. S., and Wuebbles, D.: On the Depletion of Antarctic Ozone, Nature, 321, 755–758, doi:10.1038/321755a0, 1986.

Stamnes, K., Tsay, S.-C., Jayaweera, K., and Wiscombe, W.: Numerically stable algorithm for discrete-ordinate-method radiative transfer in multiple scattering and emitting layered media, Applied Optics, 27, 2502–2509, doi:10.1364/AO.27.002502, 1988.

Stamnes, K., Tsay, S. C., Wiscombe, W., and Laszlo, I.: DISORT, a General-Purpose Fortran Program for Discrete-Ordinate-Method Radiative Transfer in Scattering and Emitting Layered Media: Documentation of Methodology, Tech. rep., Dept. of Physics and Engineering Physics Stevens Institute of Technology Hoboken, NJ 07030, URL ftp://climate1.gsfc.nasa.gov/wiscombe/Multiple_Scatt/, 2000.

Stimpfle, R. M., Wilmouth, D. M., Salawitch, R. J., and Anderson, J. G.: First measurements of ClOOCl in the stratosphere: The coupling of ClOOCl and ClO in the Arctic polar vortex, Journal Of Geophysical Research (Atmospheres), 109, D03 301, doi: 10.1029/2003JD003811, 2004.

Stolarski, R. S. and Cicerone, R. J.: Stratospheric Chlorine: a Possible Sink for Ozone, Canadian Journal of Chemistry, 52, 1610–1615, doi:10.1139/v74-233, URL http://www.nrcresearchpress.com/doi/abs/10.1139/v74-233, 1974.

Stolarski, R. S., Krueger, A. J., Schoeberl, M. R., McPeters, R. D., Newman, P. A., and Alpert, J. C.: Nimbus 7 satellite measurements of the springtime Antarctic ozone decrease, Nature, 322, 808–811, doi:10.1038/322808a0, URL http://dx.doi.org/10.1038/322808a0, 1986.

Studer, A.: Aerobic Microbial Degradation of Chloromethane, Ph.D. thesis, Swiss Federal Institute of Technology Zürich, 2001.

Sumińska-Ebersoldt, O., Lehmann, R., Wegner, T., Grooß, J.-U., Hösen, E., Weigel, R., Volk, C. M., Borrmann, S., Rex, M., Stroh, F., and von Hobe, M.: ClOOCl photolysis at high

solar zenith angles: analysis of the RECONCILE self-match flight, Atmospheric Chemistry and Physics Discussions, 11, 18 901–18 926, doi:10.5194/acpd-11-18901-2011, URL http://www.atmos-chem-phys-discuss.net/11/18901/2011/, 2011.

Thompson, D. W. J. and Solomon, S.: Interpretation of Recent Southern Hemisphere Climate Change, Science, 296, 895–899, doi:10.1126/science.1069270, URL http://www.sciencemag.org/content/296/5569/895.abstract, 2002.

Toniolo, A., Granucci, G., Inglese, S., and Persico, M.: Theoretical study of the photodissociation dynamics of ClOOCl, Physical Chemistry Chemical Physics, 3, 4266–4279, doi:10.1039/b104044h, 2001.

Trentmann, J., Bovensmann, H., Eyring, V., Müller, R. W., and Burrows, J. P.: Impact of accurate photolysis calculations on the simulation of stratospheric chemistry, Journal of Atmospheric Chemistry, 44, 225–240, 2003.

Tripathi, O. P., Godin-Beekmann, S., Lefevre, F., Marchand, M., Pazmino, A., Hauchecorne, A., Goutail, F., Schlager, H., Volk, C. M., Johnson, B., Konig-Langlo, G., Balestri, S., Stroh, F., Bui, T. P., Jost, H. J., Deshler, T., and von der Gathen, P.: High resolution simulation of recent Arctic and Antarctic stratospheric chemical ozone loss compared to observations, Journal of Atmospheric Chemistry, 55, 205–226, doi:10.1007/s10874-006-9028-8, 2006.

Troe, J.: Theory of thermal unimolecular reactions at low pressures. I. Solutions of the master equation, The Journal of Chemical Physics, 66, 4745–4757, doi:10.1063/1.433837, 1977a.

Troe, J.: Theory of thermal unimolecular reactions at low pressures. II. Strong collision rate constants. Applications, The Journal of Chemical Physics, 66, 4758–4775, doi:10.1063/1.433838, 1977b.

Troe, J.: Predictive possibilities of unimolecular rate theory, The Journal of Physical Chemistry, 83, 114–126, doi:10.1021/j100464a019, URL http://pubs.acs.org/doi/abs/10.1021/j100464a019, 1979.

Trolier, M., Mauldin, R. L., and Ravishankara, A. R.: Rate coefficient for the termolecular channel of the self-reaction of chlorine monoxide, The Journal of Physical Chemistry, 94, 4896–4907, doi:10.1021/j100375a027, URL http://pubs.acs.org/doi/abs/10.1021/j100375a027, 1990.

Urban, J., Pommier, M., Murtagh, D. P., Santee, M. L., and Orsolini, Y. J.: Nitric acid in the stratosphere based on Odin observations from 2001 to 2009 – Part 1: A global climatology, Atmospheric Chemistry and Physics, 9, 7031–7044, doi:10.5194/acp-9-7031-2009, URL http://www.atmos-chem-phys.net/9/7031/2009/, 2009.

Volk, C., Riediger, O., Strunk, M., Schmidt, U., Ravegnani, F., Ulanovsky, A., and Rudakovand, V.: In situ Tracer Measurements in the Tropical Tropopause Region During APE-THESEO, Eur. Comm. Air Pollut. Res. Report 73, pp. 661–664, 2000.

von Hobe, M.: Revisiting Ozone Depletion, Science, 318, 1878, doi:10.1126/science.1151597, 2007.

von Hobe, M., Grooß, J. U., Müller, R., Hrechanyy, S., Winkler, U., and Stroh, F.: A re-evaluation of the ClO/Cl2O2 equilibrium constant based on stratospheric in-situ observations, Atmospheric Chemistry and Physics, 5, 693–702, 2005.

von Hobe, M., Salawitch, R. J., Canty, T., Keller-Rudek, H., Moortgat, G. K., Grooß, J. U., Müller, R., and Stroh, F.: Understanding the kinetics of the ClO dimer cycle, Atmospheric Chemistry and Physics, 7, 3055–3069, doi:10.5194/acp-7-3055-2007, 2007.

von Hobe, M., Stroh, F., Beckers, H., Benter, T., and Willner, H.: The UV/Vis absorption spectrum of matrix-isolated dichlorine peroxide, ClOOCl, Physical Chemistry Chemical Physics, 11, 1571–1580, doi:10.1039/B814373K, 2009.

von Hobe, M., Grooß, J.-U., Pope, F., Peter, T., Cairo, F., Orsolini, I., Volk, C., Marchand, M., Janosi, I., Schlager, H., Stroh, F., Rex, M., Wienhold, F., and RECONCILE-Team: Reconciliation of essential process parameters for an enhanced predictability of arctic stratospheric ozone loss and its climate interactions, to be submitted to Atmospheric Chemistry and Physics, 2011.

Voulgarakis, A., Savage, N. H., Wild, O., Carver, G. D., Clemitshaw, K. C., and Pyle, J. A.: Upgrading photolysis in the p-TOMCAT CTM: model evaluation and assessment of the role of clouds, Geoscientific Model Development, 2, 59–72, doi:10.5194/gmd-2-59-2009, URL http://www.geosci-model-dev.net/2/59/2009/, 2009.

Weigel, R., Hermann, M., Curtius, J., Voigt, C., Walter, S., Böttger, T., Lepukhov, B., Belyaev, G., and Borrmann, S.: Experimental characterization of the COndensation PArticle counting System for high altitude aircraft-borne application, Atmospheric Measurement Techniques, 2, 243–258, doi:10.5194/amt-2-243-2009, 2009.

Wild, O., Zhu, X., and Prather, M. J.: Fast-J: Accurate Simulation of In- and Below-Cloud Photolysis in Tropospheric Chemical Models, Journal of Atmospheric Chemistry, 37, 245–282, URL http://dx.doi.org/10.1023/A:1006415919030, 10.1023/A:1006415919030, 2000.

Wilmouth, D. M., Hanisco, T. F., Stimpfle, R. M., and Anderson, J. G.: Chlorine-Catalyzed Ozone Destruction: Cl Atom Production from ClOOCl Photolysis, Journal of Physical Chemistry A, 113, 14 099–14 108, doi:10.1021/jp9053204, 2009.

Wiscombe, W. J.: The Delta-M Method: Rapid Yet Accurate Radiative Flux Calculations for Strongly Asymmetric Phase Functions, Journal of Atmospheric Science, 34, 1408–1422, doi:10.1175/1520-0469(1977)034<1408:TDMRYA>2.0.CO;2, URL http://dx.doi.org/10.1175/1520-0469(1977)034<1408:TDMRYA>2.0.CO;2, 1977.

WMO: Scientific assessment of ozone depetion: 1985, Geneva, Switzerland, 1985.

WMO: Scientific assessment of ozone depetion: 2010, Geneva, Switzerland, 2010.

Woods, T. N., Prinz, D. K., Rottman, G. J., London, J., Crane, P. C., Cebula, R. P., Hilsenrath, E., Brueckner, G. E., Andrews, M. D., White, O. R., VanHoosier, M. E., Floyd, L. E., Herring, L. C., Knapp, B. G., Pankratz, C. K., and Reiser, P. A.: Validation of the UARS solar ultraviolet irradiances: Comparison with the ATLAS 1 and 2 measurements, Journal of Geophysical Research, 101, 9541–9569, doi:10.1029/96JD00225, URL http://dx.doi.org/10.1029/96JD00225, 1996.

Woyke, T.: In-Situ Messung von Halogenoxiden in der polaren Stratosphäre: Untersuchungen zur Ozonchemie im Winter 1994/95, Ph.D. thesis, Universität Bonn, URL http://books.google.de/books?id=uqMwPwAACAAJ, 1997.

Young, I. A. K., Murray, C., Blaum, C. M., Cox, R. A., Jones, R. L., and Pope, F. D.: Temperature dependent structured absorption spectra of molecular chlorine, Physical Chemistry Chemical Physics, 13, 15 318–15 325, doi:10.1039/C1CP21337G, URL http://dx.doi.org/10.1039/C1CP21337G, 2011.

Zhang, H., Zhang, F., Fu, Q., Shen, Z., and Lu, P.: Two- and Four-Stream Combination Approximations for Computation of Diffuse Actinic Fluxes, Journal of the Atmospheric Sciences, 67, 3238–3252, doi:10.1175/2010JAS3370.1, URL http://dx.doi.org/10.1175/2010JAS3370.1, 2010.

Zhong, W. and Haigh, J. D.: Improved Broadband Emissivity Parameterization for Water Vapor Cooling Rate Calculations, Journal of the Atmospheric Sciences, 52, 124–138, doi:10.1175/1520-0469(1995)052<0124:IBEPFW>2.0.CO;2, URL http://dx.doi.org/10.1175/1520-0469(1995)052<0124:IBEPFW>2.0.CO;2, 1995.

Band / Volume 136
Development of thin film inorganic membranes for oxygen separation
H. J. Moon (2012), XII, 118 pp.
ISBN: 978-3-89336-781-8

Band / Volume 137
Influence of Material and Testing Parameters on the Lifetime of TBC Systems with MCrAlY and NiPtAl Bondcoats
P. Song (2012), V, 126 pp.
ISBN: 978-3-89336-783-2

Band / Volume 138
Strömungsmechanische Modellierung eines Brenngaserzeugungssystems
F. Scharf (2012), vi, 223 pp.
ISBN: 978-3-89336-784-9

Band / Volume 139
Clouds and aerosol in infrared radiative transfer calculations for the analysis of satellite observations
S. Grießbach (2012), viii, 169 pp.
ISBN: 978-3-89336-785-6

Band / Volume 140
Untersuchung zum Thin Film Low Pressure Plasma Spraying (LPPS-TF) Prozess
A. Hospach (2012), 165 pp.
ISBN: 978-3-89336-787-0

Band / Volume 141
Development of thermal spray processes with liquid feedstocks
A. Guignard (2012), 128 pp.
ISBN: 978-3-89336-788-7

Band / Volume 142
Herstellung uranbasierter Keramiken mittels interner Gelierung zur Konversion trivalenter Actinoiden
H. Daniels (2012), 154 pp.
ISBN: 978-3-89336-794-8

Band / Volume 143
Experimental and numerical studies on solute transport in unsaturated heterogeneous porous media under evaporation conditions
M. Bechtold (2012), xviii, 131 pp.
ISBN: 978-3-89336-795-5

Band / Volume 144
Konzept und Kosten eines Pipelinesystems zur Versorgung des deutschen Straßenverkehrs mit Wasserstoff
D. Krieg (2012), 228 pp.
ISBN: 978-3-89336-800-6

Band / Volume 145
Mechanistic studies on the OH-initiated atmospheric oxidation of selected aromatic hydrocarbons
S. Nehr (2012), viii, 129 pp.
ISBN: 978-3-89336-804-4

Band / Volume 146
Electron Spin Resonance Investigation of Semiconductor Materials for Application in Thin-Film Silicon Solar Cells
L. Xiao (2012), VIII, 147 pp.
ISBN: 978-3-89336-805-1

Band / Volume 147
Untersuchungen zum Sicherheits- und Transmutationsverhalten innovativer Brennstoffe für Leichtwasserreaktoren
O. Schitthelm (2012), V, 150 pp.
ISBN: 978-3-89336-806-8

Band / Volume 148
IEK-Report 2011. Klimarelevante Energieforschung
(2012), ca. 250 pp.
ISBN: 978-3-89336-808-2

Band / Volume 149
IEK-Report 2011. Climate-Relevant Energy Research
(2012), ca. 250 pp.
ISBN: 978-3-89336-809-9

Band / Volume 150
Netzintegration von Fahrzeugen mit elektrifizierten Antriebssystemen in bestehende und zukünftige Energieversorgungsstrukturen (2012)
ISBN: 978-3-89336-811-2

Band / Volume 151
Stratospheric ClOOCl chemistry at high solar zenith angles
O. Suminska-Ebersoldt (2012), VI, 126 pages
ISBN: 978-3-89336-817-4

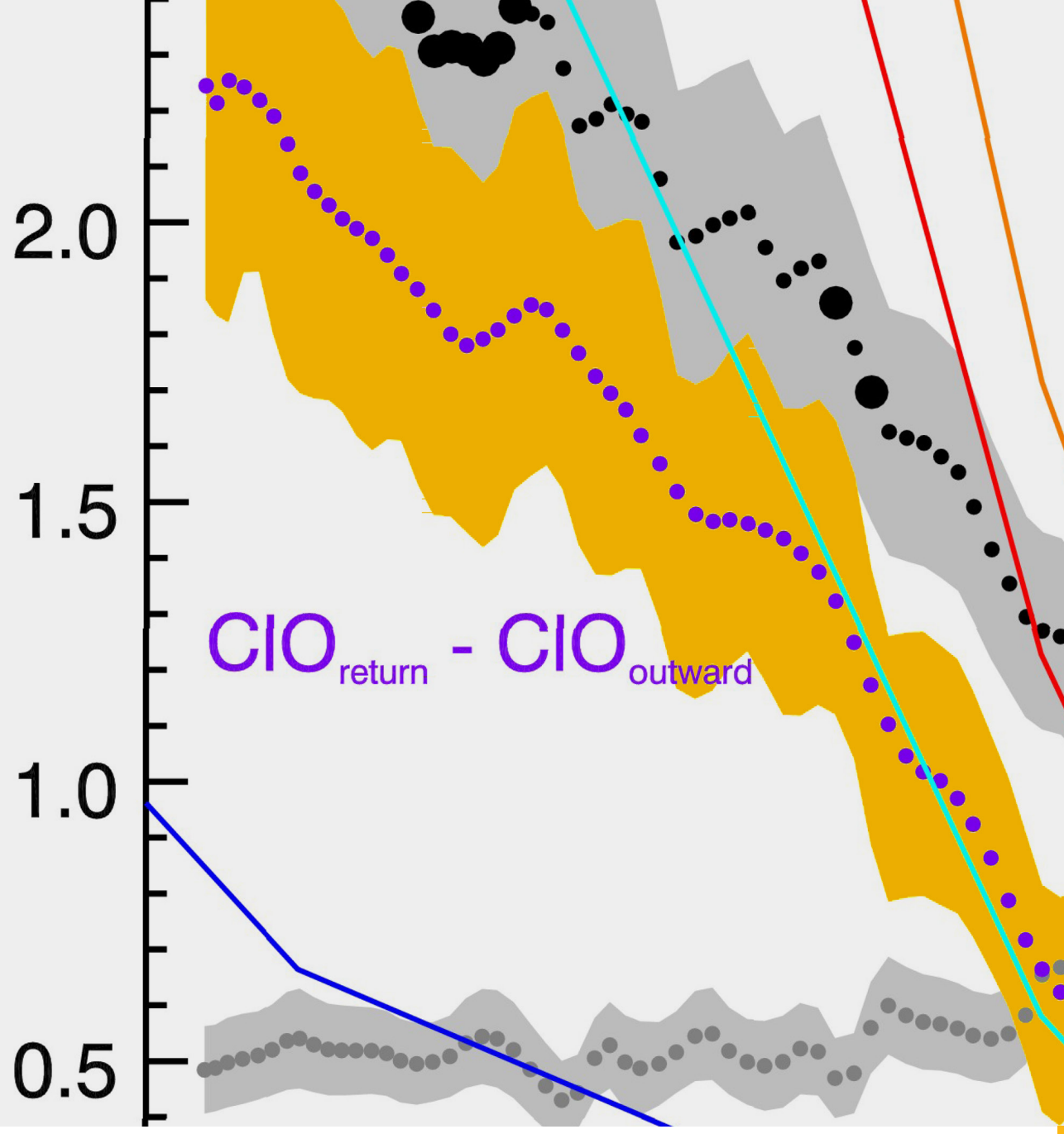

Energie & Umwelt / Energy & Environment
Band / Volume 151
ISBN 978-3-89336-817-4

JÜLICH
FORSCHUNGSZENTRUM